Structure and Reactivity of Lithium Enolates: Characterization of Solutions Structures and Rate Studies of O-Silylations

by Jocelyn Marie Gruver

This thesis/dissertation document has been electronically approved by the following individuals:

Collum,David B (Chairperson)

Njardarson,Jon (Minor Member)

Chirik,Paul (Minor Member)

STRUCTURE AND REACTIVITY OF LITHIUM ENOLATES: CHARACTERIZATION OF SOLUTION STRUCTURES AND RATE STUDIES OF O-SILYLATIONS

A Dissertation
Presented to the Faculty of the Graduate School
of Cornell University
In Partial Fulfillment of the Requirements for the Degree of
Doctor of Philosophy

by
Jocelyn Marie Gruver
August 2010

© 2010 Jocelyn Marie Gruver

STRUCTURE AND REACTIVITY OF LITHIUM ENOLATES: CHARACTERIZATION OF SOLUTION STRUCTURES AND RATE STUDIES OF O-SILYLATIONS

Jocelyn Marie Gruver, Ph. D.

Cornell University 2010

Progress toward understanding the reactivity of synthetically important lithium enolates relies on the ability to characterize their aggregation states in solution. There have been successes in characterizing solution structures of lithium enolates, however, no general method existed until the Collum group's recent efforts to solve this problem. Disrupting the aggregate's high inherent symmetry by mixing two different O-lithiated species in solution is key to developing this general method. Monitoring the resulting ensemble by ^{6}Li NMR spectroscopy in conjunction with the method of continuous variation enables characterization of the solution structure. Most O-lithiated species are disolvated cyclic dimers in TMEDA, with the exception of lithium alkoxides and bulky phenolates. The general method for characterizing O-Li species in solution has enabled rate studies of O-silylations of lithium enolates. Although O-silylations are very common and seem quite simple on the surface, studies reveal a complex mechanism involving LiCl autocatalysis due to LiCl-enolate mixed aggregates. Side product formation and other unexpected observations also contributed to the difficulty in studying the mechanism of O-silylations. Chapter III includes characterization of a C,N-chelated lithium dianion, which was completed in collaboration with the Sarpong group at the University of California, Berkeley.

BIOGRAPHICAL SKETCH

Jocelyn M. Bilas was born in the small town of Indianola, Mississippi to B.J. and Jane Bilas, joining her 3-year-old brother Jeremy. After just 3 weeks of enjoying southern living, she moved to Wilmington, Delaware where she attended Ursuline Academy from kindergarten through her freshman year. She then moved to Tampa, Florida where she spent her sophomore year at Tampa Catholic before heading back to the cold north. In 1997, she moved to DeWitt, Michigan and finished her high school career, graduating as salutatorian from Lansing Catholic Central in 1999.

Jocelyn attended Saint Mary's College in Notre Dame, Indiana. She participated in an NSF funded Research Experience for Undergraduates with Professor SonBinh T. Nguyen at Northwestern University. This research led to her senior thesis entitled "Chiral Induction Through Axial Ligand Substitution of Ruthenium(II)-Salen Complexes for the Cyclopropanation of Styrene." She graduated summa cum laude with a B.S. in chemistry with a biochemical concentration in 2003. After graduation, she worked as an analytical chemist at DuPont in Newark, Delaware.

In 2005, Jocelyn moved to upstate New York to attend Cornell University where she joined David Collum's laboratory. In October 2005, she married Scott J. Gruver. After 5 years in upstate New York, they will be relocating to the Philadelphia area where Jocelyn has accepted a position at Dow Chemical in Spring House, Pennsylvania.

This is dedicated to my wonderful parents, B.J. and Jane, for giving me the strength to follow my dreams and supporting me every step of the journey. It is also dedicated to my incredible husband, Scott, for his endless support throughout graduate school.

ACKNOWLEDGMENTS

First, I would like to acknowledge my advisor, Professor David Collum, for his teaching and encouragement. His guidance and advice were crucial to my development as a scientist. His stories and sense of humor were always welcome on days when the research was particularly difficult. I also thank my committee members Professors Paul Chirik and Jón T. Njarðarson.

I would also like to thank the Cornell NMR facility, especially Dr. Ivan Keresztes and Tony Condo for their guidance and flexibility during countless hours of NMR usage.

I also acknowledge the former Collum group members for their training, patience, and support during my early years in the Collum lab: Dr. Lara Liou, Dr. Jason Riggs, Dr. Pete Godenschwager, Dr. Tim DeVries, Dr. Lekha Gupta, and Dr. Anandarup Gowsami. A special thanks to current group members, Dr. Yun Ma, Alex Hoepker, Laura Tomasevich, Angela Bruneau, and Hari Subramanian, for making my time at Cornell enjoyable.

I thank my parents for supporting me throughout my childhood and into adulthood. They have always given me the encouragement and freedom to make my own decisions. Thank you for all of the opportunities that you have given me – words cannot express how grateful I am to have you as my mom and dad. Thank you also to my brother, Jeremy, for his all of his love and support.

Last, but certainly not least, I thank my husband Scott. I truly appreciate you quizzing me with flash cards, listening to my group meetings, and making my busy life easier even when yours was extremely busy, too. Thank you for being by my side during this journey – you are the best!

TABLE OF CONTENTS

LIST OF FIGURES

LIST OF TABLES

CHAPTER I

Solution Structures of Lithium Enolates, Phenolates, Carboxylates, and Alkoxides in the Presence of *N,N,N′,N′*-Tetramethylethylenediamine: A Prevalence of Cyclic Dimers

Solution Structures of Lithium Enolates, Phenolates, Carboxylates, and Alkoxides in the Presence of *N*,*N*,*N*′,*N*′-Tetramethylethylenediamine: A Prevalence of Cyclic Dimers[*]

Abstract

The method of continuous variation was used to characterize lithium enolates, phenolates, carboxylates, and alkoxides solvated by *N*,*N*,*N*′,*N*′-tetramethylethylenediamine (TMEDA). The method relies on characterizing an ensemble of homo- and heteroaggregates using ^{6}Li NMR spectroscopy. A combination of aggregate counts and symmetries, nearly statistical distributions, and quantitative parametric fits revealed that cyclic dimers are the dominant form. Non-statistical distributions favoring heteroaggregated dimers were observed when hindered enolates and lithium carboxylates were mixed with unhindered enolates. Nonstatistical distributions favoring homoaggregates observed when hindered (tertiary) alkoxides were paired with other O-lithiated forms were traced to the formation of higher aggregates (hexamers) of the tertiary alkoxides. Highly hindered lithium phenolates appear to form TMEDA-solvated monomers.

[*] Reprinted with permission from Gruver, J. M.; Liou, L. R.; McNeil, A. J.; Ramirez, A.; Collum, D. B. *J. Org. Chem*. **2008**, *73*, 7743. Copyright 2008 American Chemical Society.

Introduction

Ketone enolates are highly reactive intermediates used for a range of functionalizations in organic synthesis.[1] It is no surprise, therefore, that they have also commandeered the attention of structural and mechanistic chemists.[2,3] The Achilles heel of most mechanistic studies is characterizing their structures in solution.[4-7] The problem stems from a combination of the oppressive symmetry of the possible aggregates and the absence of observable O-Li scalar coupling.[8] Progress has been made by accruing data from a broad range of indirect analytical methods,[2] but these methods are often specific to the substrate-solvent combination.

We recently used the method of continuous variation[9] (the method of Job[10]) to show that lithium enolates of β -amino esters are hexameric.[11] The generality of the method was confirmed by showing that simple enolates **1**-**3** are cyclic dimers (**4**) in *N,N,N′,N′*-tetramethylethylenediamine (TMEDA), cubic tetramers (**5**) in THF, and cubic tetramers (**6**) in 1,2-dimethoxyethane (DME).[3]

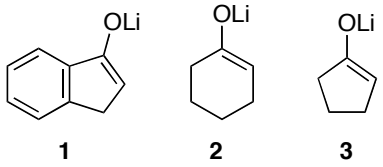

1 **2** **3**

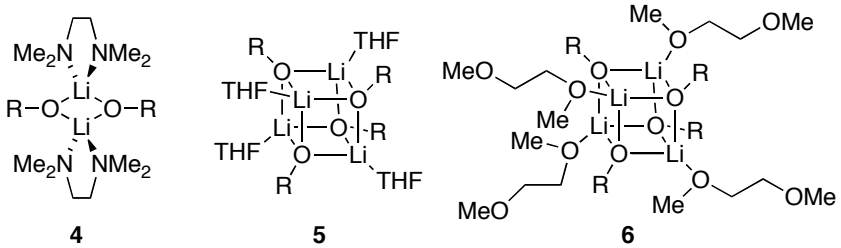

4 **5** **6**

We have now significantly expanded the range of characterized TMEDA-solvated O-lithiated species.[12] All species in Figure I.1 form cyclic dimers of general structure **4**.[6,13,14] Standard lithium alkoxides constitute the primary exception, affording higher oligomers. The protocols used to determine structure were refined.

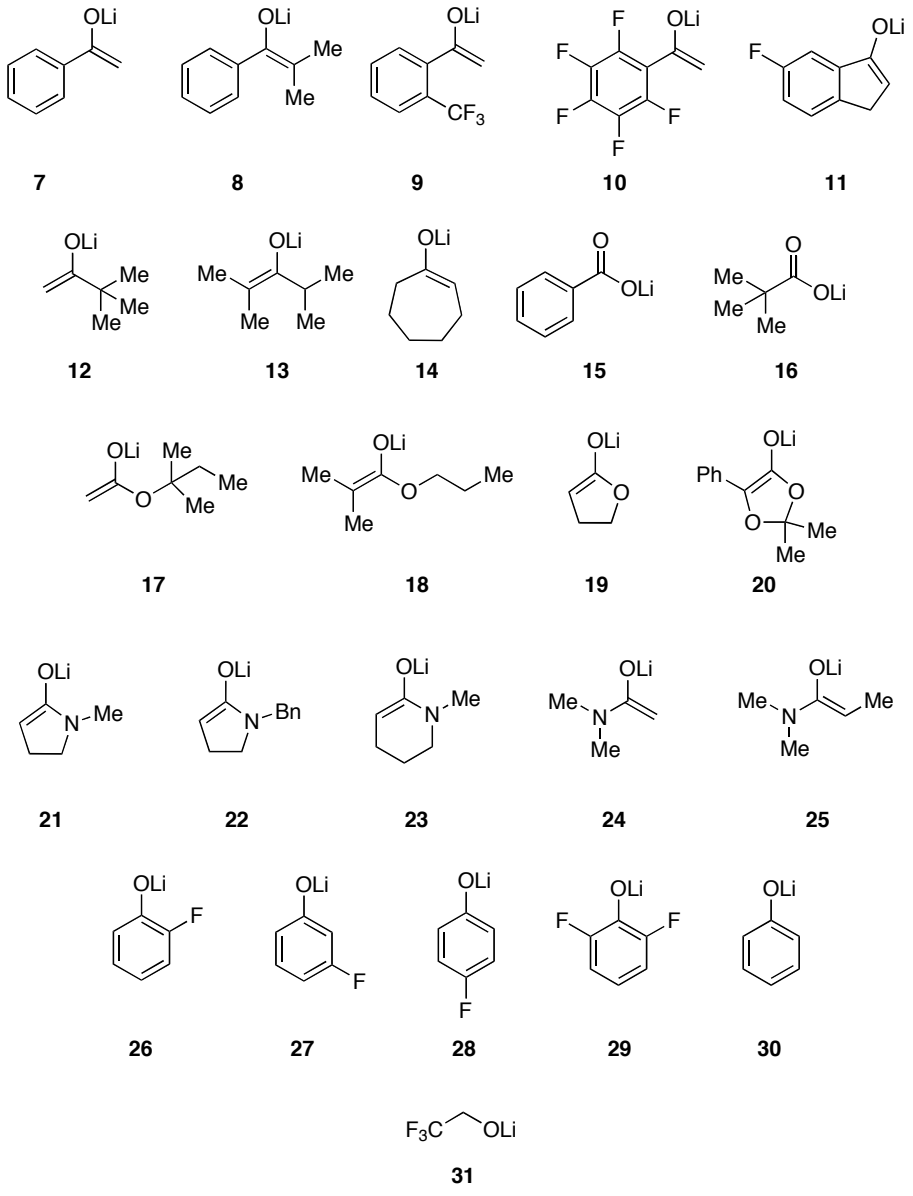

Figure I.1. O-Lithiated species found to be dimeric in TMEDA.

Results and Discussion

Method of Continuous Variation. The general strategy for characterizing enolates and related O-lithiated species using the method of continuous variation finds its origins in studies of Chabanel,[15] Gagne,[16] Günther,[17] Reich,[4i] and others.[18,19] An ensemble of homo- and heteroaggregated enolates (eq 1) is monitored as a function of the mole fractions of enolate subunits (**A** and **B**) using ^{6}Li NMR spectroscopy.[20] The number of aggregates and their symmetries reflect the aggregation state, *n*. As we show herein, the preponderant form of TMEDA-solvated enolates is a disolvated dimer of general structure **4**, representing the simplest possible ensemble (eq 2). A high tendency toward statistical distributions and parametric fits distinguish the all-dimer $\mathbf{A_2}$-**AB**-$\mathbf{B_2}$ model from $\mathbf{A_2}$-**AB**-**B** and $\mathbf{A_2}$-**AB**-$\mathbf{B_4}$ models (see Appendix I).

$$\mathbf{A_n} + \mathbf{B_n} \Longleftrightarrow \mathbf{A_n} + \mathbf{A_{n-1}B_1} + \mathbf{A_{n-2}B_2} + \mathbf{A_{n-3}B_3} + ...\mathbf{B_n} \qquad (1)$$

$$\mathbf{A_2} + \mathbf{B_2} \overset{K_1}{\rightleftharpoons} 2\ \mathbf{AB} \qquad (2)$$

Optimizing the resolution of the ^{6}Li resonances of the various aggregates is of paramount importance. Resolution is most readily achieved by pairing $\mathbf{A_n}$ and $\mathbf{B_n}$ with distinctly different ^{6}Li chemical shifts (Table I.1.)[3] A second issue is that the actual mole fractions of the **A** and **B** subunits can deviate from the intended mole fractions because of experimental error, non-quantitative enolization, selective formation of mixed aggregates with base,[6f,7,21] or formation of by-products. (Metalations using [^{6}Li,^{15}N]LDA[22] and

[^{6}Li,^{15}N]LiHMDS[23] reveal that only LDA forms detectable mixed aggregates in TMEDA/toluene.[21]) Although such deviations do not impair the qualitative analysis of aggregate numbers and their symmetries, they can distort the quantitative parametric fits. Consequently, the mole fractions were measured by simply integrating the ^{6}Li resonances. Usually, the intended and measured mole fractions are comparable, but we believe the latter are more accurate.[3] One last concern pertains to deviations from statistical behavior. The parametric fits reveal that deviations from statistical behavior are usually quite small. When large deviations occur, however, the parametric fits do not readily distinguish the all-dimer $\mathbf{A_2}$-**AB**-$\mathbf{B_2}$ model from the $\mathbf{A_2}$-**AB**-**B** and $\mathbf{A_2}$-**AB**-$\mathbf{B_4}$ models; the models become quite similar if the relative **AB** concentration becomes either very high or very low. Additional experiments exclude the latter two models (vide infra).

Table I.1. ^{6}Li NMR chemical shifts relative to a 0.30 M [^{6}Li]LiCl/MeOH standard at -90 °C in 0.24 M TMEDA/toluene.

Substrate	δ ^{6}Li	Substrate	δ ^{6}Li
1	0.22	**18**	-0.33
2	-0.02	**19**	0.29
3	0.05	**20**	0.05
7	0.14	**21**	-0.24
8	-0.05	**22**	-0.14
9	-0.12	**23**	-0.26
10	-0.34	**24**[b]	-0.14
11	0.00	**25**[c]	-0.04
12	-0.27	**26**	0.30
13	-0.42	**27**	0.03
14	-0.06	**28**	0.04
15	1.12	**29**	0.32
16	0.66	**30**	0.30
17[a]	0.33	**31**	-0.13

[a]3.0 M TMEDA/0.11 M THF/toluene/pentane. [b]-60 °C. [c]-70 °C.

Statistical Dimer Distributions. All O-lithiated species in Figure I.1 were found to be dimeric in TMEDA/toluene solution. Typical results are illustrated emblematically using enolates **1** and **7**. The homo- and heteroaggregated dimers were easily observed using ^{6}Li NMR spectroscopy (Figure I.2). The plot of relative aggregate integrations (I)[24] versus mole fraction (X) in Figure I.3 shows a nearly statistical distribution of aggregates. Inferior fits to models based on ternary ensembles $\mathbf{A}_2$-**AB**-**B** and $\mathbf{A}_2$-**AB**-$\mathbf{B}_4$ (evidenced by large residual deviations; Appendix I) support the dimer assignment.[25]

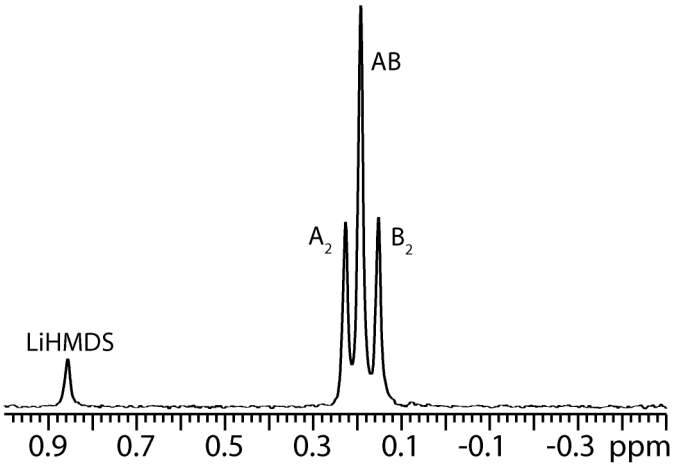

Figure I.2. ^{6}Li NMR spectrum of an equimolar mixture (mole fraction: X_7 = 0.5) of [^{6}Li]**1** (**A**) and [^{6}Li]**7** (**B**) in 0.24 M TMEDA/toluene at -50 °C.

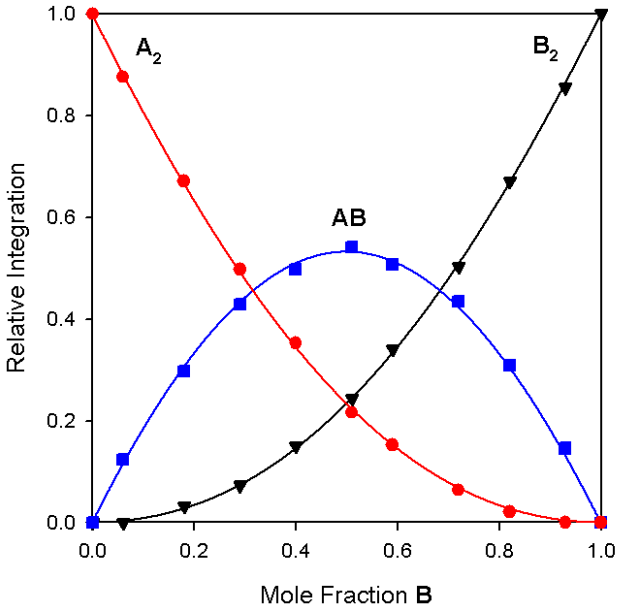

Figure I.3. Job plot showing the relative integrations versus mole fractions of **7** for 0.10 M mixtures of enolates [^{6}Li]**1** (**A**) and [^{6}Li]**7** (**B**) in 0.24 M TMEDA/toluene at -50 °C.

Nonstatistical Dimer Distributions. A non-statistical tendency toward heteroaggregation was observed when hindered enolates (**12** and **13**) were paired with their less-congested counterparts (see Figure I.4). We suspected that steric interactions destabilized the congested homoaggregated dimer. Indeed, pairing hindered enolates **12** and **13** afforded a statistical distribution that fits the $\mathbf{A}_2$-**AB**-$\mathbf{B}_2$ model.

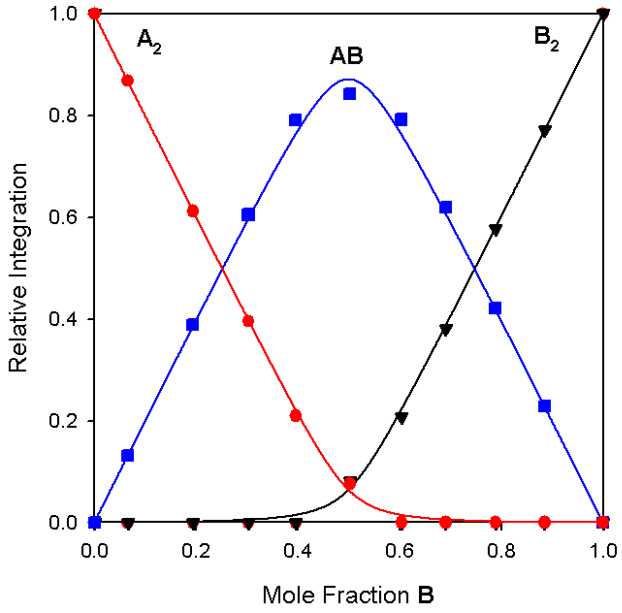

Figure I.4. Job plot showing the relative integrations versus mole fractions of **13** for 0.10 M mixtures of enolates [^{6}Li]**1** (**A**) and [^{6}Li]**13** (**B**) in 0.24 M TMEDA/toluene at -90 °C.

Similar preferences for heteroaggregates (approaching quantitative formation of the heterodimer in some cases) resulted when lithium carboxylates **15** or **16** were paired with lithium enolates. Once again, statistical behavior returned when carboxylates **15** and **16** were paired. Although TMEDA-solvated lithium carboxylates could be represented by dimer **32**, crystallographic guidance is surprisingly absent. A lithium carbamate reported by Snaith and coworkers was found to have a ring-expanded structure (**33**).[26]

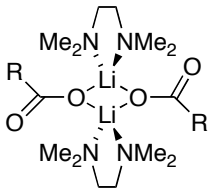

32

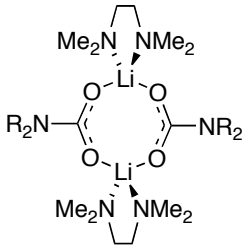

33

We admit being surprised that lithium carboxylates form homo- and heteroaggregates of well-defined structure. We expected complex aggregates displaying marginal physical properties (gelling or insolubility).[27] As salt effects on yields, selectivities, and reactivities continue to be reported,[21,28] we are encouraged by the potential importance of carboxylates in both synthetic and mechanistic organolithium chemistry.[29] There are certainly many more lithium carboxylates than lithium halides!

Higher Oligomers. Hindered lithium alkoxides (**34**-**36**) displayed a strong bias toward *homoaggregates* resulting from higher oligomers, which we believe to be hexamers. For example, tertiary alkoxides **34**-**36** in 0.24 M TMEDA/toluene each displayed a single ^{6}Li resonance at -90 ^{o}C (δ 0.48, 0.71, and 0.31 ppm, respectively). Pairing tertiary alkoxides with relatively uncongested O-lithiated species afforded very low concentrations of putative heterodimers (Figure I.5). It is telling that hindered alkoxides even resisted heteroaggregation with *hindered* enolates.[30]

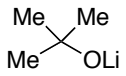

34

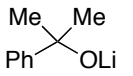

35

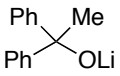

36

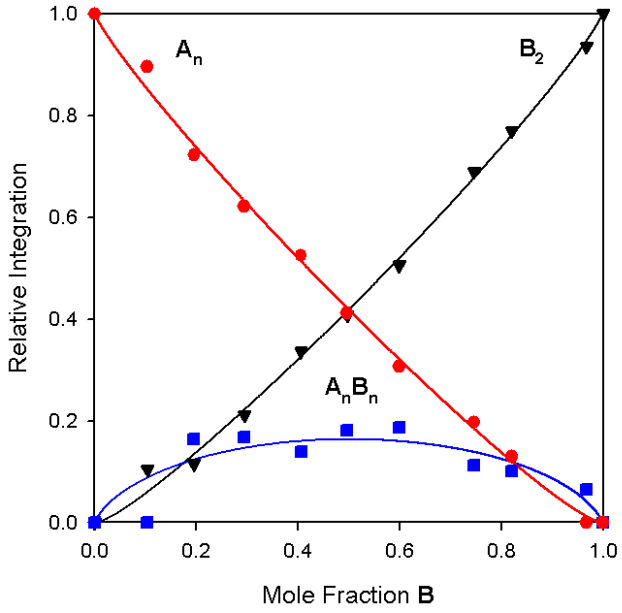

Figure I.5. Job plot showing the relative integrations versus mole fractions of **1** for 0.10 M mixtures of alkoxide [^{6}Li]**34** (**A**) and enolate [^{6}Li]**1** (**B**) in 0.24 M TMEDA/toluene at -90 °C.

We suspected that the reticence of alkoxides **34**-**36** to heteroaggregate with other O-lithiated species stemmed from a reluctance to form heterodimers of any form. Indeed, pairing *t*-BuOLi (**34**) with hindered alkoxides **35** or **36**[31] afforded remarkable spectral complexity (Figure I.6) exceeding even that anticipated for an ensemble of tetramers (**A**$_4$-**A**$_3$**B**-**A**$_2$**B**$_2$-**AB**$_3$-**B**$_4$).[3] It seems probable, therefore, that the hindered alkoxides are hexameric (possibly only partially solvated),[32-34] as indicated by x-ray crystallography[35,36] and colligative measurements for *t*-BuOLi in benzene.[37] The large number of hexamer stoichiometries (seven) and the existence of positional isomers within hexagonal drums resulted in 38 magnetically inequivalent ^{6}Li resonances.[3] The spectra appeared as though a structural assignment might be possible. Not surprisingly, however, severe overlap of

resonances (as evidenced by shoulders on peaks in Figure I.6) caused us to abort efforts to tease out additional insights.

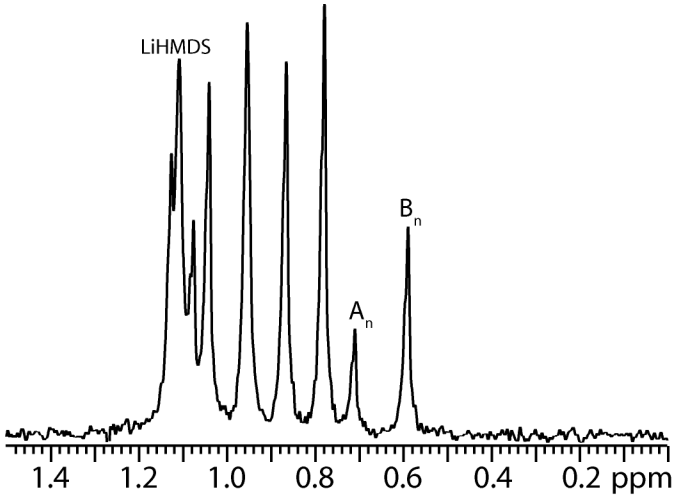

Figure I.6. ^{6}Li NMR spectrum of a 1:1 mixture of [^{6}Li]**34** and [^{6}Li]**36** in 0.24 M TMEDA/toluene at -30 °C.

We thought that hindered phenolates such as **37** might afford a monomer, but we obtained insoluble material shown to contain approximately one equiv of TMEDA by quenching an isolated sample. The corresponding disubstituted phenolate **38** is soluble and forms no detectable mixed aggregates with dimeric enolate **1** or highly oligomeric alkoxide **36**, suggesting phenolates **37** and **38** are indeed TMEDA-chelated monomers. Similar studies of primary and secondary alkoxides were thwarted by insolubility and spectral complexity, possibly attributable to higher oligomers.[38]

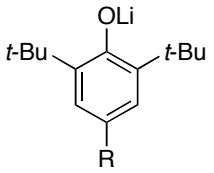

37; R = *t*-Bu
38; R = H

Conclusion

Addition of TMEDA to lithium enolates, phenolates, and carboxylates affords exclusively cyclic dimers in most instances. We are encouraged by both the success and generality of the method of continuous variation in characterizing species that have traditionally proven opaque to NMR spectroscopy. Although highly functionalized lithium enolates commonly used to effect diastereo- and enantioselective carbon-carbon bond formation may present new challenges and offer a few surprises, the protocol should prove durable. More important, these results satisfy a necessary prerequisite for understanding lithium enolate structure-reactivity relationships.

Acknowledgments. We thank the National Institutes of Health for direct support of this work and Merck, Pfizer, Boehringer-Ingelheim, R. W. Johnson, Aventis, Schering-Plough, and DuPont Pharmaceuticals (Bristol-Myers Squibb) for indirect support. We also thank Emily Jayne and Allyson Pickard for help in preparing several substrates.

Experimental Section

Reagents and Solvents. TMEDA was recrystallized as the hydrochloride salt[39] and subsequently distilled from solutions containing sodium benzophenone ketyl. Hydrocarbon solvents were distilled from blue

solutions containing sodium benzophenone ketyl with approximately 1 percent tetraglyme to dissolve the ketyl. We prepared and recrystallized [^{6}Li]LiHMDS, [^{6}Li,^{15}N]LiHMDS, [^{6}Li]LDA, and [^{6}Li,^{15}N]LDA as described previously.[22,23] Air- and moisture-sensitive materials were manipulated under argon using standard glove box, vacuum line, and syringe techniques.

Spectroscopic Analysis. Individual stock solutions of the substrates and base were prepared at room temperature. An NMR tube was flame dried on a Schlenk line and allowed to come to room temperature while under vacuum. It was then placed under argon and into a -78 °C dry ice/acetone bath. The appropriate amounts of the base followed by the substrates were added via syringe allowing about 30 seconds between additions. The tube was sealed under partial vacuum and immediately vortexed for approximately 10 seconds before being replaced into a -78 °C bath. Hindered enolates **12** and **13** required warming to 0 °C for approximately one hour to complete the enolization. Each NMR tube had 0.10 M total substrate concentration and 0.12 M lithium amide base in 0.24 M TMEDA/toluene.

^{6}Li NMR spectra were typically recorded at -90 °C on a 400 or 500 MHz spectrometer with a delay between scans set to >5 x T1 to ensure accurate integrations. In a few instances, adjusting the probe temperature was necessary to optimize resolution and line widths, although the origins of these temperature dependencies were not obvious. Chemical shifts are reported relative to a 0.30 M ^{6}LiCl/MeOH standard.

NMR resonances were integrated using standard software. After weighted Fourier transform with 64,000 points and phasing, line broadening was set between 0 and 0.2, and a baseline correction was applied if

appropriate. Deconvolution was performed in the absolute intensity mode, with application of a drift correction using default parameters for contributions from Lorentzian and Gaussian line shapes. For poorly resolved spectra, the resonances were indicated using the "mark" and "use mark" commands. The math underlying the parametric fits has been described in detail.[3,11]

APPENDIX I

A. Experimental Methods

a. Preparation of NMR Spectroscopic Samples

Stock solutions were prepared at room temperature. After flame drying the NMR tube on a Schlenk line and placing it under argon, the tube was placed in a -78 °C dry ice/acetone bath. The appropriate amounts of the base followed by the ketones and other components needed were added via syringe allowing about 30 seconds to one minute between additions. All samples had a total volume of 0.60 mL. The best results were obtained when between 100 and 300 μL were added at a time and when large concentration differences between the stock solutions and final concentrations were avoided. The tube was sealed under partial vacuum and immediately vortexed for 10 - 15 seconds before being replaced into a -78 °C bath. The samples were quickly vortexed twice more being careful to avoid excessive warming (above -20 °C). Inverting the NMR tubes to mix the samples or allowing them to warm often resulted in low quality spectra or significant deviations from the expected result.

b. Integration of NMR Resonances by Deconvolution

NMR resonances were integrated using Varian's software, VNMR. After weighted Fourier transform with 64,000 points and phasing, line broadening was set between 0 and 0.2 and a baseline correction was applied if appropriate. Deconvolution was performed in the absolute intensity mode, with application of a drift correction, with the default parameters for contributions from Lorentzian and Gaussian line shapes, and using the line

list for well resolved spectra. For poorly resolved spectra, the resonances were indicated using the “mark” and “use mark” commands.

B. Combinations of O-lithiated Species in TMEDA.

Table AI.1. Complete list of combinations of O-lithiated species.

Substrate A	Substrate B	Page	Structure	Statistical?
		21	Dimers	Yes
	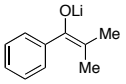	22	Dimers	Yes
	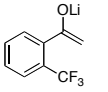	23	Dimers	Yes
	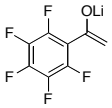	24	Dimers	Yes
		25	Dimers	Heteroaggregate Favored
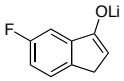		26	Dimers	Heteroaggregate Favored
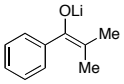		27	Dimers	Yes
		28	Dimers	Yes
	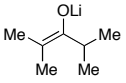	29	Dimers	Heteroaggregate Favored
	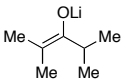	30	Dimers	Yes
	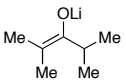	31	Dimers	Yes
		32	Dimers	Yes

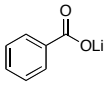		33	Dimers	Heteroaggregate Favored
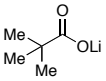		34	Dimers	Heteroaggregate Favored
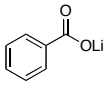	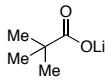	35	Dimers	Yes
	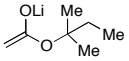	36	Dimers	Yes
	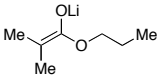	37	Dimers	Yes
		38	Dimers	Yes
	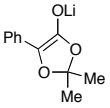	39	Dimers	Yes
		40	Dimers	Yes
		41	Dimers	Yes
		42	Dimers	Yes
		43	Dimers	Yes
		44	Dimers	Yes
	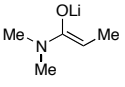	45	Dimers	Yes
		46	Dimers	Yes

		47	Dimers	Yes
	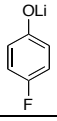	48	Dimers	Yes
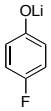		49	Dimers	Heteroaggregate Favored
	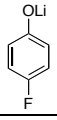	50	Dimers	Yes
		51	Dimers	Yes
		52	Dimers	Yes
		53	**A** = Higher oligomer **B** = Dimer	Homoaggregate Favored
	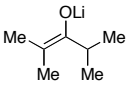	54	**A** = Higher oligomer **B** = Dimer	Homoaggregate Favored
		55-56	Higher oligomers	Homoaggregate Slightly Favored
		63	Higher oligomers	--
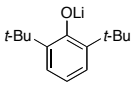		687	**A** = Monomer **B** =Dimer	--
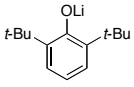		67	**A** = Monomer **B** = Higher oligomer	--

C. Job Plots in TMEDA.

i.

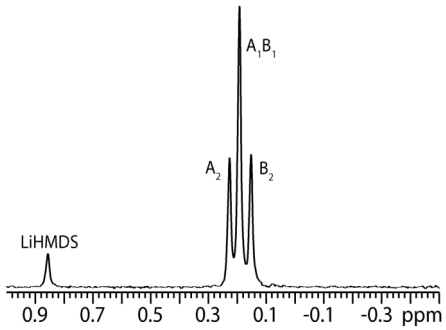

ii.

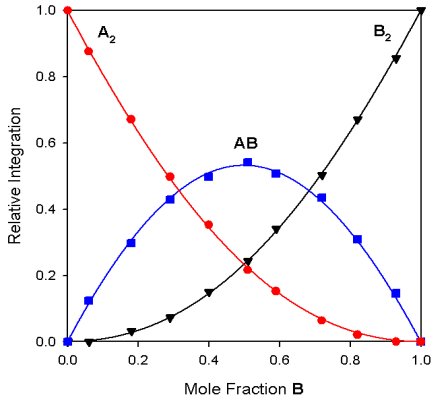

iii.

Calc. X_B	$\mathbf{A}_2$	$\mathbf{A}_1\mathbf{B}_1$	$\mathbf{B}_2$
0.00	1.00	0.00	0.00
0.06	0.88	0.12	0.00
0.18	0.67	0.30	0.03
0.29	0.50	0.43	0.07
0.40	0.35	0.50	0.15
0.51	0.22	0.54	0.24
0.59	0.15	0.51	0.34
0.72	0.06	0.43	0.50
0.82	0.02	0.31	0.67
0.93	0.00	0.15	0.85
1.00	0.00	0.00	1.00

Figure AI.1. i. ^{6}Li NMR spectrum of a 50:50 mixture of [^{6}Li]**1** (**A**) and [^{6}Li]**7** (**B**) in 0.24 M TMEDA/toluene at -50 °C. **ii.** Plot of the relative integration versus the mole fraction of **7** (**B**) for a mixture of [^{6}Li]**1** (**A**) and [^{6}Li]**7** (**B**) $\phi_0 = 0.88$; $\phi_1 = 1.00$; $\phi_2 = 0.88$; RMS = 0.006. **iii.** Relative integrations for aggregates in a mixture of **1** (**A**) and **7** (**B**) at various mole fractions of **A** and **B.**

i.

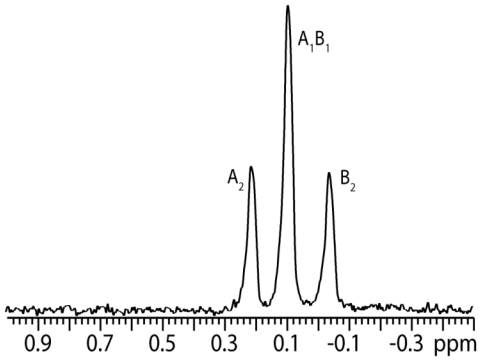

ii.

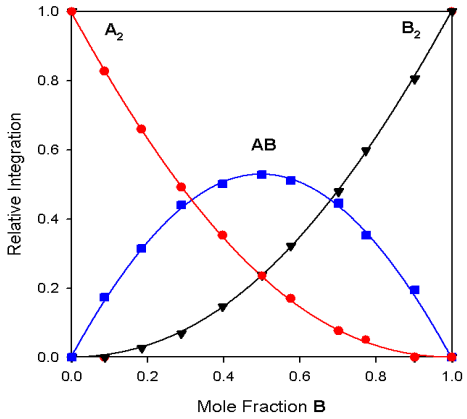

iii.

Calc. X_B	$\mathbf{A}_2$	$\mathbf{A}_1\mathbf{B}_1$	$\mathbf{B}_2$
0.00	1.00	0.00	0.00
0.09	0.81	0.19	0.00
0.18	0.63	0.35	0.01
0.29	0.44	0.50	0.06
0.40	0.29	0.59	0.11
0.50	0.18	0.63	0.20
0.58	0.11	0.59	0.31
0.70	0.09	0.40	0.51
0.77	0.02	0.36	0.62
0.90	0.00	0.19	0.81
1.00	0.00	0.00	1.00

Figure AI.2. i. ^{6}Li NMR spectrum of a 50:50 mixture of [^{6}Li]**1** (**A**) and [^{6}Li]**8** (**B**) in 0.24 M TMEDA/toluene at -90 °C. **ii.** Plot of the relative integration versus the mole fraction of **8** (**B**) for a mixture of [^{6}Li]**1** (**A**) and [^{6}Li]**8** (**B**) $\phi_0 = 0.89$; $\phi_1 = 1.00$; $\phi_2 = 0.89$; RMS = 0.01. **iii.** Relative integrations for aggregates in a mixture of **1** (**A**) and **8** (**B**) at various mole fractions of **A** and **B**.

i.

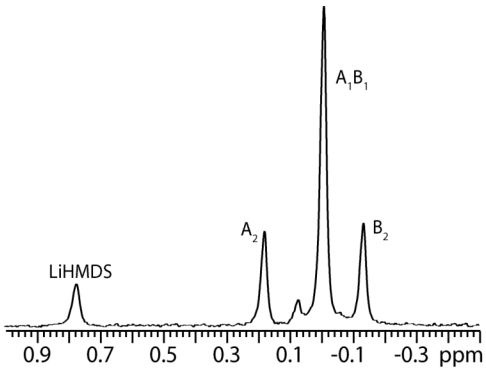

ii.

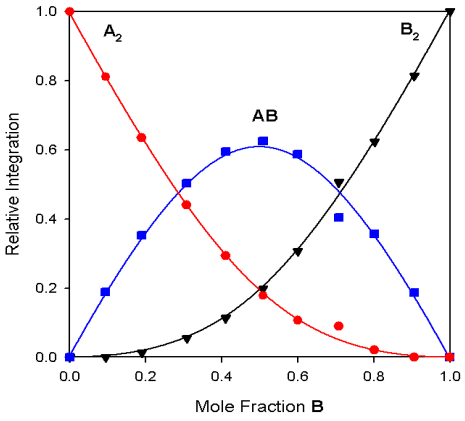

iii.

Calc. X_B	$\mathbf{A}_2$	$\mathbf{A}_1\mathbf{B}_1$	$\mathbf{B}_2$
0.00	1.00	0.00	0.00
0.10	0.81	0.19	0.00
0.19	0.63	0.35	0.01
0.31	0.44	0.50	0.06
0.41	0.29	0.59	0.11
0.51	0.18	0.63	0.20
0.60	0.11	0.59	0.31
0.71	0.09	0.40	0.51
0.80	0.02	0.36	0.62
0.91	0.00	0.19	0.81
1.00	0.00	0.00	1.00

Figure AI.3. i. ^{6}Li NMR spectrum of a 50:50 mixture of [^{6}Li]**1** (**A**) and [^{6}Li]**9** (**B**) in 0.24 M TMEDA/toluene at -90 °C. **ii.** Plot of the relative integration versus the mole fraction of **9** (**B**) for a mixture of [^{6}Li]**1** (**A**) and [^{6}Li]**9** (**B**) $\phi_0 = 0.64$; $\phi_1 = 1.00$; $\phi_2 = 0.64$; RMS = 0.02. **iii.** Relative integrations for aggregates in a mixture of **1** (**A**) and **9** (**B**) at various mole fractions of **A** and **B**.

i.

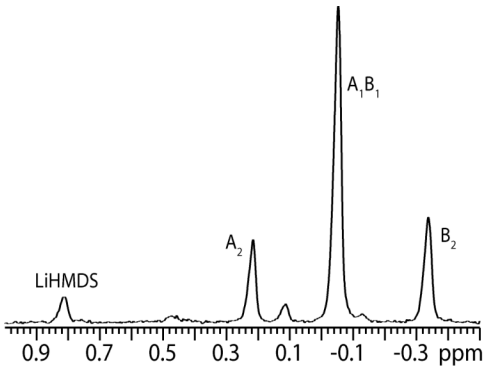

ii.

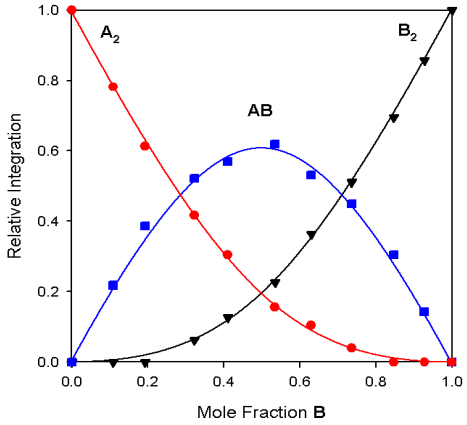

iii.

Calc. X_B	$\mathbf{A}_2$	$\mathbf{A}_1\mathbf{B}_1$	$\mathbf{B}_2$
0.00	1.00	0.00	0.00
0.11	0.78	0.22	0.00
0.19	0.61	0.39	0.00
0.32	0.42	0.52	0.06
0.41	0.30	0.57	0.13
0.54	0.16	0.62	0.23
0.63	0.10	0.53	0.36
0.74	0.04	0.45	0.51
0.85	0.00	0.31	0.70
0.93	0.00	0.14	0.86
1.00	0.00	0.00	1.00

Figure AI.4. i. ^{6}Li NMR spectrum of a 50:50 mixture of [^{6}Li]**1** (**A**) and [^{6}Li]**10** (**B**) in 0.24 M TMEDA/toluene at -90 °C. **ii.** Plot of the relative integration versus the mole fraction of **10** (**B**) for a mixture of [^{6}Li]**1** (**A**) and [^{6}Li]**10** (**B**) $\phi_0 =$ 0.64; $\phi_1 = 1.00$; $\phi_2 = 0.64$; RMS = 0.01. **iii.** Relative integrations for aggregates in a mixture of **1** (**A**) and **10** (**B**) at various mole fractions of **A** and **B**.

i.

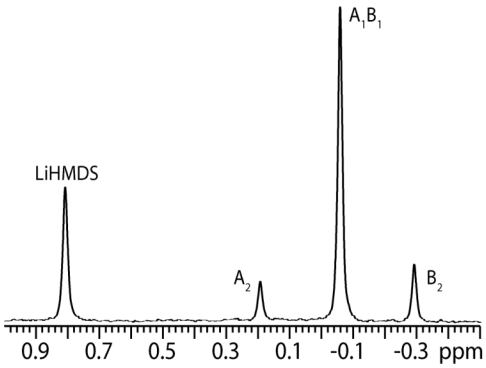

ii.

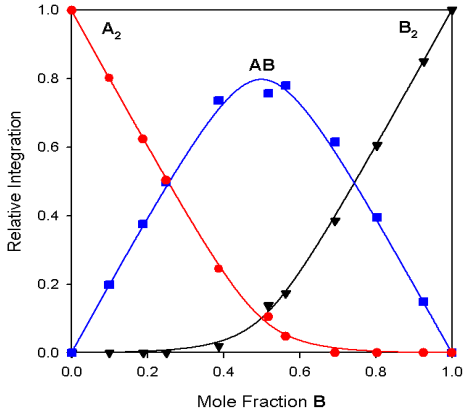

iii.

Calc. X_B	$\mathbf{A}_2$	$\mathbf{A}_1\mathbf{B}_1$	$\mathbf{B}_2$
0.00	1.00	0.00	0.00
0.10	0.80	0.20	0.00
0.19	0.62	0.38	0.00
0.25	0.50	0.50	0.00
0.39	0.25	0.74	0.02
0.52	0.11	0.76	0.14
0.56	0.05	0.78	0.17
0.69	0.00	0.62	0.39
0.80	0.00	0.40	0.61
0.93	0.00	0.15	0.85
1.00	0.00	0.00	1.00

Figure AI.5. i. ^{6}Li NMR spectrum of a 50:50 mixture of [^{6}Li]**1** (**A**) and [^{6}Li]**12** (**B**) in 0.24 M TMEDA/toluene at -90 °C. **ii.** Plot of the relative integration versus the mole fraction of **12** (**B**) for a mixture of [^{6}Li]**1** (**A**) and [^{6}Li]**12** (**B**) $\phi_0 =$ 0.76; $\phi_1 = 3.00$; $\phi_2 = 0.76$; RMS = 0.01. **iii.** Relative integrations for aggregates in a mixture of **1** (**A**) and **12** (**B**) at various mole fractions of **A** and **B**.

i.

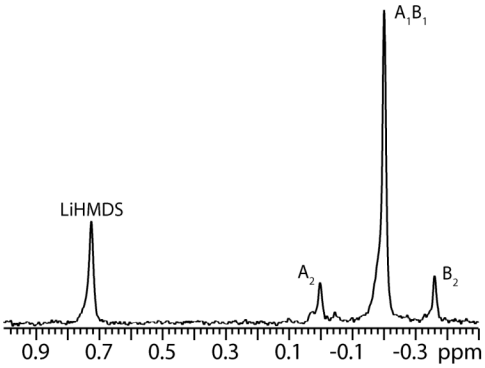

ii.

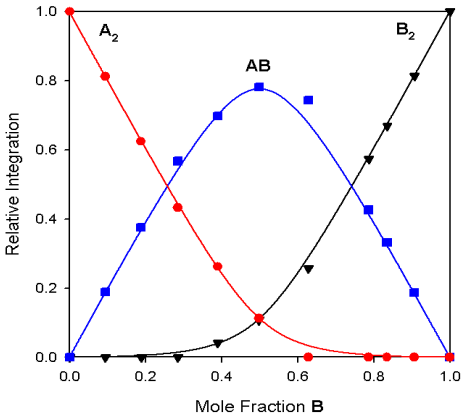

iii.

Calc. X_B	$\mathbf{A}_2$	$\mathbf{A}_1\mathbf{B}_1$	$\mathbf{B}_2$
0.00	1.00	0.00	0.00
0.09	0.81	0.19	0.00
0.19	0.62	0.38	0.00
0.28	0.43	0.57	0.00
0.39	0.26	0.70	0.04
0.50	0.11	0.78	0.11
0.63	0.00	0.74	0.26
0.79	0.00	0.43	0.57
0.84	0.00	0.33	0.67
0.91	0.00	0.19	0.81
1.00	0.00	0.00	1.00

Figure AI.6. i. ^{6}Li NMR spectrum of a 50:50 mixture of [^{6}Li]**11** (**A**) and [^{6}Li]**12** (**B**) in 0.24 M TMEDA/toluene at -90 °C. **ii.** Plot of the relative integration versus the mole fraction of **12** (**B**) for a mixture of [^{6}Li]**11** (**A**) and [^{6}Li]**12** (**B**) ϕ_0 = 0.87; ϕ_1 = 3.00; ϕ_2 = 0.87; RMS = 0.07. **iii.** Relative integrations for aggregates in a mixture of **11** (**A**) and **12** (**B**) at various mole fractions of **A** and **B**.

i.

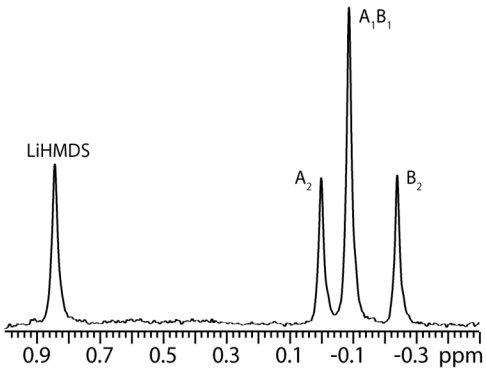

ii.

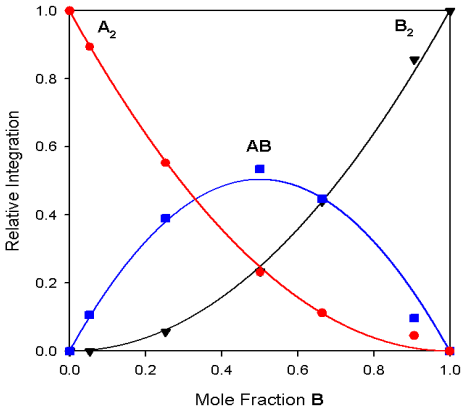

iii.

Calc. X_B	$\mathbf{A}_2$	$\mathbf{A}_1\mathbf{B}_1$	$\mathbf{B}_2$
0.00	1.00	0.00	0.00
0.05	0.89	0.11	0.00
0.25	0.55	0.39	0.06
0.50	0.23	0.54	0.23
0.66	0.11	0.45	0.44
0.91	0.05	0.10	0.86
1.00	0.00	0.00	1.00

Figure AI.7. i. ^{6}Li NMR spectrum of a 50:50 mixture of [^{6}Li]**8** (**A**) and [^{6}Li]**12** (**B**) in 0.24 M TMEDA/toluene at -90 °C. **ii.** Plot of the relative integration versus the mole fraction of **12** (**B**) for a mixture of [^{6}Li]**8** (**A**) and [^{6}Li]**12** (**B**) $\phi_0 = 0.93$; $\phi_1 = 1.00$; $\phi_2 = 0.93$; RMS = 0.02. **iii.** Relative integrations for aggregates in a mixture of **8** (**A**) and **12** (**B**) at various mole fractions of **A** and **B**.

i.

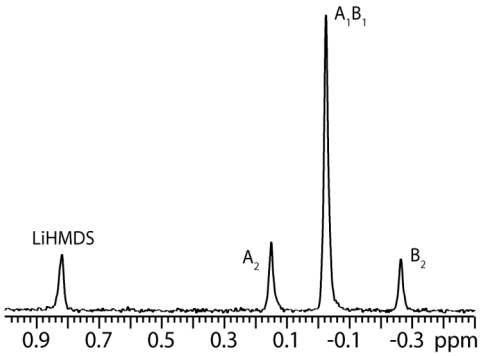

ii.

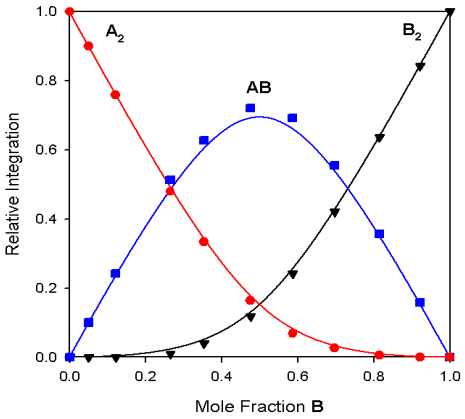

iii.

Calc. X_B	$\mathbf{A}_2$	$\mathbf{A}_1\mathbf{B}_1$	$\mathbf{B}_2$
0.00	1.00	0.00	0.00
0.05	0.90	0.10	0.00
0.12	0.76	0.24	0.00
0.27	0.48	0.51	0.01
0.35	0.33	0.63	0.04
0.48	0.16	0.72	0.12
0.59	0.07	0.69	0.24
0.70	0.03	0.55	0.42
0.82	0.01	0.36	0.64
0.92	0.00	0.16	0.84
1.00	0.00	0.00	1.00

Figure AI.8. i. ^{6}Li NMR spectrum of a 50:50 mixture of [^{6}Li]**7** (**A**) and [^{6}Li]**12** (**B**) in 0.24 M TMEDA/toluene at -90 °C. **ii.** Plot of the relative integration versus the mole fraction of **12** (**B**) for a mixture of [^{6}Li]**7** (**A**) and [^{6}Li]**12** (**B**) ϕ_0 = 1.32; ϕ_1 = 3.00; ϕ_2 = 1.32; RMS = 0.04. **iii.** Relative integrations for aggregates in a mixture of **7** (**A**) and **12** (**B**) at various mole fractions of **A** and **B**.

i.

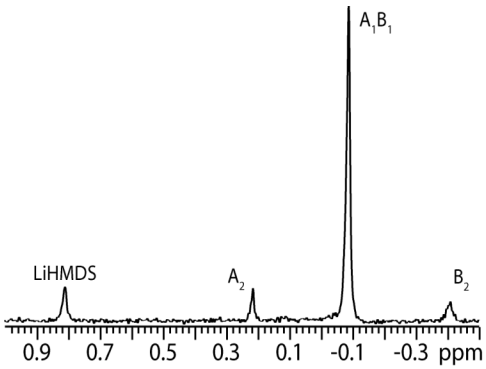

ii.

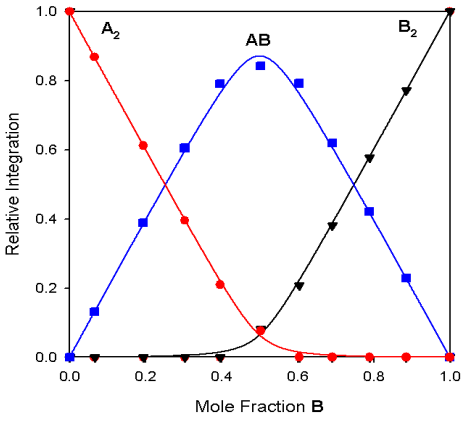

iii.

Calc. X_B	$\mathbf{A}_2$	$\mathbf{A}_1\mathbf{B}_1$	$\mathbf{B}_2$
0.00	1.00	0.00	0.00
0.07	0.87	0.13	0.00
0.20	0.61	0.39	0.00
0.30	0.40	0.61	0.00
0.40	0.21	0.79	0.00
0.50	0.08	0.84	0.08
0.60	0.00	0.79	0.21
0.69	0.00	0.62	0.38
0.79	0.00	0.42	0.58
0.89	0.00	0.23	0.77
1.00	0.00	0.00	1.00

Figure AI.9. i. ^{6}Li NMR spectrum of a 50:50 mixture of [^{6}Li]**1** (**A**) and [^{6}Li]**13** (**B**) in 0.24 M TMEDA/toluene at -90 °C. **ii.** Plot of the relative integration versus the mole fraction of **13** (**B**) for a mixture of [^{6}Li]**1** (**A**) and [^{6}Li]**13** (**B**) ϕ_0 = 0.74; ϕ_1 = 5.00; ϕ_2 = 0.74; RMS = 0.01. **iii.** Relative integrations for aggregates in a mixture of **1** (**A**) and **13** (**B**) at various mole fractions of **A** and **B**.

i.

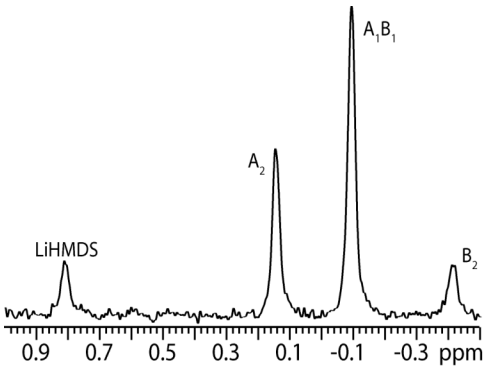

ii.

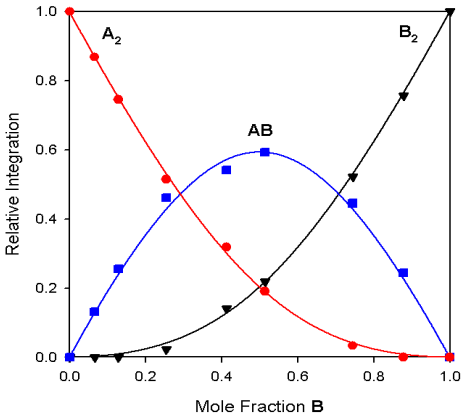

iii.

Calc. X_B	$\mathbf{A}_2$	$\mathbf{A}_1\mathbf{B}_1$	$\mathbf{B}_2$
0.00	1.00	0.00	0.00
0.07	0.87	0.13	0.00
0.13	0.75	0.26	0.00
0.25	0.52	0.46	0.02
0.41	0.32	0.54	0.14
0.51	0.19	0.59	0.22
0.75	0.03	0.45	0.52
0.88	0.00	0.24	0.76
1.00	0.00	0.00	1.00

Figure AI.10. i. ^{6}Li NMR spectrum of a 50:50 mixture of [^{6}Li]**7** (**A**) and [^{6}Li]**13** (**B**) in 0.24 M TMEDA/toluene at -90 °C. **ii.** Plot of the relative integration versus the mole fraction of **13** (**B**) for a mixture of [^{6}Li]**7** (**A**) and [^{6}Li]**13** (**B**) $\phi_0 =$ 0.69; $\phi_1 = 1.00$; $\phi_2 = 0.69$; RMS = 0.01. **iii.** Relative integrations for aggregates in a mixture of **7** (**A**) and **13** (**B**) at various mole fractions of **A** and **B**.

i.

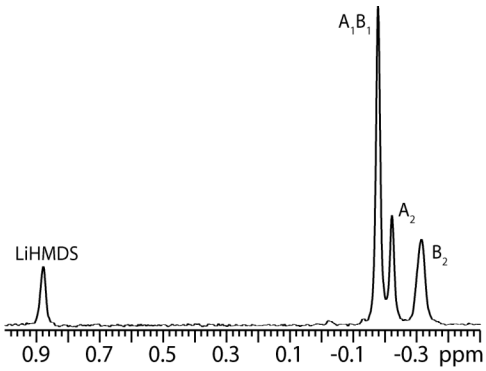

ii.

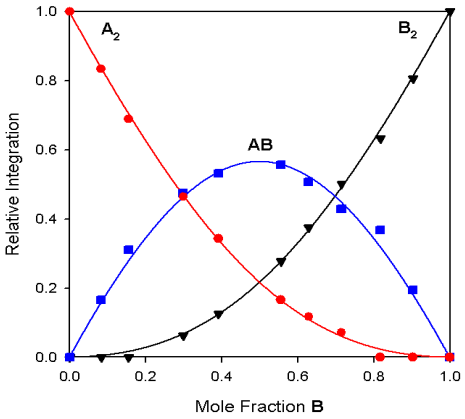

iii.

Calc. X_B	$\mathbf{A}_2$	$\mathbf{A}_1\mathbf{B}_1$	$\mathbf{B}_2$
0.00	1.00	0.00	0.00
0.08	0.83	0.17	0.00
0.16	0.69	0.31	0.00
0.30	0.46	0.47	0.06
0.39	0.34	0.53	0.13
0.56	0.17	0.56	0.28
0.63	0.12	0.51	0.38
0.72	0.07	0.43	0.50
0.82	0.00	0.37	0.63
0.90	0.00	0.19	0.81
1.00	0.00	0.00	1.00

Figure AI.11. i. ^{6}Li NMR spectrum of a 50:50 mixture of [^{6}Li]**12** (**A**) and [^{6}Li]**13** (**B**) in 0.24 M TMEDA/toluene at -90 °C. **ii.** Plot of the relative integration versus the mole fraction of **13** (**B**) for a mixture of [^{6}Li]**12** (**A**) and [^{6}Li]**13** (**B**) ϕ_0 = 0.77; ϕ_1 = 1.00; ϕ_2 = 0.77; RMS = 0.01. **iii.** Relative integrations for aggregates in a mixture of **12** (**A**) and **13** (**B**) at various mole fractions of **A** and **B**.

i.

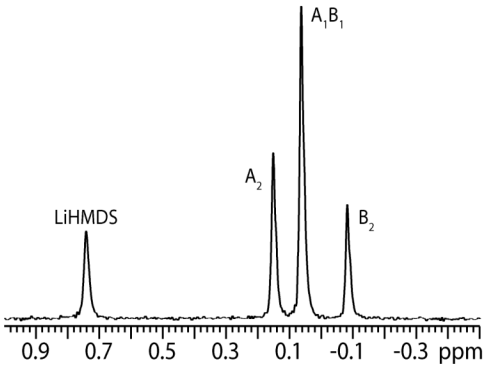

ii.

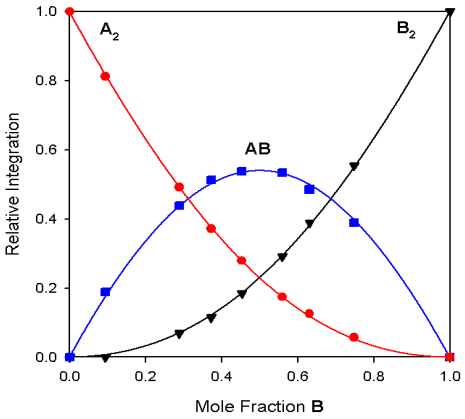

iii.

Calc. X_B	$\mathbf{A}_2$	$\mathbf{A}_1\mathbf{B}_1$	$\mathbf{B}_2$
0.00	1.00	0.00	0.00
0.09	0.81	0.19	0.00
0.29	0.49	0.44	0.07
0.37	0.37	0.51	0.12
0.45	0.28	0.54	0.18
0.56	0.17	0.53	0.29
0.63	0.13	0.49	0.39
0.75	0.06	0.39	0.55
1.00	0.00	0.00	1.00

Figure AI.12. i. ^{6}Li NMR spectrum of a 50:50 mixture of [^{6}Li]**1** (**A**) and [^{6}Li]**14** (**B**) in 0.24 M TMEDA/toluene at -90 °C. **ii.** Plot of the relative integration versus the mole fraction of **14** (**B**) for a mixture of [^{6}Li]**1** (**A**) and [^{6}Li]**14** (**B**) $\phi_0 = 0.85$; $\phi_1 = 1.00$; $\phi_2 = 0.85$; RMS = 0.01. **iii.** Relative integrations for aggregates in a mixture of **1** (**A**) and **14** (**B**) at various mole fractions of **A** and **B**.

i.

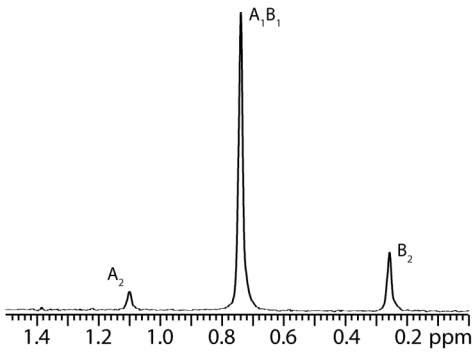

ii.

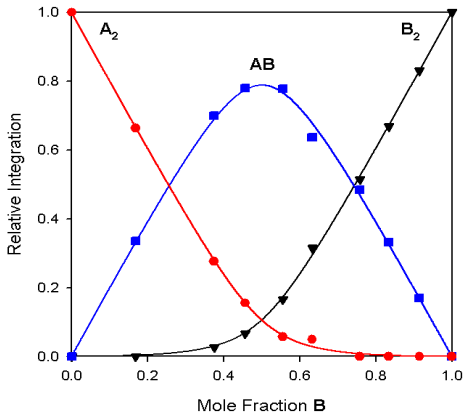

iii.

Calc. X_B	$\mathbf{A}_2$	$\mathbf{A}_1\mathbf{B}_1$	$\mathbf{B}_2$
0.00	1.00	0.00	0.00
0.17	0.66	0.34	0.00
0.38	0.28	0.70	0.03
0.46	0.16	0.78	0.07
0.56	0.06	0.78	0.17
0.63	0.05	0.64	0.32
0.76	0.00	0.49	0.52
0.83	0.00	0.33	0.67
0.92	0.00	0.17	0.83
1.00	0.00	0.00	1.00

Figure AI.13. i. ^{6}Li NMR spectrum of a 50:50 mixture of [^{6}Li]**15** (**A**) and [^{6}Li]**1** (**B**) in 0.24 M TMEDA/toluene at -78 °C. **ii.** Plot of the relative integration versus the mole fraction of **1** (**B**) for a mixture of [^{6}Li]**15** (**A**) and [^{6}Li]**1** (**B**) ϕ_0 = 0.81; ϕ_1 = 3.00; ϕ_2 = 0.81; RMS = 0.01. **iii.** Relative integrations for aggregates in a mixture of **15** (**A**) and **1** (**B**) at various mole fractions of **A** and **B**.

i.

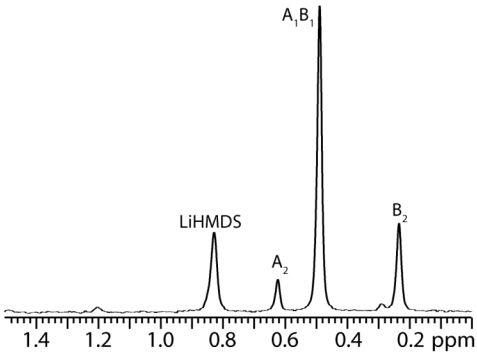

ii.

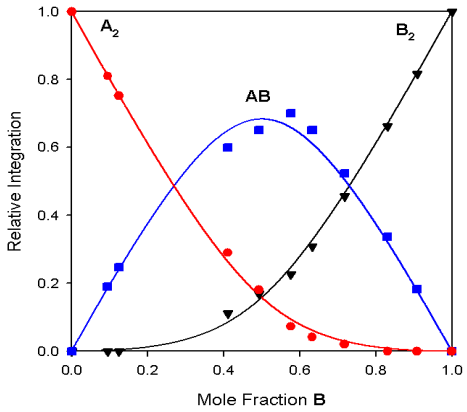

iii.

Calc. X_B	$\mathbf{A}_2$	$\mathbf{A}_1\mathbf{B}_1$	$\mathbf{B}_2$
0.00	1.00	0.00	0.00
0.10	0.81	0.19	0.00
0.12	0.75	0.25	0.00
0.41	0.29	0.60	0.11
0.49	0.18	0.65	0.17
0.58	0.07	0.70	0.23
0.63	0.04	0.65	0.31
0.72	0.02	0.52	0.46
0.83	0.00	0.34	0.66
0.91	0.00	0.18	0.82
1.00	0.00	0.00	1.00

Figure AI.14. i. ^{6}Li NMR spectrum of a 50:50 mixture of [^{6}Li]**16** (**A**) and [^{6}Li]**1** (**B**) in 0.24 M TMEDA/toluene at -90 °C. **ii.** Plot of the relative integration versus the mole fraction of **1** (**B**) for a mixture of [^{6}Li]**16** (**A**) and [^{6}Li]**1** (**B**) ϕ_0 = 1.34; ϕ_1 = 3.00; ϕ_2 = 1.34; RMS = 0.02. **iii.** Relative integrations for aggregates in a mixture of **16** (**A**) and **1** (**B**) at various mole fractions of **A** and **B**.

i.

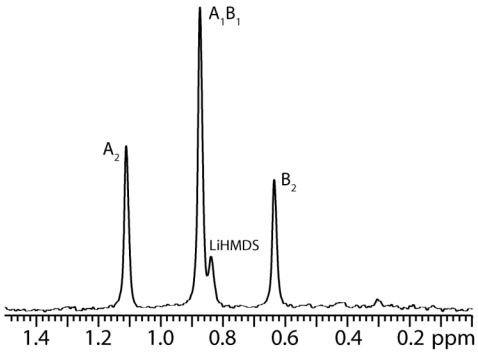

ii.

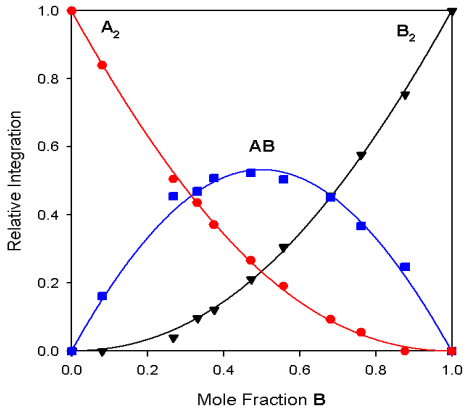

iii.

Calc. X_B	$\mathbf{A}_2$	$\mathbf{A}_1\mathbf{B}_1$	$\mathbf{B}_2$
0.00	1.00	0.00	0.00
0.08	0.84	0.16	0.00
0.27	0.51	0.46	0.04
0.33	0.44	0.47	0.10
0.38	0.37	0.51	0.12
0.47	0.27	0.52	0.21
0.56	0.19	0.50	0.31
0.68	0.09	0.45	0.46
0.76	0.06	0.37	0.58
0.88	0.00	0.25	0.75
1.00	0.00	0.00	1.00

Figure AI.15. i. ^{6}Li NMR spectrum of a 50:50 mixture of [^{6}Li]**15** (**A**) and [^{6}Li]**16** (**B**) in 0.24 M TMEDA/toluene at -78 °C. **ii.** Plot of the relative integration versus the mole fraction of **16** (**B**) for a mixture of [^{6}Li]**15** (**A**) and [^{6}Li]**16** (**B**) ϕ_0 = 0.88; ϕ_1 = 1.00; ϕ_2 = 0.88; RMS = 0.01. **iii.** Relative integrations for aggregates in a mixture of **15** (**A**) and **16** (**B**) at various mole fractions of **A** and **B**.

i.

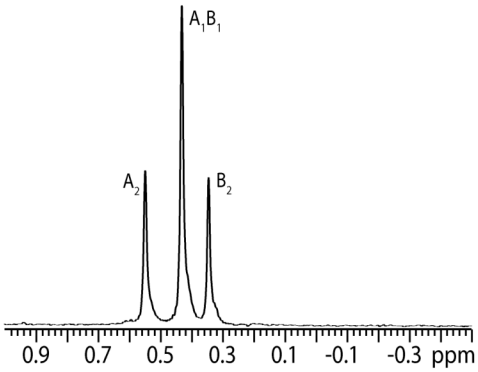

ii.

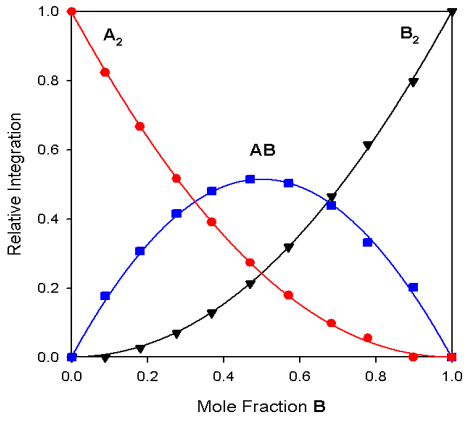

iii.

Calc. X_B	$\mathbf{A}_2$	$\mathbf{A}_1\mathbf{B}_1$	$\mathbf{B}_2$
0.00	1.00	0.00	0.00
0.09	0.82	0.18	0.00
0.18	0.67	0.31	0.03
0.28	0.52	0.42	0.07
0.37	0.39	0.48	0.13
0.47	0.27	0.51	0.21
0.57	0.18	0.50	0.32
0.68	0.10	0.44	0.46
0.78	0.06	0.33	0.61
0.90	0.00	0.20	0.80
1.00	0.00	0.00	1.00

Figure AI.16. i. ^{6}Li NMR spectrum of a 50:50 mixture of [^{6}Li]**1** (**A**) and [^{6}Li]**17** (**B**) in 3.0 M TMEDA/toluene/pentane and 0.11 M THF at -90 °C. **ii.** Plot of the relative integration versus the mole fraction of **17** (**B**) for a mixture of [^{6}Li]**1** (**A**) and [^{6}Li]**17** (**B**) $\phi_0 = 0.94$; $\phi_1 = 1.00$; $\phi_2 = 0.94$; RMS = 0.01. **iii.** Relative integrations for aggregates in a mixture of **1** (**A**) and **17** (**B**) at various mole fractions of **A** and **B**.

i.

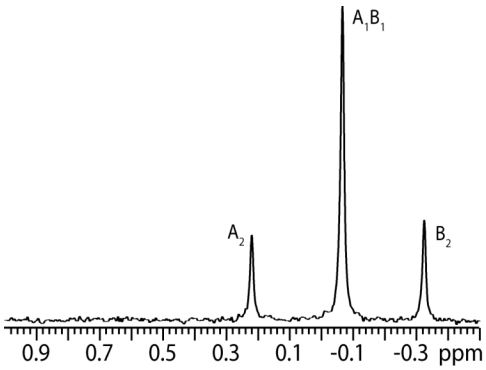

ii.

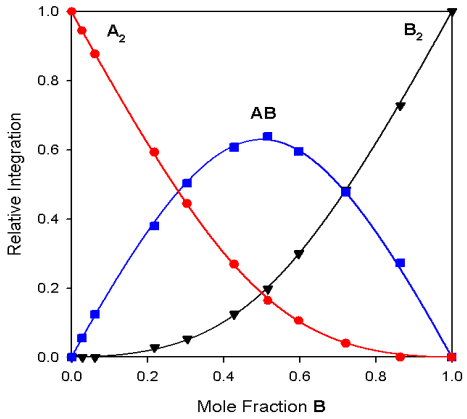

iii.

Calc. X_B	$\mathbf{A}_2$	$\mathbf{A}_1\mathbf{B}_1$	$\mathbf{B}_2$
0.00	1.00	0.00	0.00
0.03	0.94	0.06	0.00
0.06	0.88	0.12	0.00
0.22	0.59	0.38	0.03
0.30	0.44	0.50	0.05
0.43	0.27	0.61	0.12
0.52	0.16	0.64	0.20
0.60	0.11	0.60	0.30
0.72	0.04	0.48	0.48
0.86	0.00	0.27	0.73
1.00	0.00	0.00	1.00

Figure AI.17. i. ^{6}Li NMR spectrum of a 50:50 mixture of [^{6}Li]**1** (**A**) and [^{6}Li]**18** (**B**) in 0.24 M TMEDA/toluene at -90 °C. **ii.** Plot of the relative integration versus the mole fraction of **18** (**B**) for a mixture of [^{6}Li]**1** (**A**) and [^{6}Li]**18** (**B**) ϕ_0 = 0.59; ϕ_1 = 1.00; ϕ_2 = 0.59; RMS = 0.005. **iii.** Relative integrations for aggregates in a mixture of **1** (**A**) and **18** (**B**) at various mole fractions of **A** and **B**.

i.

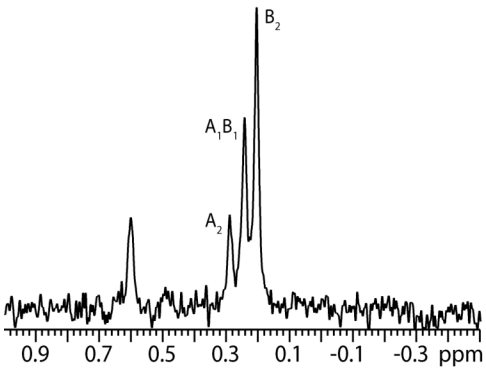

ii.

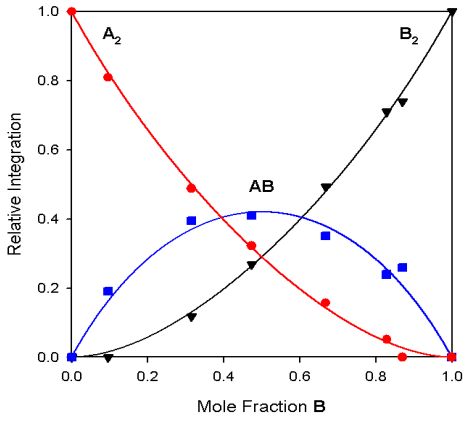

iii.

Calc. X_B	$\mathbf{A}_2$	$\mathbf{A}_1\mathbf{B}_1$	$\mathbf{B}_2$
0.00	1.00	0.00	0.00
0.10	0.81	0.19	0.00
0.32	0.49	0.40	0.12
0.47	0.32	0.41	0.27
0.67	0.16	0.35	0.49
0.83	0.05	0.24	0.71
0.87	0.00	0.26	0.74
1.00	0.00	0.00	1.00

Figure AI.18. i. ^{6}Li NMR spectrum of a 50:50 mixture of [^{6}Li]**19** (**A**) and [^{6}Li]**1** (**B**) in 0.24 M TMEDA/toluene at -90 °C. **ii.** Plot of the relative integration versus the mole fraction of **1** (**B**) for a mixture of [^{6}Li]**19** (**A**) and [^{6}Li]**1** (**B**) ϕ_0 = 1.38; ϕ_1 = 1.00; ϕ_2 = 1.38; RMS = 0.02. **iii.** Relative integrations for aggregates in a mixture of **19** (**A**) and **1** (**B**) at various mole fractions of **A** and **B**.

i.

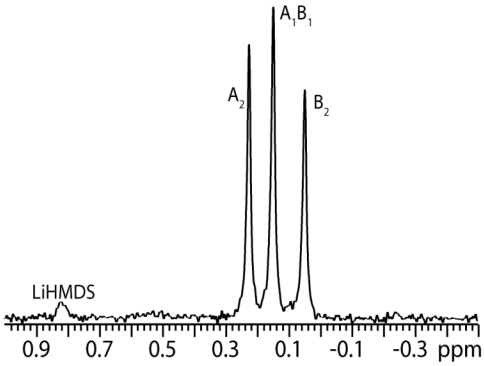

ii.

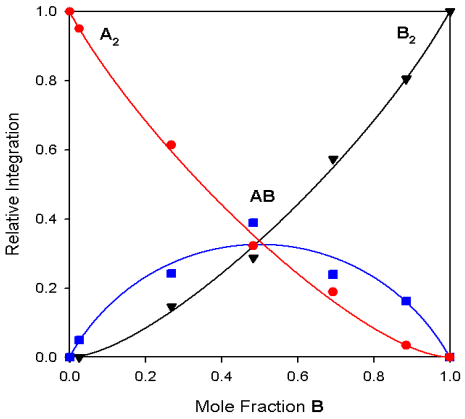

iii.

Calc. X_B	$\mathbf{A}_2$	$\mathbf{A}_1\mathbf{B}_1$	$\mathbf{B}_2$
0.00	1.00	0.00	0.00
0.03	0.95	0.05	0.00
0.27	0.61	0.24	0.15
0.48	0.32	0.39	0.29
0.69	0.19	0.24	0.57
0.89	0.03	0.16	0.81
1.00	0.00	0.00	1.00

Figure AI.19. i. ^{6}Li NMR spectrum of a 50:50 mixture of [^{6}Li]**1** (**A**) and [^{6}Li]**20** (**B**) in 0.24 M TMEDA/toluene at -90 °C. **ii.** Plot of the relative integration versus the mole fraction of **20** (**B**) for a mixture of [^{6}Li]**1** (**A**) and [^{6}Li]**20** (**B**) ϕ_0 = 0.83; ϕ_1 = 1.00; ϕ_2 = 0.83; RMS = 0.03. **iii.** Relative integrations for aggregates in a mixture of **1** (**A**) and **20** (**B**) at various mole fractions of **A** and **B**.

i.

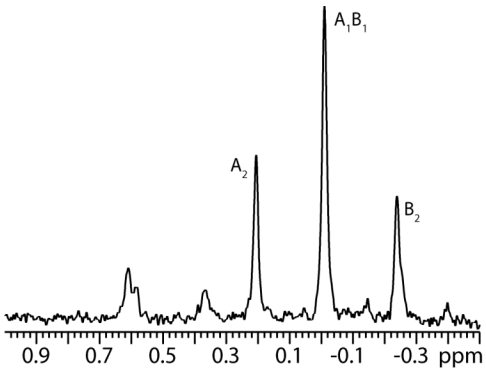

ii.

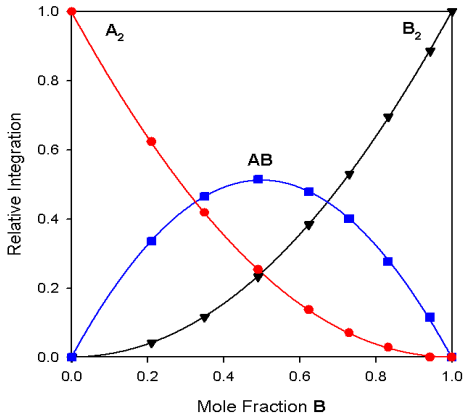

iii.

Calc. X_B	$\mathbf{A}_2$	$\mathbf{A}_1\mathbf{B}_1$	$\mathbf{B}_2$
0.00	1.00	0.00	0.00
0.00	1.00	0.00	0.00
0.00	1.00	0.00	0.00
0.21	0.62	0.34	0.04
0.35	0.42	0.47	0.12
0.49	0.25	0.51	0.23
0.62	0.14	0.48	0.38
0.73	0.07	0.40	0.53
0.83	0.03	0.28	0.70
0.94	0.00	0.12	0.89
1.00	0.00	0.00	1.00

Figure AI.20. i. ^{6}Li NMR spectrum of a 50:50 mixture of [^{6}Li]**1** (**A**) and [^{6}Li]**21** (**B**) in 0.24 M TMEDA/toluene at -90 °C. **ii.** Plot of the relative integration versus the mole fraction of **21** (**B**) for a mixture of [^{6}Li]**1** (**A**) and [^{6}Li]**21** (**B**) ϕ_0= 0.95; ϕ_1 = 1.00; ϕ_2 = 0.95; RMS = 0.002. **iii.** Relative integrations for aggregates in a mixture of **1** (**A**) and **21** (**B**) at various mole fractions of **A** and **B**.

i.

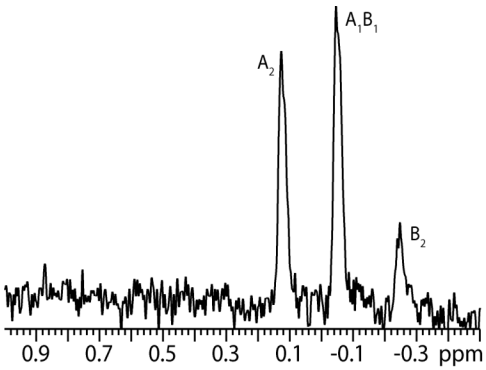

ii.

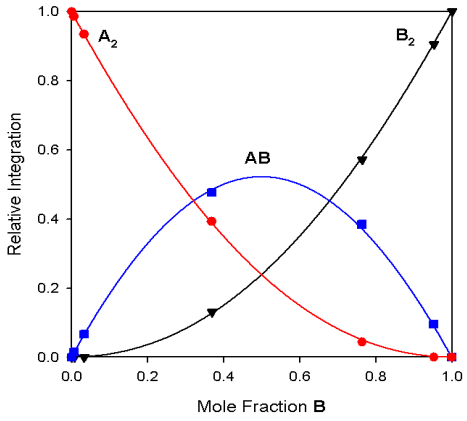

iii.

Calc. X_B	$\mathbf{A}_2$	$\mathbf{A}_1\mathbf{B}_1$	$\mathbf{B}_2$
0.00	1.00	0.00	0.00
0.01	0.99	0.02	0.00
0.03	0.93	0.07	0.00
0.37	0.39	0.48	0.13
0.76	0.04	0.38	0.57
0.95	0.00	0.10	0.91
1.00	0.00	0.00	1.00

Figure AI.21. i. ^{6}Li NMR spectrum of a 50:50 mixture of [^{6}Li]**7** (**A**) and [^{6}Li]**21** (**B**) in 0.24 M TMEDA/toluene at -90 °C. **ii.** Plot of the relative integration versus the mole fraction of **21** (**B**) for a mixture of [^{6}Li]**7** (**A**) and [^{6}Li]**21** (**B**) ϕ_0 = 0.92; ϕ_1 = 1.00; ϕ_2 = 0.92; RMS = 0.004. **iii.** Relative integrations for aggregates in a mixture of **7** (**A**) and **21** (**B**) at various mole fractions of **A** and **B**.

i.

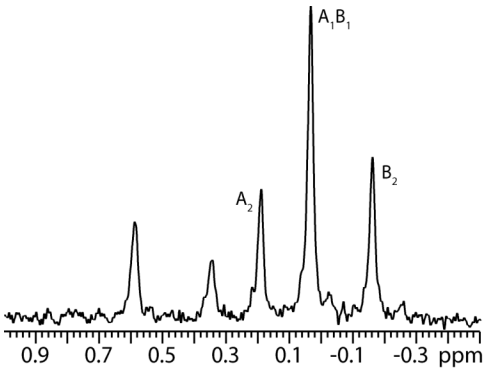

ii.

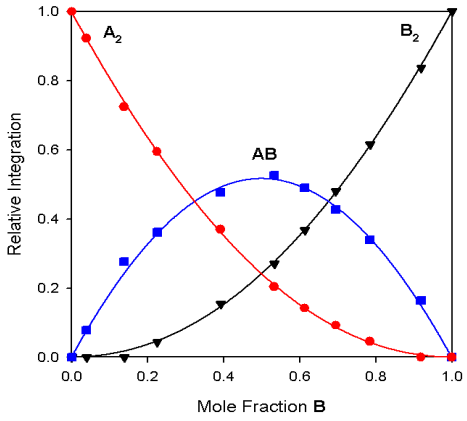

iii.

Calc. X_B	$\mathbf{A}_2$	$\mathbf{A}_1\mathbf{B}_1$	$\mathbf{B}_2$
0.00	1.00	0.00	0.00
0.04	0.92	0.08	0.00
0.14	0.72	0.28	0.00
0.23	0.60	0.36	0.04
0.39	0.37	0.48	0.15
0.53	0.20	0.53	0.27
0.61	0.14	0.49	0.37
0.69	0.09	0.43	0.48
0.79	0.05	0.34	0.62
0.92	0.00	0.16	0.84
1.00	0.00	0.00	1.00

Figure AI.22. i. ^{6}Li NMR spectrum of a 50:50 mixture of [^{6}Li]**1** (**A**) and [^{6}Li]**22** (**B**) in 0.24 M TMEDA/toluene at -90 °C. **ii.** Plot of the relative integration versus the mole fraction of **22** (**B**) for a mixture of [^{6}Li]**1** (**A**) and [^{6}Li]**22** (**B**) $\phi_0 = 0.94$; $\phi_1 = 1.00$; $\phi_2 = 0.94$; RMS = 0.01. **iii.** Relative integrations for aggregates in a mixture of **1** (**A**) and **22** (**B**) at various mole fractions of **A** and **B**.

i.

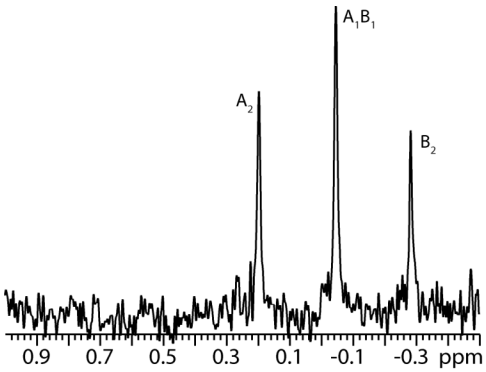

ii.

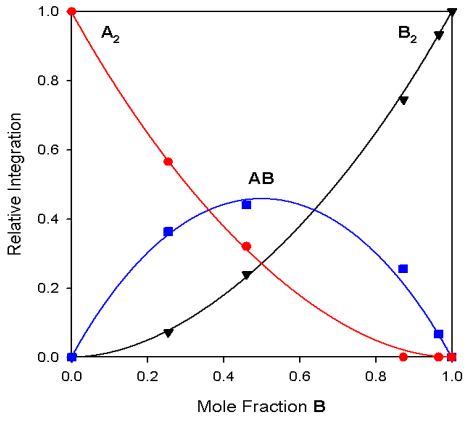

iii.

Calc. X_B	$\mathbf{A}_2$	$\mathbf{A}_1\mathbf{B}_1$	$\mathbf{B}_2$
0.00	1.00	0.00	0.00
0.25	0.57	0.36	0.07
0.46	0.32	0.44	0.24
0.87	0.00	0.26	0.75
0.97	0.00	0.07	0.93
1.00	0.00	0.00	1.00

Figure AI.23. i. ^{6}Li NMR spectrum of a 50:50 mixture of [^{6}Li]**1** (**A**) and [^{6}Li]**23** (**B**) in 0.24 M TMEDA/toluene at -90 °C. **ii.** Plot of the relative integration versus the mole fraction of **23** (**B**) for a mixture of [^{6}Li]**1** (**A**) and [^{6}Li]**23** (**B**) ϕ_0 = 1.18; ϕ_1 = 1.00; ϕ_2 = 1.18; RMS = 0.01. **iii.** Relative integrations for aggregates in a mixture of **1** (**A**) and **23** (**B**) at various mole fractions of **A** and **B**.

i.

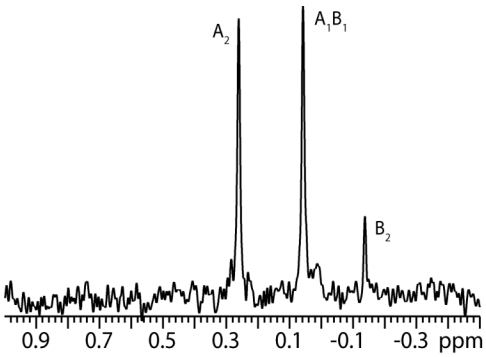

ii.

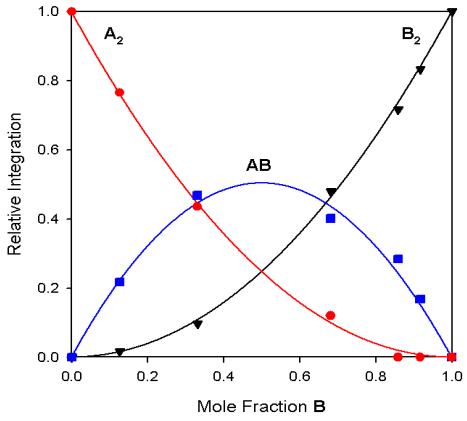

iii.

Calc. X_B	$\mathbf{A}_2$	$\mathbf{A}_1\mathbf{B}_1$	$\mathbf{B}_2$
0.00	1.00	0.00	0.00
0.13	0.77	0.22	0.02
0.33	0.44	0.47	0.10
0.68	0.12	0.40	0.48
0.86	0.00	0.28	0.72
0.92	0.00	0.17	0.83
1.00	0.00	0.00	1.00

Figure AI.24. i. ^{6}Li NMR spectrum of a 50:50 mixture of [^{6}Li]**1** (**A**) and [^{6}Li]**24** (**B**) in 0.24 M TMEDA/toluene at -60 °C. **ii.** Plot of the relative integration versus the mole fraction of **24** (**B**) for a mixture of [^{6}Li]**1** (**A**) and [^{6}Li]**24** (**B**) $\phi_0 = 0.98$; $\phi_1 = 1.00$; $\phi_2 = 0.98$; RMS = 0.01. **iii.** Relative integrations for aggregates in a mixture of **1** (**A**) and **24** (**B**) at various mole fractions of **A** and **B**.

i.

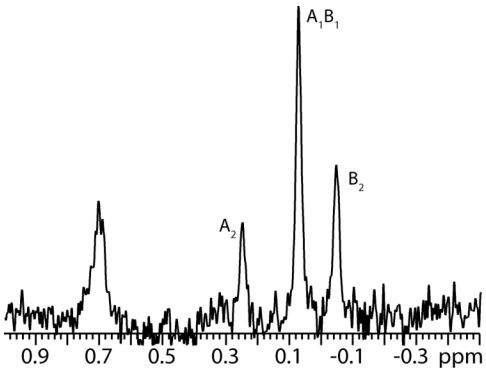

ii.

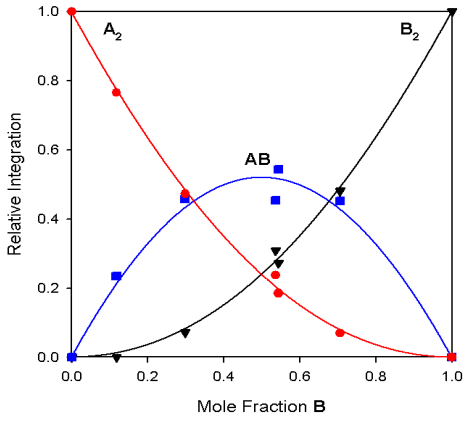

iii.

Calc. X_B	$\mathbf{A}_2$	$\mathbf{A}_1\mathbf{B}_1$	$\mathbf{B}_2$
0.00	1.00	0.00	0.00
0.12	0.77	0.24	0.00
0.30	0.47	0.46	0.07
0.54	0.24	0.45	0.31
0.54	0.19	0.54	0.27
0.71	0.07	0.45	0.48
1.00	0.00	0.00	1.00

Figure AI.25. i. ^{6}Li NMR spectrum of a 50:50 mixture of [^{6}Li]**1** (**A**) and [^{6}Li]**25** (**B**) in 0.24 M TMEDA/toluene at -70 °C. **ii.** Plot of the relative integration versus the mole fraction of **25** (**B**) for a mixture of [^{6}Li]**1** (**A**) and [^{6}Li]**25** (**B**) $\phi_0 = 0.92$; $\phi_1 = 1.00$; $\phi_2 = 0.92$; RMS = 0.02. **iii.** Relative integrations for aggregates in a mixture of **1** (**A**) and **25** (**B**) at various mole fractions of **A** and **B**.

i.

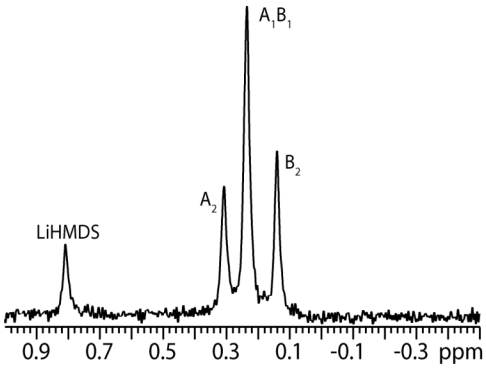

ii.

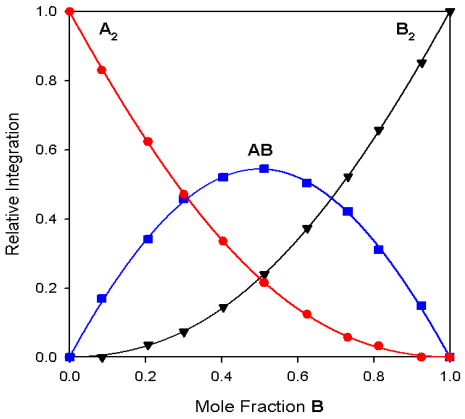

iii.

Calc. X_B	$\mathbf{A}_2$	$\mathbf{A}_1\mathbf{B}_1$	$\mathbf{B}_2$
0.00	1.00	0.00	0.00
0.09	0.83	0.15	0.00
0.21	0.62	0.31	0.04
0.30	0.47	0.42	0.07
0.40	0.34	0.50	0.14
0.51	0.22	0.55	0.24
0.63	0.12	0.52	0.37
0.73	0.06	0.46	0.52
0.81	0.03	0.34	0.66
0.93	0.00	0.17	0.85
1.00	0.00	0.00	1.00

Figure AI.26. i. ^{6}Li NMR spectrum of a 50:50 mixture of [^{6}Li]**26** (**A**) and [^{6}Li]**7** (**B**) in 0.24 M TMEDA/toluene at -90 °C. **ii.** Plot of the relative integration versus the mole fraction of **7** (**B**) for a mixture of [^{6}Li]**26** (**A**) and [^{6}Li]**7** (**B**) $\phi_0 = 0.84$; $\phi_1 = 1.00$; $\phi_2 = 0.84$; RMS = 0.004. **iii.** Relative integrations for aggregates in a mixture of **26** (**A**) and **7** (**B**) at various mole fractions of **A** and **B**.

i.

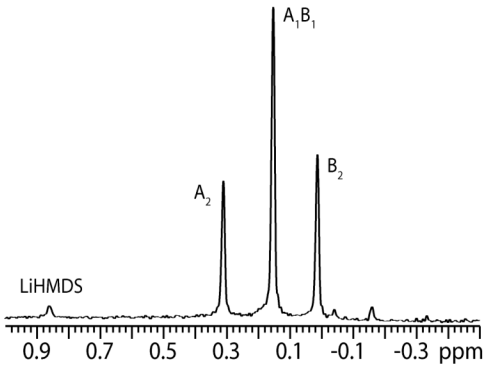

ii.

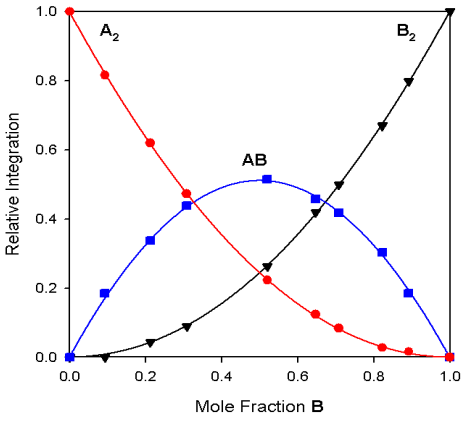

iii.

Calc. X_B	$\mathbf{A}_2$	$\mathbf{A}_1\mathbf{B}_1$	$\mathbf{B}_2$
0.00	1.00	0.00	0.00
0.09	0.82	0.19	0.00
0.21	0.62	0.34	0.04
0.31	0.47	0.44	0.09
0.52	0.22	0.51	0.26
0.65	0.12	0.46	0.42
0.71	0.08	0.42	0.50
0.82	0.03	0.30	0.67
0.89	0.02	0.19	0.80
1.00	0.00	0.00	1.00

Figure AI.27. i. ^{6}Li NMR spectrum of a 50:50 mixture of [^{6}Li]**26** (**A**) and [^{6}Li]**27** (**B**) in 0.24 M TMEDA/toluene at -90 °C. **ii.** Plot of the relative integration versus the mole fraction of **27** (**B**) for a mixture of [^{6}Li]**26** (**A**) and [^{6}Li]**27** (**B**) $\phi_0 = 0.96$; $\phi_1 = 1.00$; $\phi_2 = 0.96$; RMS = 0.01. **iii.** Relative integrations for aggregates in a mixture of **26** (**A**) and **27** (**B**) at various mole fractions of **A** and **B**.

i.

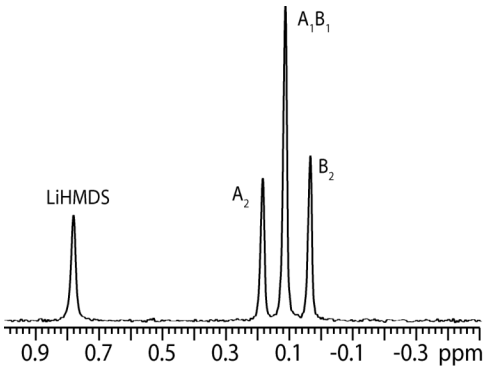

ii.

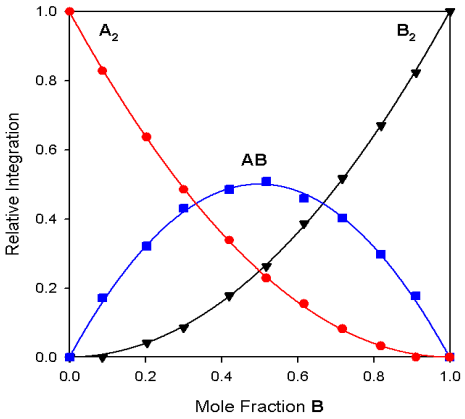

iii.

Calc. X_B	$\mathbf{A}_2$	$\mathbf{A}_1\mathbf{B}_1$	$\mathbf{B}_2$
0.00	1.00	0.00	0.00
0.09	0.83	0.17	0.00
0.20	0.64	0.32	0.04
0.30	0.49	0.43	0.09
0.42	0.34	0.49	0.18
0.52	0.23	0.51	0.26
0.62	0.15	0.46	0.39
0.72	0.08	0.40	0.52
0.82	0.03	0.30	0.67
0.91	0.00	0.18	0.82
1.00	0.00	0.00	1.00

Figure AI.28. i. ^{6}Li NMR spectrum of a 50:50 mixture of [^{6}Li]**1** (**A**) and [^{6}Li]**28** (**B**) in 0.24 M TMEDA/toluene at -90 °C. **ii.** Plot of the relative integration versus the mole fraction of **28** (**B**) for a mixture of [^{6}Li]**1** (**A**) and [^{6}Li]**28** (**B**) ϕ_0 = 1.00; ϕ_1 = 1.00; ϕ_2 = 1.00; RMS = 0.01. **iii.** Relative integrations for aggregates in a mixture of **1** (**A**) and **28** (**B**) at various mole fractions of **A** and **B**.

i.

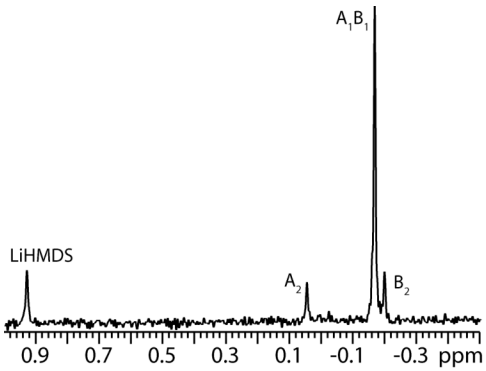

ii.

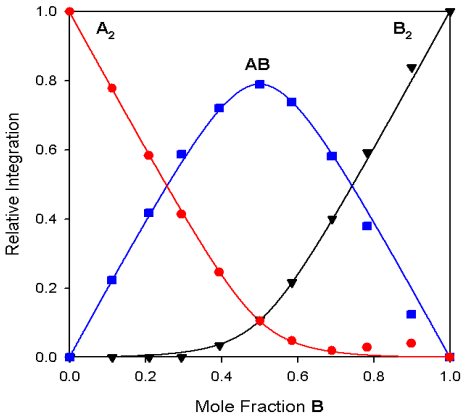

iii.

Calc. X_B	$\mathbf{A}_2$	$\mathbf{A}_1\mathbf{B}_1$	$\mathbf{B}_2$
0.00	1.00	0.00	0.00
0.11	0.78	0.22	0.00
0.21	0.58	0.42	0.00
0.29	0.41	0.59	0.00
0.39	0.25	0.72	0.03
0.50	0.11	0.79	0.11
0.59	0.05	0.74	0.22
0.69	0.02	0.58	0.40
0.78	0.03	0.38	0.59
0.90	0.04	0.12	0.84
1.00	0.00	0.00	1.00

Figure AI.29. i. ^{6}Li NMR spectrum of a 50:50 mixture of [^{6}Li]**28** (**A**) and [^{6}Li]**12** (**B**) in 0.24 M TMEDA/toluene at -50 °C. **ii.** Plot of the relative integration versus the mole fraction of **12** (**B**) for a mixture of [^{6}Li]**28** (**A**) and [^{6}Li]**12** (**B**) $\phi_0 = 0.80$; $\phi_1 = 3.00$; $\phi_2 = 0.80$; RMS = 0.02. **iii.** Relative integrations for aggregates in a mixture of **28** (**A**) and **12** (**B**) at various mole fractions of **A** and **B**.

i.

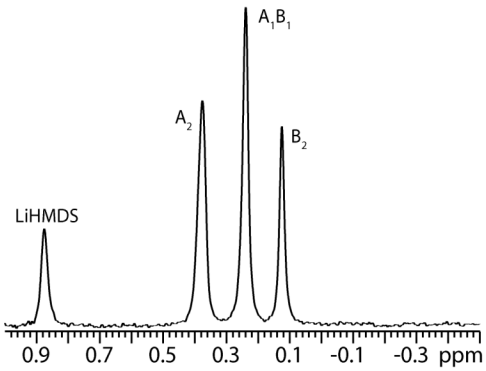

ii.

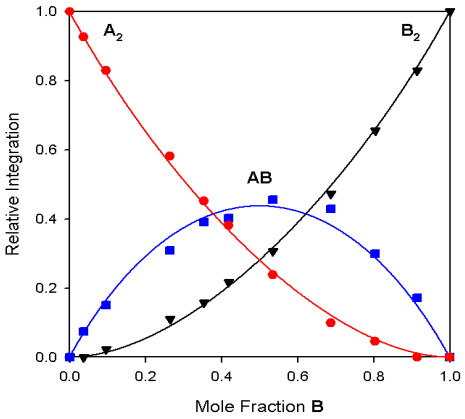

iii.

Calc. X_B	$\mathbf{A}_2$	$\mathbf{A}_1\mathbf{B}_1$	$\mathbf{B}_2$
0.00	1.00	0.00	0.00
0.04	0.93	0.07	0.00
0.10	0.83	0.15	0.02
0.26	0.58	0.31	0.11
0.35	0.45	0.39	0.16
0.42	0.38	0.40	0.22
0.53	0.24	0.46	0.31
0.69	0.10	0.43	0.47
0.80	0.05	0.30	0.66
0.91	0.00	0.17	0.83
1.00	0.00	0.00	1.00

Figure AI.30. i. ^{6}Li NMR spectrum of a 50:50 mixture of [^{6}Li]**26** (**A**) and [^{6}Li]**28** (**B**) in 0.24 M TMEDA/toluene at -90 °C. **ii.** Plot of the relative integration versus the mole fraction of **28** (**B**) for a mixture of [^{6}Li]**26** (**A**) and [^{6}Li]**28** (**B**) ϕ_0 = 1.29; ϕ_1 = 1.00; ϕ_2 = 1.29; RMS = 0.02. **iii.** Relative integrations for aggregates in a mixture of **26** (**A**) and **28** (**B**) at various mole fractions of **A** and **B**.

i.

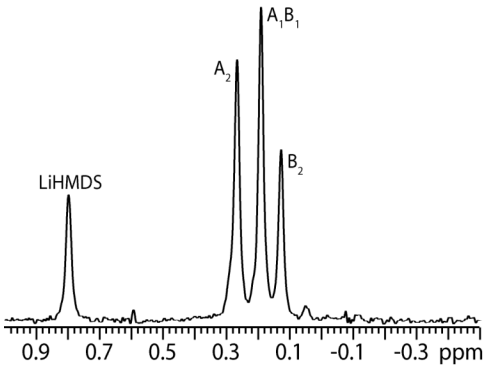

ii.

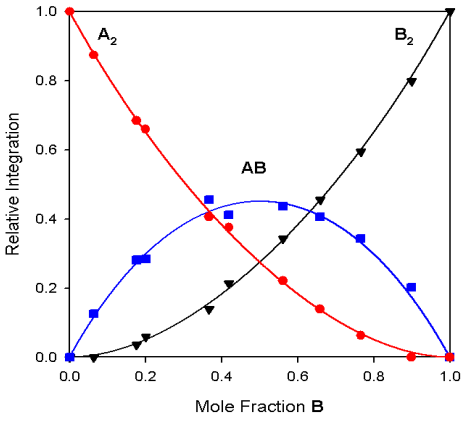

iii.

Calc. X_B	$\mathbf{A}_2$	$\mathbf{A}_1\mathbf{B}_1$	$\mathbf{B}_2$
0.00	1.00	0.00	0.00
0.06	0.87	0.13	0.00
0.18	0.68	0.28	0.04
0.20	0.66	0.28	0.06
0.37	0.41	0.46	0.14
0.42	0.38	0.41	0.21
0.56	0.22	0.44	0.34
0.66	0.14	0.41	0.46
0.77	0.06	0.34	0.60
0.60	0.00	0.20	0.80
1.00	0.00	0.00	1.00

Figure AI.31. i. ^{6}Li NMR spectrum of a 50:50 mixture of [^{6}Li]**30** (**A**) and [^{6}Li]**7** (**B**) in 0.24 M TMEDA/toluene at -90 °C. **ii.** Plot of the relative integration versus the mole fraction of **7** (**B**) for a mixture of [^{6}Li]**30** (**A**) and [^{6}Li]**7** (**B**) ϕ_0 = 1.22; ϕ_1 = 1.00; ϕ_2 = 1.22; RMS = 0.01. **iii.** Relative integrations for aggregates in a mixture of **30** (**A**) and **7** (**B**) at various mole fractions of **A** and **B**.

i.

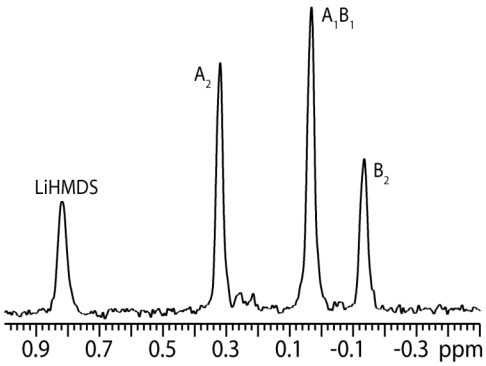

ii.

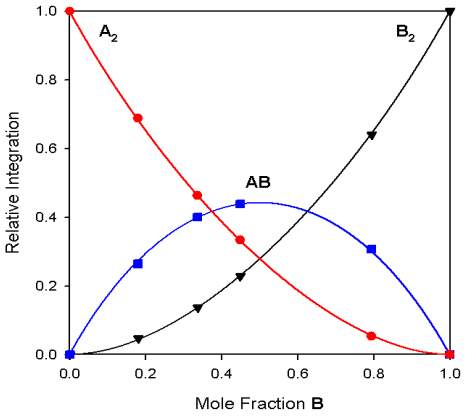

iii.

Calc. X_B	$\mathbf{A}_2$	$\mathbf{A}_1\mathbf{B}_1$	$\mathbf{B}_2$
0.00	1.00	0.00	0.00
0.18	0.69	0.31	0.05
0.34	0.46	0.44	0.14
0.45	0.33	0.40	0.23
0.79	0.05	0.26	0.64
1.00	0.00	0.00	1.00

Figure AI.32. i. ^{6}Li NMR spectrum of a 50:50 mixture of [^{6}Li]**29** (**A**) and [^{6}Li]**31** (**B**) in 0.24 M TMEDA/toluene at -90 °C. **ii.** Plot of the relative integration versus the mole fraction of **31** (**B**) for a mixture of [^{6}Li]**29** (**A**) and [^{6}Li]**31** (**B**) ϕ_0 = 1.26; ϕ_1 = 1.00; ϕ_2 = 1.26; RMS = 0.003. **iii.** Relative integrations for aggregates in a mixture of **29** (**A**) and **31** (**B**) at various mole fractions of **A** and **B**.

i.

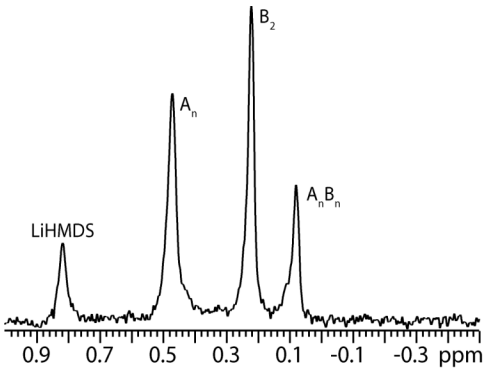

ii.

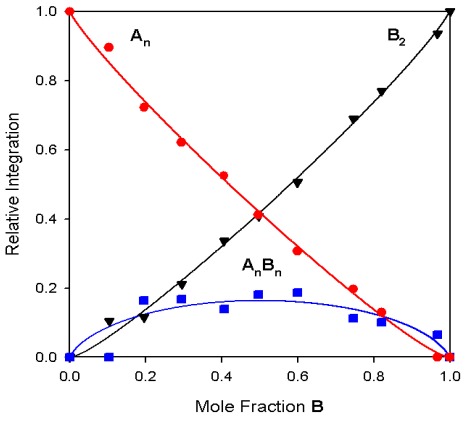

iii.

Calc. X_B	$\mathbf{A}_n$	$\mathbf{A}_n\mathbf{B}_n$	$\mathbf{B}_2$
0.00	1.00	0.00	0.00
0.10	0.90	0.00	0.10
0.20	0.72	0.16	0.12
0.30	0.62	0.17	0.21
0.41	0.53	0.14	0.34
0.50	0.41	0.18	0.41
0.60	0.31	0.19	0.51
0.75	0.20	0.11	0.69
0.82	0.13	0.10	0.77
0.98	0.00	0.07	0.94
1.00	0.00	0.00	1.00

Figure AI.33. i. ^{6}Li NMR spectrum of a 50:50 mixture of [^{6}Li]**34** (**A**) and [^{6}Li]**1** (**B**) in 0.24 M TMEDA/toluene at -90 °C. **ii.** Plot of the relative integration versus the mole fraction of **1** (**B**) for a mixture of [^{6}Li]**34** (**A**) and [^{6}Li]**1** (**B**) $\phi_0 = 5.11$; $\phi_1 = 1.00$; $\phi_2 = 5.11$; RMS = 0.02. **iii.** Relative integrations for aggregates in a mixture of **34** (**A**) and **1** (**B**) at various mole fractions of **A** and **B**.

i.

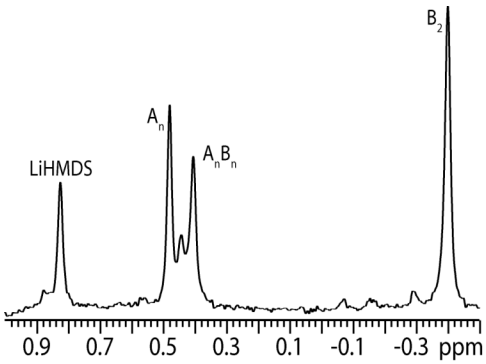

ii.

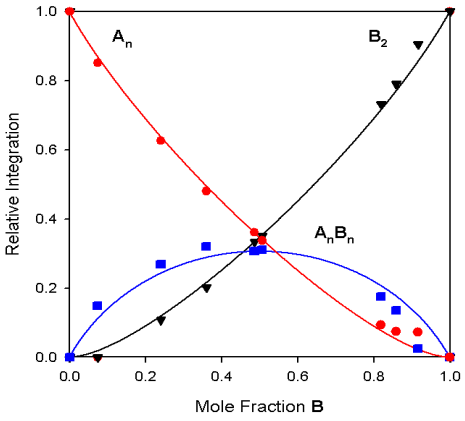

iii.

Calc. X_B	$\mathbf{A}_n$	$\mathbf{A}_n\mathbf{B}_n$	$\mathbf{B}_2$
0.00	1.00	0.00	0.00
0.07	0.85	0.15	0.00
0.24	0.63	0.27	0.11
0.36	0.48	0.32	0.20
0.49	0.36	0.31	0.33
0.51	0.34	0.31	0.35
0.82	0.09	0.18	0.73
0.86	0.07	0.14	0.79
0.92	0.07	0.02	0.91
1.00	0.00	0.00	1.00
1.00	0.00	0.00	1.00

Figure AI.34. i. ^{6}Li NMR spectrum of a 50:50 mixture of [^{6}Li]**34** (**A**) and [^{6}Li]**13** (**B**) in 0.24 M TMEDA/toluene at -90 °C. **ii.** Plot of the relative integration versus the mole fraction of **13** (**B**) for a mixture of [^{6}Li]**34** (**A**) and [^{6}Li]**13** (**B**) ϕ_0 = 2.27; ϕ_1 = 1.00; ϕ_2 = 2.27; RMS = 0.03. **iii.** Relative integrations for aggregates in a mixture of **34** (**A**) and **13** (**B**) at various mole fractions of **A** and **B**.

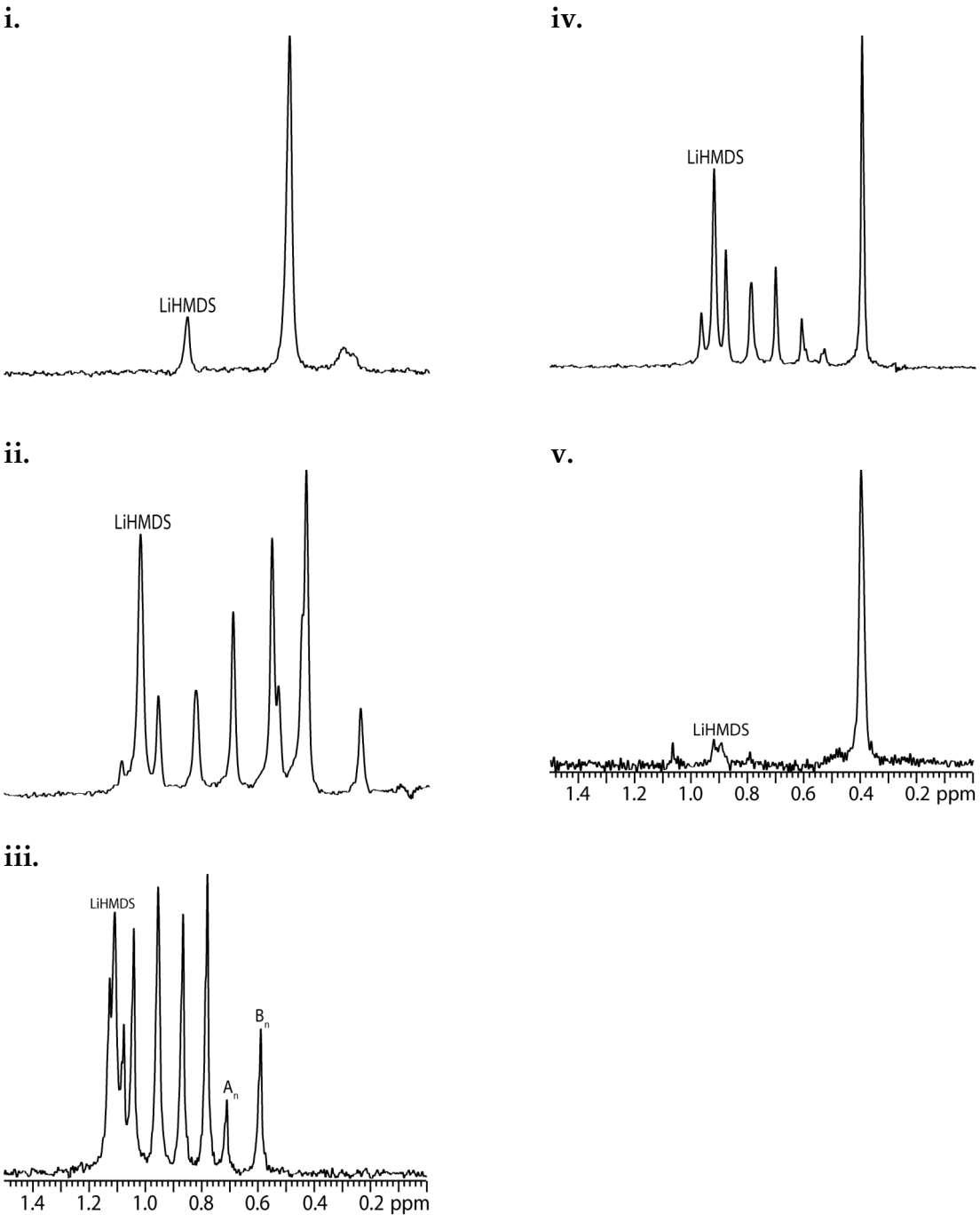

Figure AI.35. ^{6}Li NMR spectra of [^{6}Li]**34** (**A**) and [^{6}Li]**36** (**B**) and 0.12 M [^{6}Li]LiHMDS in 0.24 M TMEDA/toluene at -30 °C. **i.** 0.10 M [^{6}Li]**34** (**A**) **ii.** 70:30 mixture of [^{6}Li]**34** (**A**) and [^{6}Li]**36** (**B**) **iii.** 50:50 mixture of [^{6}Li]**34** (**A**) and [^{6}Li]**36** (**B**) **iv.** 30:70 mixture of [^{6}Li]**34** (**A**) and [^{6}Li]**36** (**B**) **v.** 0.10 M [^{6}Li]**36** (**B**).

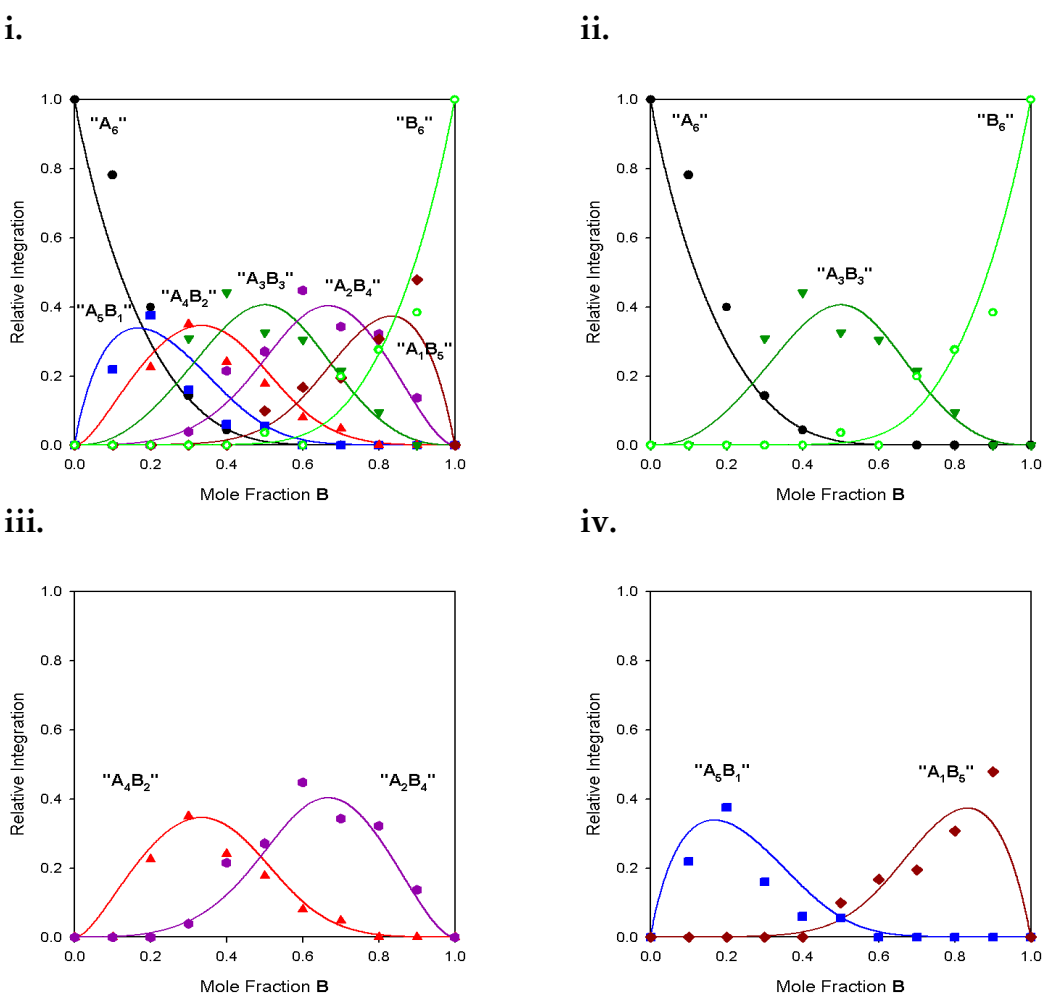

Figure AI.36. Plots of the relative integration versus mole fraction **36** (**B**) for an ensemble of [^{6}Li]**34** (**A**) and [^{6}Li]**36** (**B**) in 0.24 M TMEDA/toluene at -30 °C fit to a hexamer ensemble. Plot is shown together **(i)** and separately **(ii, iii,** and **iv)** for clarity. ϕ_{60} = 0.69; ϕ_{61} = 0.84; ϕ_{62} = 1.61; ϕ_{63} = 1.96; ϕ_{64} = 1.40; ϕ_{65} = 0.91; ϕ_{66} = 1.00; PMΣ = 0.05.

D. Residual Plots.

i. **ii.**

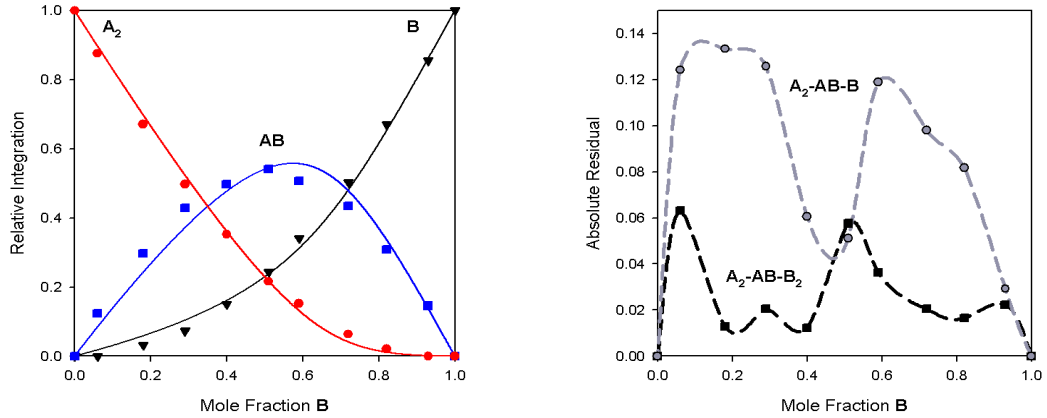

iii. **iv.**

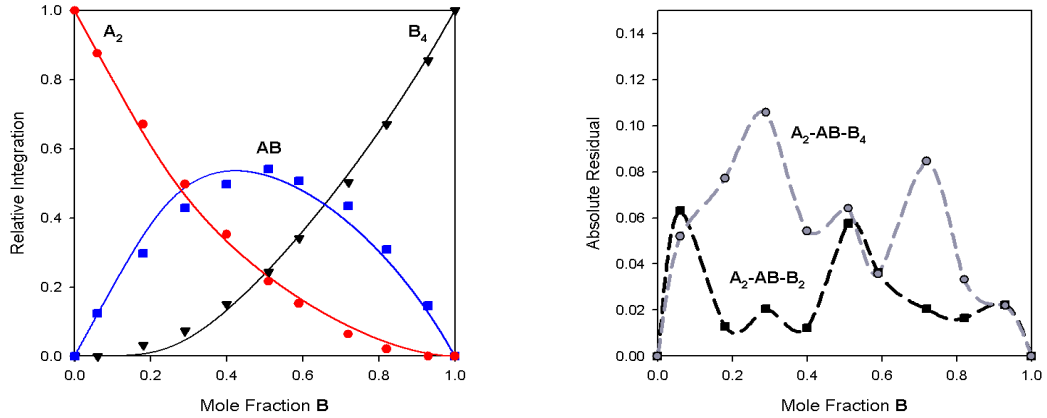

Figure AI.37. Plots of the relative integration versus mole fraction 7 (**B**) for an ensemble of [^{6}Li]**1** (**A**) and [^{6}Li]**7** (**B**) in 0.24 M TMEDA/toluene at -90 °C fit to an ensemble of **A_2-AB-B** and **A_2-AB-B_4**. **i.** Plot and fit of the relative integration versus the calculated mole fraction of **7 (B)** fit to **A_2-AB-B**; ϕ_{10} = 0.49; ϕ_{11} = 0.00; ϕ_{20} = 0.00; ϕ_{21} = 1.04; ϕ_{22} = 0.15; RMS = 0.35. **ii.** Plot of the sum of the absolute residuals for **A_2-AB-B_2** and **A_2-AB-B** versus mole fraction of **7 (B)**. **iii.** Plot and fit of the relative integration versus the calculated mole fraction of **7 (B)** fit to **A_2-AB-B_4**; ϕ_{20} = 0.00; ϕ_{21} = 0.53; ϕ_{22} = 1.55; ϕ_{40} = 0.91; $\phi_{41} = \phi_{42} = \phi_{43} = \phi_{44}$ = 0.00; RMS = 0.35. **iv.** Plot of the sum of the absolute residuals for **A_2-AB-B_2** and **A_2-AB-B_4** versus mole fraction of **7 (B)**.

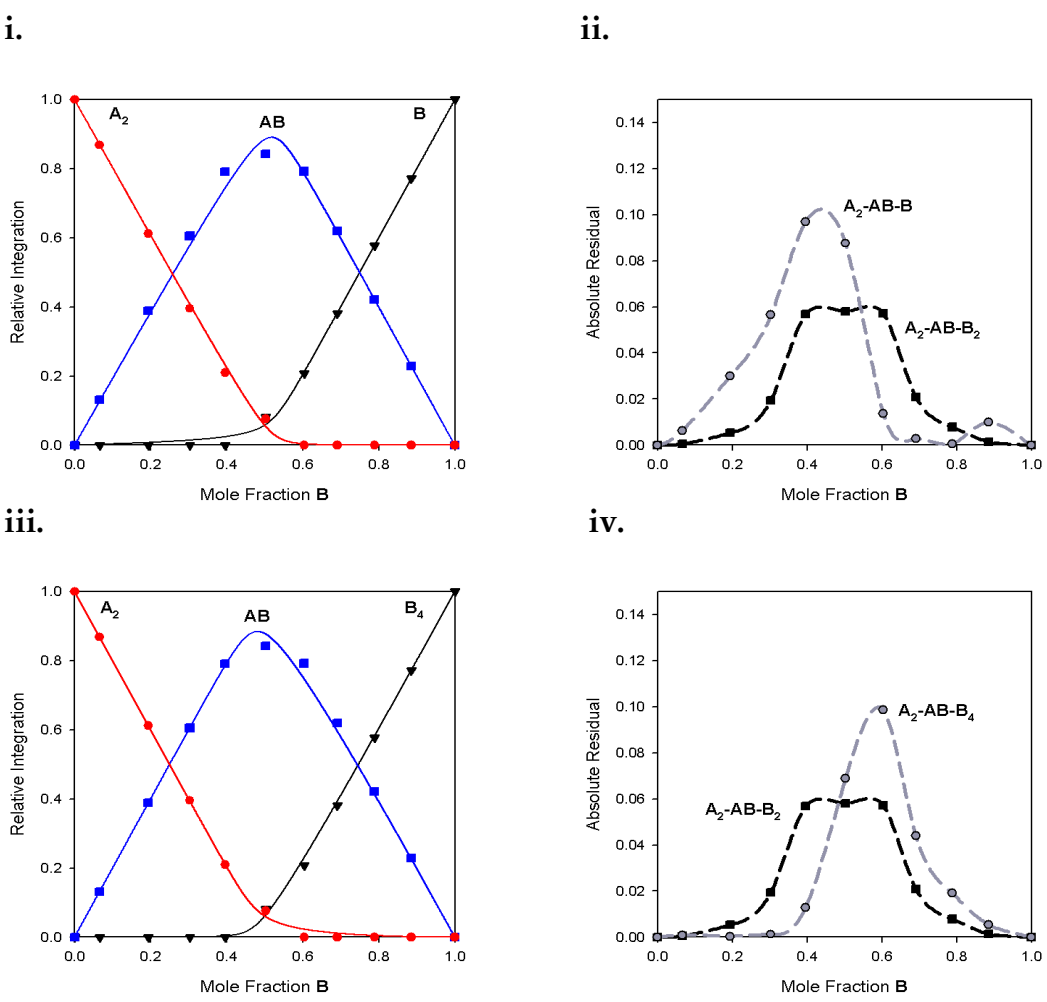

Figure AI.38. Plots of the relative integration versus mole fraction **13** (**B**) for an ensemble of [^{6}Li]**1** (**A**) and [^{6}Li]**13** (**B**) in 0.24 M TMEDA/toluene at -90 °C fit to an ensemble of **A_2-AB-B** and **A_2-AB-B_4**. **i.** Plot and fit of the relative integration versus the calculated mole fraction of **13 (B)** fit to **A_2-AB-B**; ϕ_{10} = 0.18; ϕ_{11} = 0.00; ϕ_{20} = 0.00; ϕ_{21} = 5.71; ϕ_{22} = 0.19; RMS = 0.02. **ii.** Plot of the sum of the absolute residuals for **A_2-AB-B_2** and **A_2-AB-B** versus mole fraction of **13 (B)**. **iii.** Plot and fit of the relative integration versus the calculated mole fraction of **13 (B)** fit to **A_2-AB-B_4**; ϕ_{20} = 0.00; ϕ_{21} = 1.54; ϕ_{22} = 0.54; ϕ_{40} = 1.14; ϕ_{41} = ϕ_{42} = ϕ_{43} = ϕ_{44} = 0.00; RMS = 0.01. **iv.** Plot of the sum of the absolute residuals for **A_2-AB-B_2** and **A_2-AB-B_4** versus mole fraction of **13 (B)**.

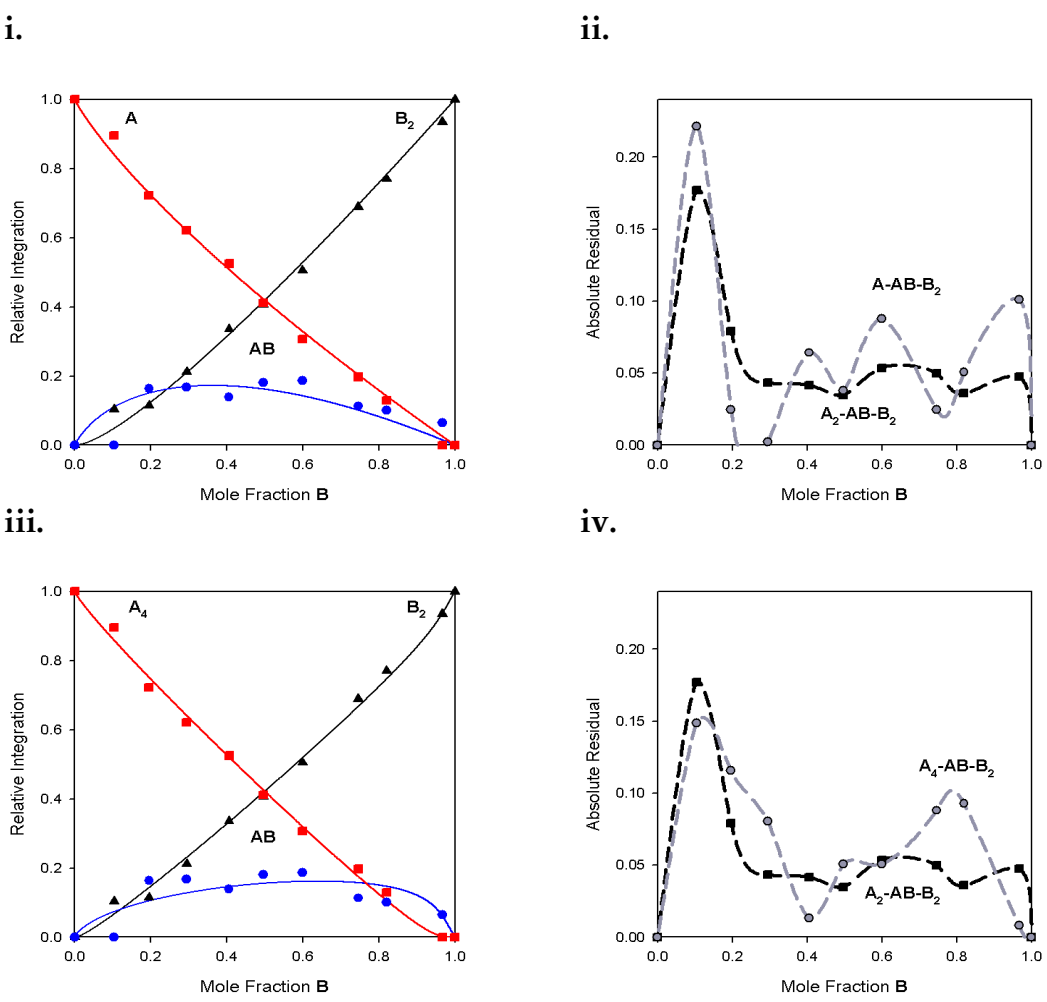

Figure AI.39. Plots of the relative integration versus mole fraction **1** (**B**) for an ensemble of [^{6}Li]**34** (**A**) and [^{6}Li]**1** (**B**) in 0.24 M TMEDA/toluene at -90 °C fit to an ensemble of **A_2-AB-B** and **A_2-AB-B_4**. **i.** Plot and fit of the relative integration versus the calculated mole fraction of **1 (B)** fit to **A_2-AB-B**; ϕ_{10} = 0.00; ϕ_{11} = 0.69; ϕ_{20} = 7.26; ϕ_{21} = 1.22; ϕ_{22} = 0.00; RMS = 0.03. **ii.** Plot of the sum of the absolute residuals for **A_2-AB-B_2** and **A_2-AB-B** versus mole fraction of **1 (B)**. **iii.** Plot and fit of the relative integration versus the calculated mole fraction of **1 (B)** fit to **A_2-AB-B_4**; ϕ_{20} = 1.54; ϕ_{21} = 0.19; ϕ_{22} = 0.00; ϕ_{40} = 0.00 = ϕ_{41} = ϕ_{42} = ϕ_{43}; ϕ_{44} = 5.34; RMS = 0.03. **iv.** Plot of the sum of the absolute residuals for **A_2-AB-B_2** and **A_2-AB-B_4** versus mole fraction of **1 (B)**.

As illlustrated by the plots, the fits are indistinguishable within error. Further investigation was necessary to characterize [^{6}Li]**34**.

E. ^{13}C NMR Spectra.

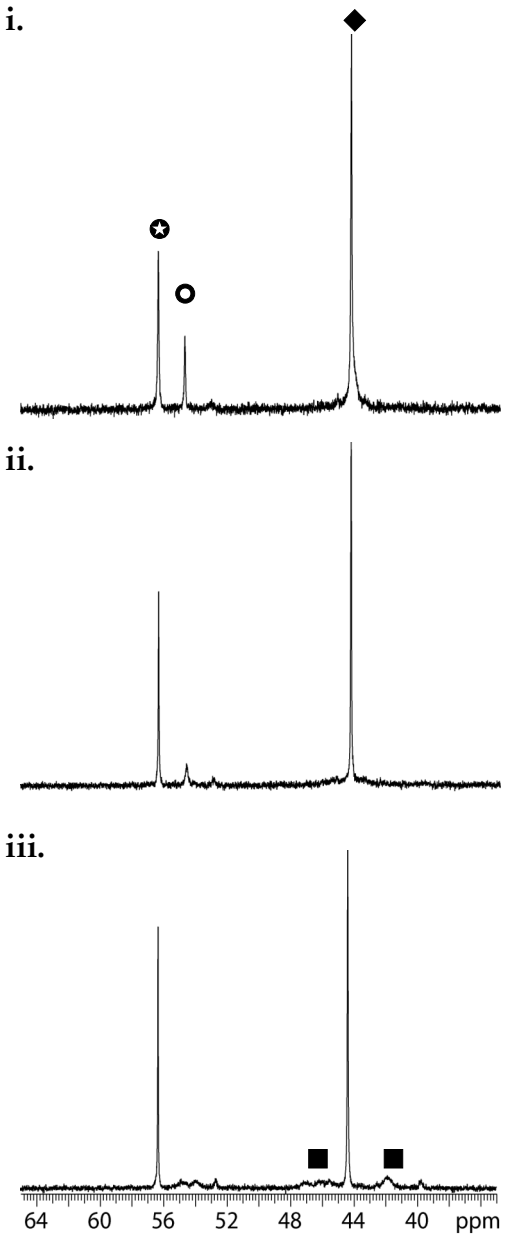

Figure AI.40. ^{13}C NMR spectra of [^{6}Li]**13** 0.24 M TMEDA/toluene at **i.** -100 °C; **ii.** -80 °C; **iii.** -70 °C. (■) bound $\underline{C}H_3$-N-; (◆) free $\underline{C}H_3$-N-; (O) bound -$\underline{C}H_2$-; (✪) free -$\underline{C}H_2$-

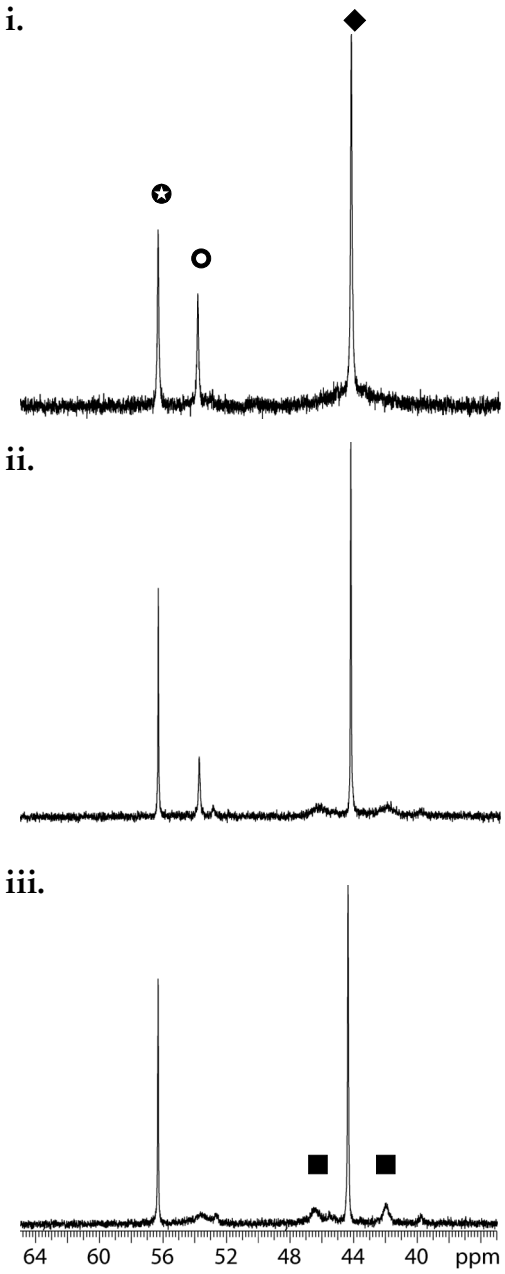

Figure AI.41. ^{13}C NMR spectra of [^{6}Li]**28** 0.24 M TMEDA / toluene at **i.** -100 °C; **ii.** -80 °C; **iii.** -70 °C. (■) bound $\underline{C}H_3$-N-; (◆) free $\underline{C}H_3$-N-; (O) bound -$\underline{C}H_2$-; (✪) free -$\underline{C}H_2$-

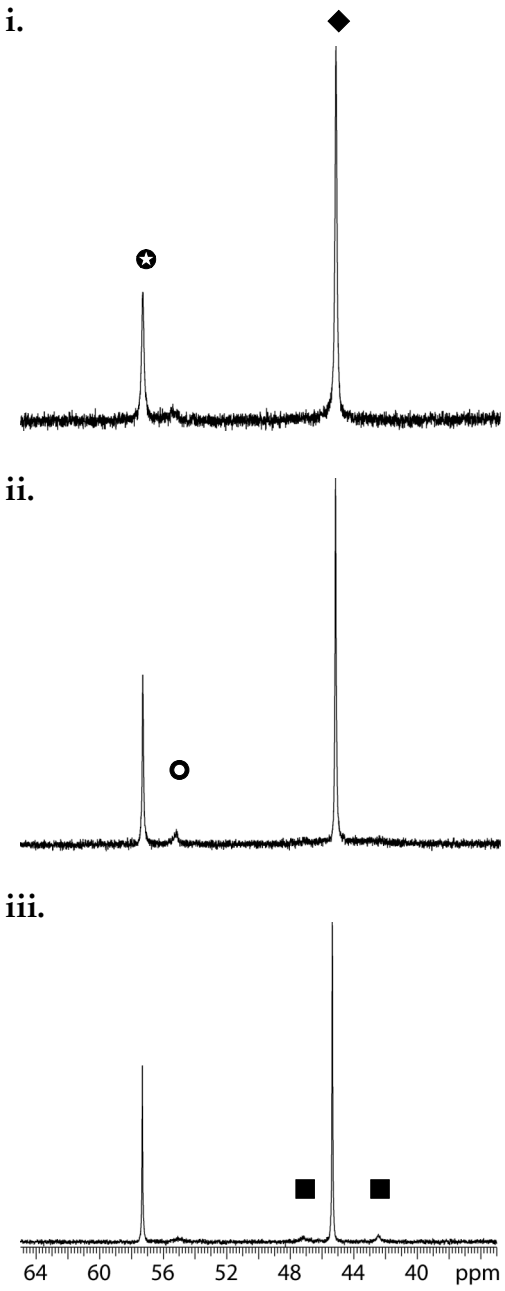

Figure AI.42. ^{13}C NMR spectra of [^{6}Li]**15** 0.24 M TMEDA/toluene at **i.** -100 °C; **ii.** -80 °C; **iii.** -70 °C. (■) bound $\underline{C}H_3$-N-; (◆) free $\underline{C}H_3$-N-; (O) bound -$\underline{C}H_2$-; (✪) free -$\underline{C}H_2$-

F. Alkoxide Studies.

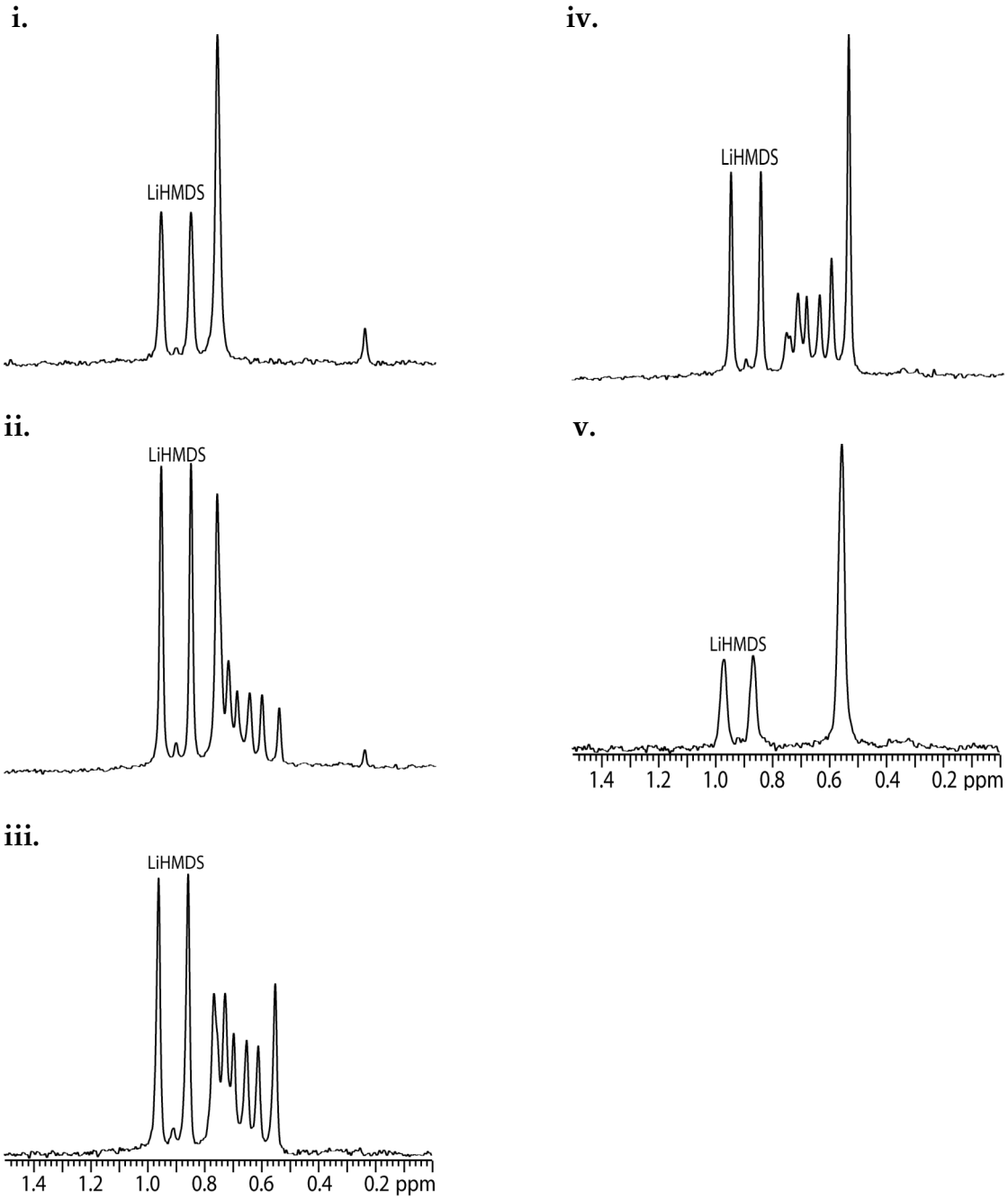

Figure AI.43. ^{6}Li NMR spectra of [^{6}Li]**35** (**A**) and [^{6}Li]**34** (**B**) and 0.12 M [^{6}Li, ^{15}N]LiHMDS in 0.24 M TMEDA/toluene at -70 °C. **i.** 0.10 M [^{6}Li]**35** (**A**) **ii.** 70:30 mixture of [^{6}Li]**35** (**A**) and [^{6}Li]**34** (**B**) **iii.** 50:50 mixture of [^{6}Li]**35** (**A**) and [^{6}Li]**34** (**B**) **iv.** 30:70 mixture of [^{6}Li]**35** (**A**) and [^{6}Li]**34** (**B**) **v.** 0.10 M [^{6}Li]**34** (**B**).

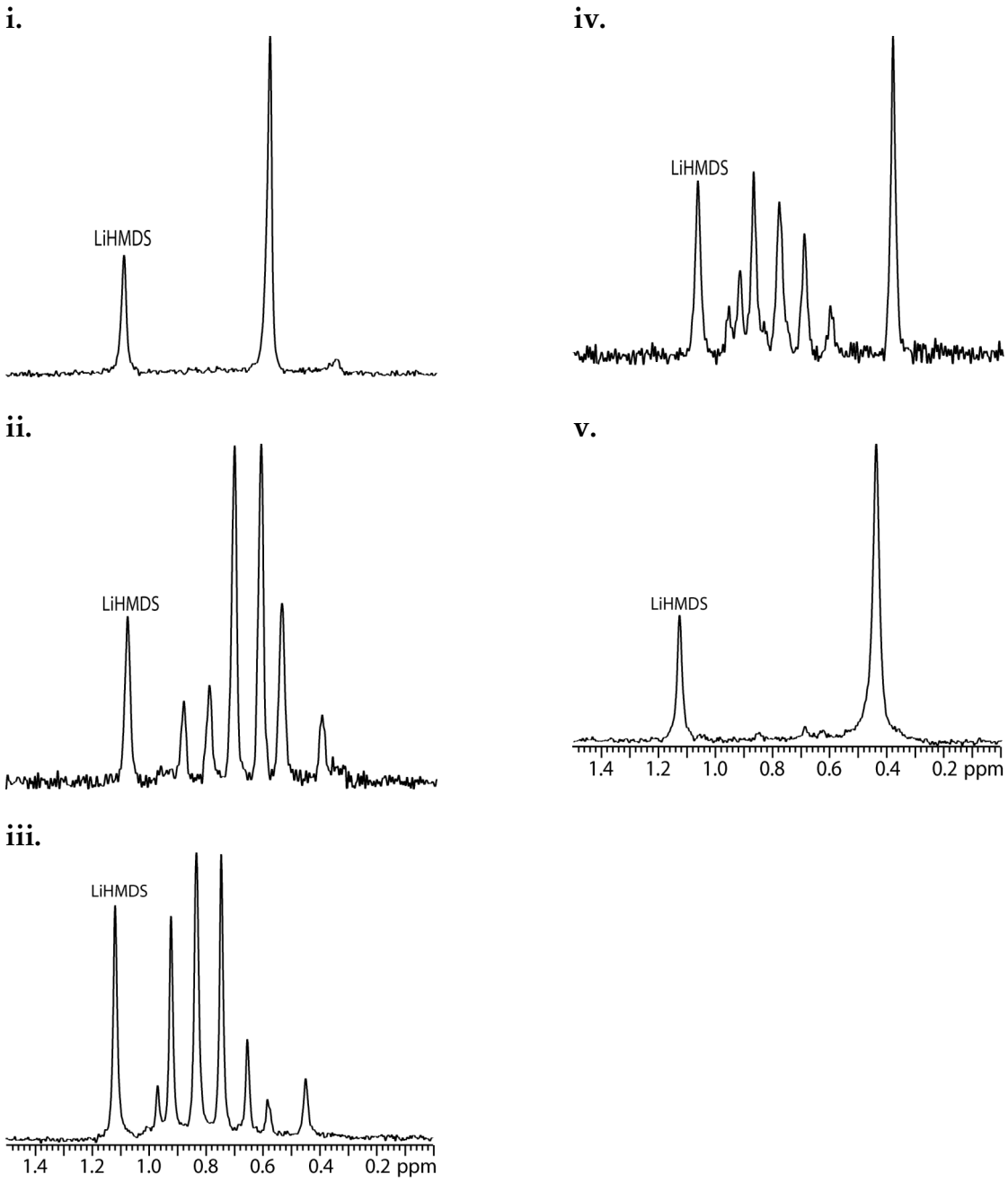

Figure AI.44. ^{6}Li NMR spectra of [^{6}Li]**34** (**A**) and [^{6}Li]**36** (**B**) in 0.24 M TMCDA/toluene at -30 °C. **i.** 0.10 M [^{6}Li]**34** (**A**) **ii.** 70:30 mixture of [^{6}Li]**34** (**A**) and [^{6}Li]**36** (**B**) **iii.** 50:50 mixture of [^{6}Li]**34** (**A**) and [^{6}Li]**36** (**B**) **iv.** 30:70 mixture of [^{6}Li]**34** (**A**) and [^{6}Li]**36** (**B**) **v.** 0.10 M [^{6}Li]**36** (**B**).

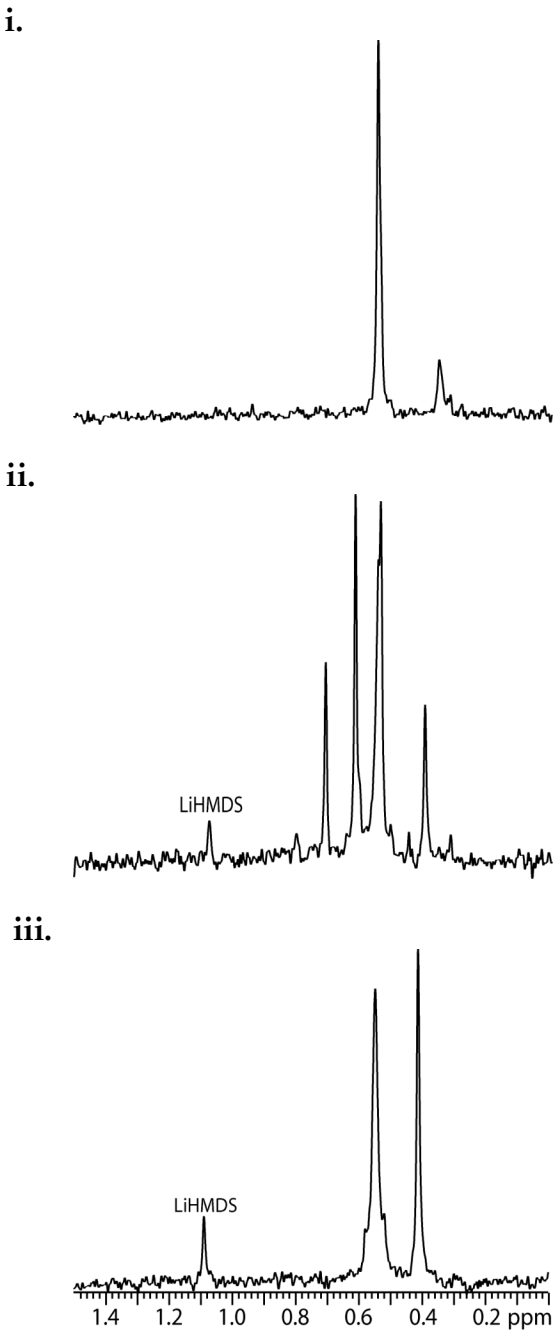

Figure AI.45. ^{6}Li NMR spectra of [^{6}Li]**34** (**A**) and [^{6}Li]**36** (**B**) in neat toluene at -30 °C. **i.** 0.10 M [^{6}Li]**34** (**A**) **ii.** 50:50 mixture of [^{6}Li]**34** (**A**) and [^{6}Li]**36** (**B**) **iii.** 0.10 M [^{6}Li]**36** (**B**).

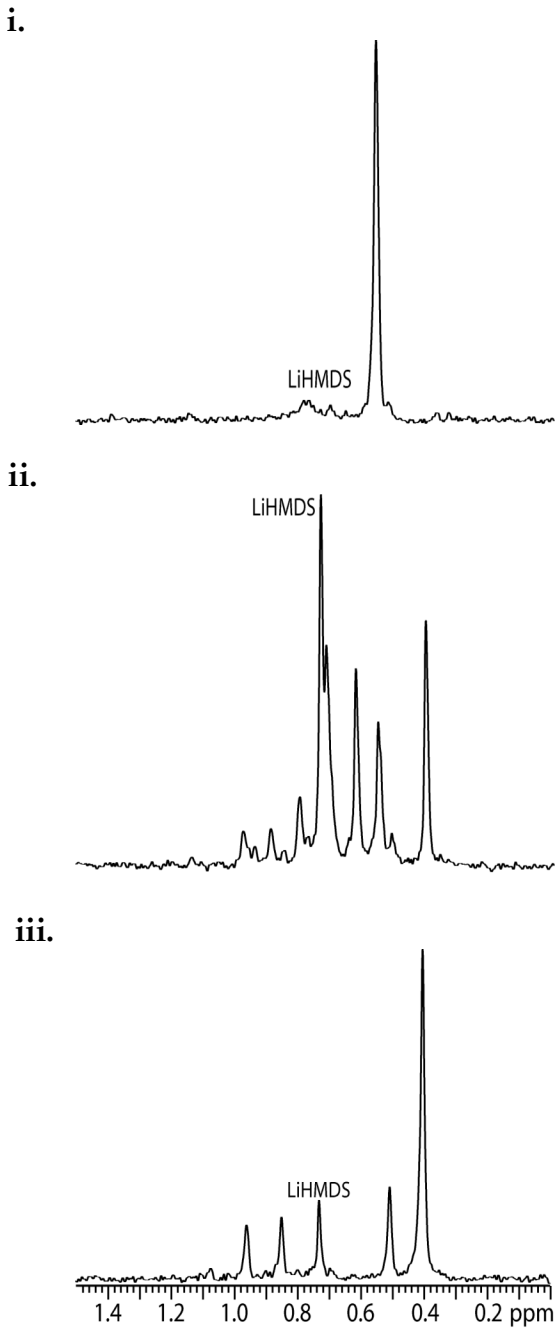

Figure AI.46. ^{6}Li NMR spectra of [^{6}Li]**34** (**A**) and [^{6}Li]**36** (**B**) in 0.24 M DMEA / toluene at -30 °C. **i.** 0.10 M [^{6}Li]**34** (**A**) **ii.** 50:50 mixture of [^{6}Li]**34** (**A**) and [^{6}Li]**36** (**B**) **iii.** 0.10 M [^{6}Li]**36** (**B**).

G. Hindered Phenolate Studies.

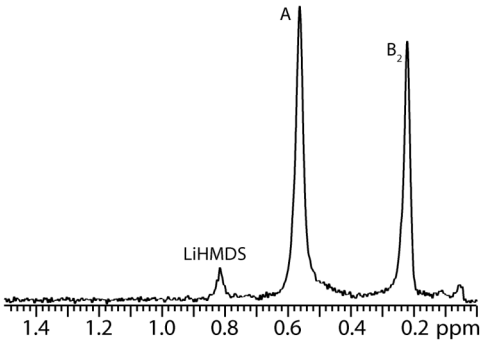

Figure AI.47. ^{6}Li NMR spectrum of a 50:50 mixture of [^{6}Li]**38** (**A**) and [^{6}Li]**1** (**B**) in 0.24 M TMEDA/toluene at -90 °C.

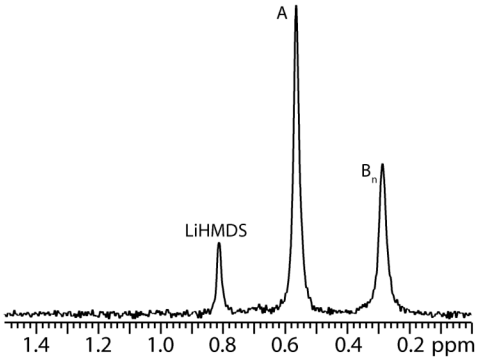

Figure AI.48. ^{6}Li NMR spectrum of a 50:50 mixture of [^{6}Li]**38** (**A**) and [^{6}Li]**36** (**B**) in 0.24 M TMEDA/toluene at -90 °C.

REFERENCES

1. (a) Green, J. R. In *Science of Synthesis*; Georg Thieme Verlag: New York, 2005; Vol. 8a, pp 427-486. (b) Schetter, B.; Mahrwald, R. *Angew. Chem., Int. Ed.* **2006**, *45*, 7506. (c) Arya, P.; Qin, H. *Tetrahedron* **2000**, *56*, 917. (d) Caine, D. In *Comprehensive Organic Synthesis*; Trost, B. M.; Fleming, I., Eds.; Pergamon: New York, **1989**, Vol. 1, p 1. Martin, S. F. *Ibid.*, Vol. 1, p. 475. (e) Plaquevent, J.-C.; Cahard, D.; Guillen, F.; Green, J. R. In *Science of Synthesis*; Georg Thieme Verlag: New York, 2005; Vol. 26, pp 463-511. (f) *Comprehensive Organic Functional Group Transformations II*; Katritzky, Alan R.; Taylor, Richard J. K., Eds.; Elsevier: Oxford, UK, 1995, pp 834-835. (g) Cativiela, C.; Diaz-de-Villegas, M. D. *Tetrahedron: Asymmetry* **2007**, *18*, 569. (h) Dugger, R. W.; Ragan, J. A.; Ripin, D. H. B. *Org. Process Res. Dev.* **2005**, *9*, 253. (i) Farina, V.; Reeves, J. T.; Senanayake, C. H.; Song, J. J. *Chem. Rev.* **2006**, *106*, 2734. Wu, G.; Huang, M. *Chem. Rev.* **2006**, *106*, 2596.

2. Representative examples and leading references to rate studies: (a) Jackman, L. M.; Lange, B. C. *Tetrahedron* **1977**, *33*, 2737. (b) Jackman, L. M.; Bortiatynski, J. *Adv. Carbanion Chem.* **1992**, *1*, 45. (c) Jackman, L. M.; Chen, X. *J. Am. Chem. Soc.* **1997**, *119*, 8681. (d) Wang, D. Z.; Kim, Y.-J.; Streitwieser, A. *J. Am. Chem. Soc.* **2000**, *122*, 10754. (e) Kim, Y.-J.; Streitwieser, A. *Org. Lett.* **2002**, *4*, 573. (f) Kim, Y.-J.; Wang, D. Z. *Org. Lett.* **2001**, *3*, 2599. (f) Zune, C.; Jerome, R. *Prog. Polymer Sci.* **1999**, *24*, 631. (g) Baskaran, D. *Prog. Polym. Sci.* **2003**, *28*, 521. (h) For an extensive bibliography of the structural and mechanistic studies of lithium enolates, see ref 3.

3. Liou, L. R. McNeil, A. J. Ramirez, A.; Toombes, G. E. S.; Gruver, J. M.; Collum, D. B. *J. Am. Chem. Soc.* **2008**, *130*, 4859.

4. For selected examples of and leading references to structural studies of lithium enolates in solution, see: (a) Yamataka, K.; Yamada, H.; Tomioka, H. In *The Chemistry of Organolithium Compounds*; Rappoport, Z.; Marek, I., Eds.; Wiley: New York, 2004, Vol. 2, p 908. (b) Zabicky, J. In *The Chemistry of Organolithium Compounds*; Rappoport, Z.; Marek, I., Eds.; Wiley: New York, 2004, Vol. 2, p 376. (c) Jackman, L. M.; Bortiatynski, J. *Adv. Carbanion Chem.* **1992**, *1*, 45. (d) Jackman, L. M.; Lange, B. C. *Tetrahedron* **1977**, *33*, 2737. (e) Zune, C.; Jerome, R. *Prog. Polymer Sci.* **1999**, *24*, 631. (f) Baskaran, D. *Prog. Polym. Sci.* **2003**, *28*, 521. (g) Pospisil, P. J.; Wilson, S. R.; Jacobsen, E. N. *J. Am. Chem. Soc.* **1992**, *114*, 7585. (h) Kim, Y.-J.; Streitwieser, A. *Org. Lett.* **2002**, *4*, 573. (i) Biddle, M. M.; Reich, H. J. *J. Org. Chem.* **2006**, *71*, 4031.

5. The rate law provides the stoichiometry of the transition structure relative to the reactant (Edwards, J. O.; Greene, E. F.; Ross, J. *J. Chem. Educ.* **1968**, *45*,

381); knowing the structure of the reactant is essential. For a review describing some recent advances and details of studying organolithium reaction mechanism, see: Collum, D. B.; McNeil, A. J.; Ramirez, A. *Angew. Chem., Int. Ed.* **2007**, *46*, 3002.

6. The crystallographic literature of lithium enolates[7] reveals a prevalence of chelated dimers for TMEDA solvates: (a) Nichols, M. A.; Leposa, C. M.; Hunter, A. D.; Zeller, M. *J. Chem. Crystallogr.* **2007**, *37*, 825. (b) Seebach, D.; Amstutz, R.; Laube, T.; Schweizer, W. B.; Dunitz, J. D. *JACS* **1985**, *107*, 5403. (c) Meyers, A. I.; Seefeld, M. A.; Lefker, B. A.; Blake, J. F.; Williard, P. G. *J. Am. Chem. Soc.* **1998**, *120*, 7429. (d) Boche, G.; Langlotz, I.; Marsch, M.; Harms, K. *Chem. Ber.* **1994**, *127*, 2059. (e) Hahn, E.; Maetzke, T.; Plattner, D. A.; Seebach, D. *Chem. Ber.* **1990**, *123*, 2059. (f) Henderson, K. W.; Dorigo, A. E.; Williard, P. G.; Bernste, P. R. *Angew. Chem., Int. Ed.* **1996**, *35*, 1322. (g) See reference 21c and 28a.

7. (a) Seebach, D. *Angew. Chem., Int. Ed. Engl.* **1988**, *27*, 1624. (b) Setzer, W. N.; Schleyer, P. v. R. *Adv. Organomet. Chem.* **1985**, *24*, 353. (c) Williard, P. G. In *Comprehensive Organic Synthesis*; Trost, B. M.; Fleming, I., Eds.; Pergamon: New York, 1991; Vol. 1, Chapter 1.1.

8. The rapid relaxation of the highly quadrupolar ^{17}O nucleus would preclude observing ^{6}Li-^{17}O coupling.

9. (a) Gil, V. M. S.; Oliveira, N. C. *J. Chem. Educ.* **1990**, *67*, 473. (b) Huang, C. Y. *Method Enzymol.* **1982**, *87*, 509. (c) Hirose, K. *J. Incl. Phenom.* **2001**, *39*, 193. (d) Likussar, W.; Boltz, D. F. *Anal. Chem.* **1971**, *43*, 1265.

10. Job, P. *Ann. Chim.* **1928**, *9*, 113.

11. (a) McNeil, A. J.; Toombes, G. E. S.; Gruner, S. M.; Lobkovsky, E.; Collum, D. B.; Chandramouli, S. V.; Vanasse, B. J.; Ayers, T. A. *J. Am. Chem. Soc.* **2004**, *126*, 16559. (b) McNeil, A. J.; Toombes, G. E. S.; Chandramouli, S. V.; Vanasse, B. J.; Ayers, T. A.; O'Brien, M. K.; Lobkovsky, E.; Gruner, S. M.; Marohn, J. A.; Collum, D. B. *J. Am. Chem. Soc.* **2004**, *126*, 5938. (c) McNeil, A. J.; Collum, D. B. *J. Am. Chem. Soc.* **2005**, *127*, 5655.

12. TMEDA is one of the most prevalent ligands in organolithium chemistry: (a) Snieckus, V. *Chem. Rev.* **1990**, *90*, 879. (b) Clayden, J. *Organolithiums: Selectivity for Synthesis*; Pergamon: New York, 2002. (c) *Polyamine-Chelated Alkali Metal Compounds*; Langer, A. W., Jr., Ed.; American Chemical Society:

Washington, 1974. (d) For a discussion of the effect of TMEDA on anionic polymerizations of methyl methacrylate, see: Baskaran, D.; Muller, A. H. E.; Sivaram, S. *Macromol. Chem. Phys.* **2000**, *201*, 1901.

13. ^{6}Li NMR spectra recorded on mixtures of **1** and **3** in Me_2NEt, a non-chelating analog of TMEDA display a distribution of resonances characteristic of an ensemble of tetramers.[3]

14. Free and bound TMEDA have been observed by ^{13}C NMR spectroscopy for a select group of homodimers derived from **1**, **2**, **3**, **13**, **15**, and **28**, suggesting chelation.

15. (a) Goralski, P.; Chabanel, M. *Inorg. Chem.* **1987**, *26*, 2169. (b) Goralski, P.; Legoff, D.; Chabanel, M. *J. Organomet. Chem.* **1993**, *456*, 1.

16. Kissling R. M.; Gagne, M. R. *J. Org. Chem.* **2001**, *66*, 9005.

17. Günther, H. *J. Brazil. Chem.* **1999**, *10*, 241.

18. (a) Novak, D. P.; Brown, T. L. *J. Am. Chem. Soc.* **1972**, *94*, 3793. (b) Desjardins, S.; Flinois, K.; Oulyadi, H.; Davoust, D.; Giessner-Prettre, C.; Parisel, O.; Maddaluno, J. *Organometallics* **2003**, *22*, 4090. (c) Weingarten, H.; Van Wazer, J. R. *J. Am. Chem. Soc.* **1965**, *87*, 724.

19. For a more recent example, see: Jacobson, M. A.; Keresztes, I.; Williard, P. G. *J. Am. Chem. Soc.* **2005**, *127*, 4965.

20. After surveying a subset of the community, we have chosen to refer to $(LiX)_n$ and $(LiX)_m(LiX')_n$ as a "homoaggregate" and "heteroaggregate", respectively, and reserve the term "mixed aggregate" for $(LiX)_m(LiY)_n$.

21. (a) Collum, D. B. *Acc. Chem. Res.* **1993**, *26*, 227. (b) Williard, P. G.; Hintze, M. J. *J. Am. Chem. Soc.* **1990**, *112*, 8602. (c) Henderson, K. W.; Dorigo, A. E.; Williard, P. G.; Bernstein, P. R. *Angew. Chem., Int. Ed. Engl.* **1996**, *35*, 1322. (d) See ref 28e.

22. Kim, Y.-J.; Bernstein, M. P.; Galiano-Roth, A. S.; Romesberg, F. E.; Fuller, D. J.; Harrison, A. T.; Collum, D. B.; Williard, P. G. *J. Org. Chem.* **1991**, *56*, 4435.

23. Romesberg, F. E.; Bernstein, M. P.; Gilchrist, J. H.; Harrison, A. T.; Fuller, D. J.; Collum, D. B. *J. Am. Chem. Soc.* **1993**, *115*, 3475.

24. The relative integration $(I_n)^3$ was previously referred to as aggregate mole fraction (X_n).[11] The change was made to avoid using two, distinctly different mole fraction terms and to include provisions for mixtures of aggregates with different aggregation numbers.

25. The mathematics underlying the parametric fits has been described in detail in refs 3 and 11.

26. Ball, S.C.; Cragg-Hine, I.; Davidson, M.G.; Davies, R.P.; Edwards, A.J.; Lopez-Solera, I.; Raithby, P.R.; Snaith, R. *Angew. Chem., Int. Ed. Engl.* (1995), **34**, 921.

27. Wisian-Neilson, P.; Islam, M. S.; Ganapathiappan, S.; Scott, D. L.; Raghuveer, K. S.; Ford, R. R. *Macromolecules* **1989**, *22*, 4382. Kim, Y. H.; Webster, O. W.; *J. Am. Chem. Soc.* **1990** *112*, 4592.

28. Leading references to salt effects: (a) Tchoubar, B.; Loupy, A. *Salt Effects in Organic and Organometallic Chemistry*; VCH: New York, 1992; Chapters 4, 5, and 7. (b) Seebach, D. In *Proceedings of the Robert A. Welch Foundation Conferences on Chemistry and Biochemistry*; Wiley: New York, 1984; p 93. (c) Gossage, R. A.; Jastrzebski, J. T. B. H.; van Koten, G. *Angew. Chem., Int. Ed.* **2005**, *44*, 1448. (d) Seebach, D. *Angew. Chem., Int. Ed. Engl.* **1988**, *27*, 1624. (e) Ramirez, A.; Sun, X.; Collum, D. B. *J. Am. Chem. Soc.* **2006**, *128*, 10326. (f) Also, see ref 11a.

29. Cottet, F.; Schlosser, M. *Eur. J. Org. Chem.* **2004**, 3793. Green, J. R. In *Science of Synthesis*; Georg Thieme Verlag: New York, 2005; Vol. 8a, pp 427.

30. A mixed aryloxide/alkoxide tetramer has been characterized crystallographically: Ko, B.-T.; Lin, C.-C. *J. Am. Chem. Soc.* **2001**, *123*, 7973.

31. The phenyl moieties on **32** and **33** were necessary to maximize the resolution in the ^{6}Li NMR spectrum when paired with *t*-BuOLi (**31**).

32. Collum, D. B. *Acc. Chem. Res.* **1992**, *25*, 448.

33. A solvent-free hexameric imidate crystallizes from solutions containing TMEDA: Maetzke, T.; Seebach, D. *Organometallics* **1990**, *9*, 3032.

34. For early discussions of steric effects on solvation and aggregation, see: Settle, F. A.; Haggerty, M.; Eastham, J. F. *J. Am. Chem. Soc.* **1964**, *86*, 2076. Lewis, H. L.; Brown, T. L. *J. Am. Chem. Soc.* **1970**, *92*, 4664. Brown, T. L.; Gerteis, R. L.; Rafus, D. A.; Ladd, J. A. *J. Am. Chem. Soc.* **1964**, *86*, 2135.

35. Unsolvated *t*-BuOLi (**31**) is octameric in the solid state: Allan, J. F.; Nassar, R.; Specht, E.; Beatty, A.; Calin, N.; Henderson, K. W. *J. Am. Chem. Soc.* **2004**, *126*, 484.

36. Unsolvated Me_2PhCOLi (**32**) is hexameric in the solid state: Chisholm, M. H.; Drake, S. R.; Naiini, A. A.; Streib, W. E. *Polyhedron,* (1991), **10**, 805.

37. (a) Kamienski, C. W.; Lewis, D. H. *J. Org. Chem.* **1965**, *30*, 3498. (b) Golovanov, I. B.; Simonov, A. P.; Priskunov, A. K.; Talalseva, T. V.; Tsareva, G. V.; Kocheshkov, *Dokl. Adka. Nauk. SSSR* **1963**, *149*, 835. (c) Simonov, A. P.; Shigorin, D. N.; Talalseva, T. V.; Kocheshkov, K. A. *Bull. Acad. Sci. USSR Div. Chem. Sci.* **1962**, *6*, 1056.

38. (a) Arnett, E. M.; Moe, K. D. *J. Am. Chem. Soc.* **1991**, *113*, 7288. (b) Arnett, E. M.; Fisher, F. J.; Nichols, M. A.; Ribeiro, A. A. *J. Am. Chem. Soc.* **1990**, *112*, 801. (c) Seebach, D.; Bauer, von W. *Helv. Chim. Acta* **1984**, *67*, 1972. (d) Shobatake, K.; Nakamoto, K. *Inorg. Chim. Acta* **1980**, *4*, 485. (e) den Besten, R.; Harder, S.; Brandsma, L. *J. Organomet. Chem.* **1990**, *385*, 153. (f) Halaska, V.; Lochmann, L. *Collect. Czech. Chem. Commun.* **1973**, *38*, 1780. (g) Simonov, A. P.; Shigorin, D. N.; Talalseva, T. V.; Kocheshkov, K. A. *Bull. Acad. Sci. USSR Div. Chem. Sci.* **1962**, *6*, 1056. (h) Armstrong, D. R.; Davies, J. E.; Davies, R. P.; Raithby, P. R.; Snaith, R.; Wheatley, A. E. H. *New J. Chem.* **1999**, 35. (i) Lochmann, L.; Lim, D. *J. Organomet. Chem.* **1973**, *50*, 9. (j) Also, see ref 4.

39. (a) Freund, M.; Michaels, H. *Ber. Dtsch. Chem. Ges.* **1897**, *30*, 1374. 8. (b) Chadwick, S. T.; Rennels, R. A.; Rutherford, J. L.; Collum, D. B. *J. Am. Chem. Soc.* **2000**, *122*, 8640. (c) Rennels, R. A.; Maliakal, A. J.; Collum, D. B. *J. Am. Chem. Soc.* **1998**, *120*, 421.

CHAPTER II

O-Silylations of Lithium Enolates

O-Silylations of Lithium Enolates

Abstract

O-Silylations of lithium enolates using trimethylsilyl chloride (TMSCl) in THF are described. O-Silylation of the cyclohexanone-derived enolate exhibits first-order behavior at low THF concentrations. At high THF concentrations, sigmoidal behavior is observed due to autocatalysis likely caused by in situ generated LiCl. There were a number of unexpected observations throughout the study, including side product formation, autocatalytic behavior, and extreme sensitivity to the reaction conditions. A variety of other silylating agents were also explored. Silyl triflates gave unusual results that provided insight into lithium triflate chemistry.

Introduction

The Collum group is one of the few groups in the world dedicated to understanding structure-reactivity relationships in organolithium chemistry, beginning with a synthetically important observation and ending with a detailed description of the rate-limiting transition structure(s)—start to finish. Sound structural assignments of reactive species in their ground state *must* precede rate and mechanistic studies, which provide explicit information about the transition structures. With a general protocol for characterizing enolates in place, detailed rate studies naturally follow.

We recently used the method of continuous variation[1] (the method of Job[2]) to show that simple enolates **1**-**3** are cyclic dimers in *N*,*N*,*N*′,*N*′-tetramethylethylenediamine (TMEDA) (**4**), cubic tetramers in tetrahydrofuran

(THF) (**5**), and cubic tetramers in 1,2-dimethoxyethane (DME) (**6**).[3]

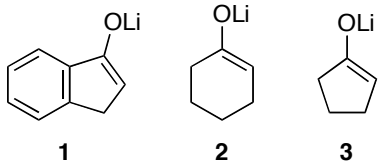

1 **2** **3**

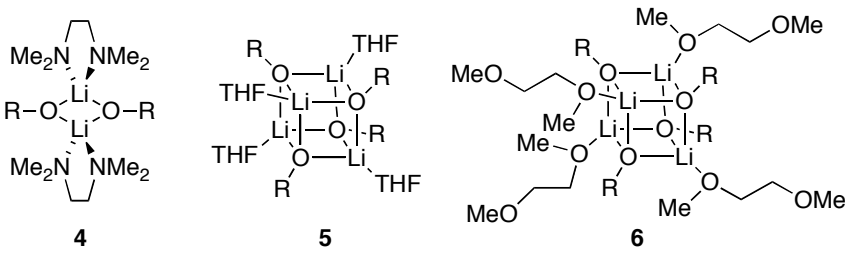

4 **5** **6**

With the structural assignment in place, enolate reactivity was explored. We initially focused on O-silylations of ketone enolates (eq 1), which are prevalent throughout organic chemistry. O-silylations derive special importance from a growing number of catalytic methods that use silyl ethers as substrates.[4] O-Silylations also have the outward appearance of simplicity, suggesting that the reaction could serve as a benchmark to compare reactivities of a variety of enolates in a wide range of solvent conditions.

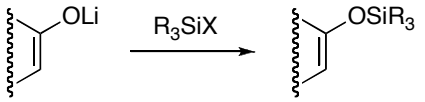

(1)

Structural and rate studies reveal that the assumption of simplicity was wrong, instead providing a window into the effects of LiCl on enolate structure and reactivity. Monitoring enolate decay at high THF concentrations

results in sigmoidal behavior, which is indicative of autocatalysis likely caused by LiCl. We thought that we may be able to influence—and possibly preclude—mixed aggregates and autocatalysis by using silyl triflates[5] and silyl imidazoles.[6] While we did not obtain the expected results, we did gain insight into the reactivity of lithium triflate, which led to a new method for synthesizing silyl enol ethers under mild conditions and in the absence of a lithium amide base.

Throughout the O-silylation studies, we observed several other unexpected behaviors including the formation of side products and intermediates using NMR and in situ IR spectroscopies. We also had difficulty obtaining sufficiently reproducible data for more detailed rate studies due to observed induction periods being unusually sensitive to the reaction conditions. O-Silylations were clearly more complex than had been assumed, and one cannot help but wonder if these complexities are negatively affecting research in both industrial and academic laboratories.

Background

Lithium salts (LiX) generated during an organolithium reaction can profoundly alter structures, reactivity, or selectivity of the reaction.[7] In particular, the beneficial effects of LiCl on the chemistry of LDA and other organolithium reactions have been well documented.[8-10] Our group recently showed that LDA–mediated ortholithiations of a variety of arenes are accelerated substantially by the addition of as little as 0.5 mol % LiCl (relative to LDA).[11]

While a large part of the literature refers to lithium amide-LiX mixed aggregation effects,[7-10] lithium enolates are also affected by addition of lithium

salts. It has been shown that the addition of either LiCl or LiBr to the isobutyrophenone-derived lithium enolate in dioxolane alters the enolate aggregate structure.[12] Using ^{1}H NMR spectroscopy, Jackman and co-workers initially determined that the enolate-LiX mixed aggregate was a tetrahedron of enolate ions surrounding a central halide ion (X = Cl, Br), along with one external lithium ion. With improved techniques, however, they later determined that the complex is actually the enolate-LiCl 3:1 mixed cubic tetramer in dioxolane.[13] X-ray crystallographic studies on diisopropyl ketone-derived lithium enolate mixed with LiX salts (X = Br, I) in TMEDA have revealed a disolvated cyclic heterodimer.[14] Further evidence that lithium salts can drastically alter enolate aggregate structures, a unique TMEDA solvated crystal structure has been obtained that includes three types of ions – lithium amide (LiHMDS), lithium enolate (derived from pinacolone), and lithium bromide.[15]

While enolate-LiX mixed aggregate structures are an important part of understanding salt effects, studying their reactivity is also a significant part of the puzzle. In an extensive review by Seebach,[10] three types of salt effects are discussed. First, adding LiX to a reaction may cause a variation in product ratios. For example, a lithium enolate homoaggregate may produce a single product, however, an enolate-LiX mixed aggregate may result in a different product. With this knowledge, one then has the ability to control product formation. A second example illustrates how addition of a chiral salt additive to an achiral enolate produces chiral mixed aggregate, which can lead to the formation of enantiomerically pure products. This is very beneficial since the chiral salt is easily removed during an aqueous workup instead of cleaving a chiral auxiliary that was covalently bound to the enolate. Lastly, Seebach

discusses how lithium salts may convert insoluble polylithiated compounds into soluble mixed aggregated species.

Enolate-LiX mixed aggregates do not always serve as the reactive species in a reaction, evidenced by studies of O- and C-methylation of lithioisobutyrophenone.[16] The C/O product ratio of this reaction in dioxolane was determined and, in theory, should remain constant if the reactive species remains unchanged. Adding LiCl to this reaction did not alter the C/O ratio. This indicates that the reactivity of the tetrameric lithioisobutyrophenone[12,13] is not affected by replacing one of the corners with a chloride ion.

Clearly, addition of lithium salts to enolate solutions can have significant effects on the structure and reactivity of lithium enolates. This fact is certainly important considering halide derivatives are often utilized in enolate reactions, specifically alkylations using alkyl chlorides or silylations using TMSCl. Our group's interest in enolate structure-reactivity relationships is a result of just this. Stemming from a collaboration with Aventis, it was determined that LiBr generated during an alkylation was actually inhibiting the reaction.[17] ^{6}Li NMR spectroscopic studies of enolate-LiBr mixtures revealed an absence of enolate homoaggregate due to the formation of mixed aggregates, the structure(s) of which has not been characterized. Although enolate structure and reactivity may not always be influenced by the addition of lithium salts, it is an important consideration that cannot be ignored.

Results

General Methods. Lithium enolates were prepared from [^{6}Li]LiHMDS or [^{6}Li]LDA in THF at -78 °C. TMSCl over CaH_2 was freshly distilled. TMSCl

was then added to Et_3N (3:1 mole ratio) and centrifuged to separate the $Et_3N{\cdot}HCl$ salt. Upon complete enolate formation, 10 equiv TMSCl in Et_3N was added directly to the reaction vessel. The lithium amide base and the silylating agent were mixed in the reaction vessel at -78 °C prior to ketone addition for the in situ trap studies.

The O-silylations were performed under pseudo-first-order conditions ([TMSCl] ≥ 10 x [enolate]). Rates were monitored using in situ IR spectroscopy and ^1H NMR spectroscopy.

TMSCl Silylations of the Cyclohexanone-derived Enolate. O-Silylation of the cyclohexanone-derived enolate (eq 2) with TMSCl at low THF concentrations follows an exponential decay—a first-order dependence on enolate concentration—indicating a direct reaction of the tetramer (Figure II.1).

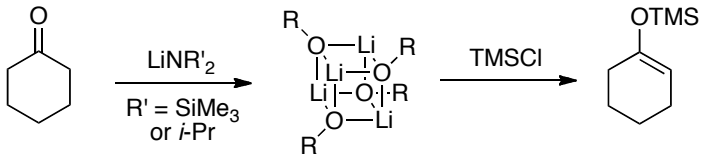

(2)

7 **8** **9a**

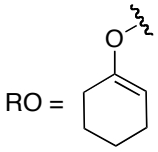

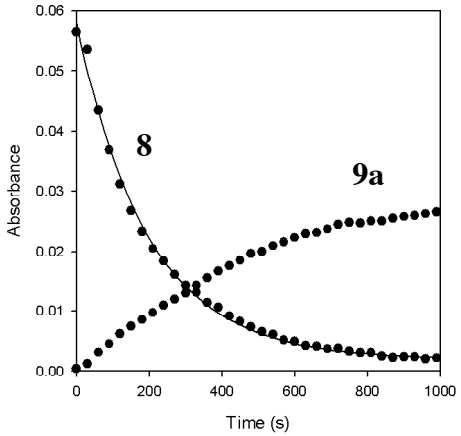

Figure II.1. Plot of the decay of **8** (0.05 M) and formation of **9a** in 2.0 M THF/pentane at -50 °C. TMSCl (6.0 equiv) was added to the enolate solution. Decay of **8** is fit to $y = ae^{-kx}$ ($k = 4.5 \times 10^{-3}$, $a = 4.1 \times 10^{-2}$).

At elevated THF concentration (≥ 3.0 M), however, the silylation displays markedly higher rates and clear evidence of autocatalysis in the form of a sigmoidal decay (Figure II.2A). Initial studies point to LiCl as the source of autocatalysis. Adding 1 mol % of $Et_3N{\cdot}HCl$ to lithium amide base at the outset partially eliminates the induction period of the sigmoidal curve and enhances reactivity (Figure II.2B). The Et_3N byproduct is a poor ligand for lithium amides[18] and has no effect on the silylation reaction.

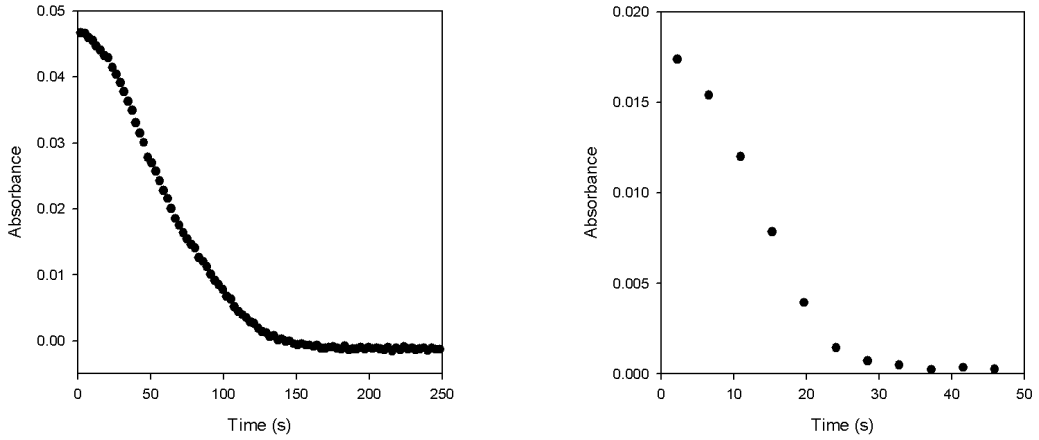

Figure II.2. (**A**) Plot of the decay of **8** (0.05 M) in neat THF at -78 °C. (**B**) Plot of the decay of **8** (0.05 M) in neat THF at -78 °C with 1 mol % $Et_3N{\cdot}HCl$ added to LiHMDS. TMSCl (6.0 equiv) was added to the enolate solution.

Serially injecting TMSCl in 10% increments also confirms LiCl as the source of autocatalytic behavior. Monitoring enolate decay during the early injections shows linear behavior (Figure II.3A). However, as the concentration of LiCl increases, the enolate reacts more rapidly and appears to follow an exponential decay (Figure II.3B-C). An attempt at duplicating this experiment resulted in unusual data; plotting the decay of the enolate gives consecutive sigmoidal curves, behaving almost identically (Figure II.4). The cause of the multiple sigmoidal curves is unknown, but may point to a problem with equilibration of the reactive species.

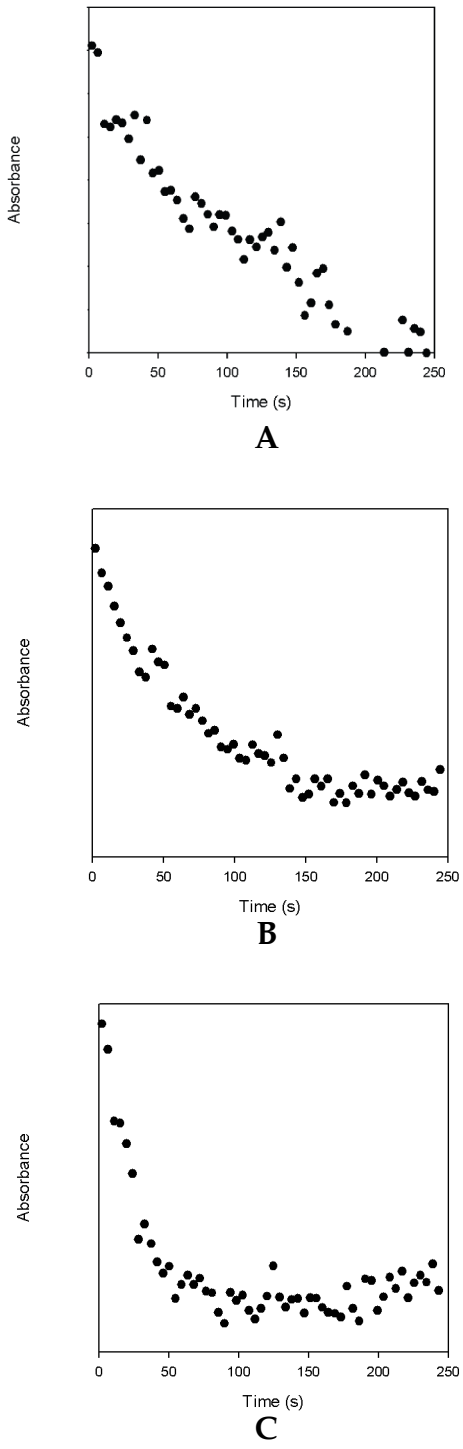

Figure II.3. Plots of the decay of **8** (0.025 M) in neat THF at -78 °C after serially injecting 0.10 equiv TMSCl until a total of 1.0 equiv was added. (**A**) 2nd injection (0.20 equiv), (**B**) 4th injection (0.40 equiv), and (**C**) 9th injection (0.90 equiv).

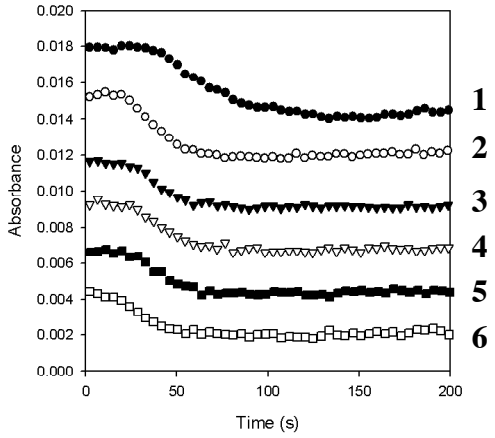

Figure II.4. Plot of the decay of **8** (0.025 M) in neat THF at -78 °C after serially injecting 0.10 equiv TMSCl. Each curve depicts enolate decay upon injecting 10% TMSCl. The injection number is indicated next to the curve.

Due to the unexpected behavior observed by in situ IR, we turned to ^{6}Li NMR spectroscopy to aid in understanding the enolate-LiCl interactions. LiCl was generated in situ from recrystallized $Et_3N{\cdot}HCl$.[19] The studies reveal the formation of mixed dimer **10** and traces of mixed trimer **11** in neat THF (Figure II.5).

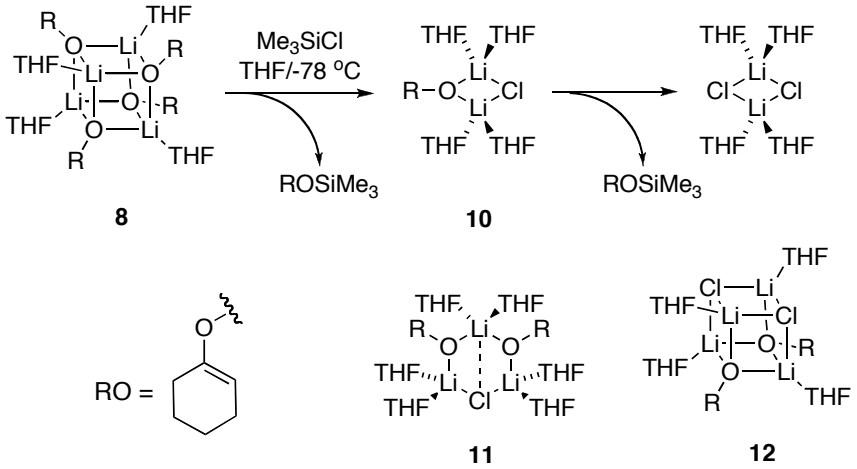

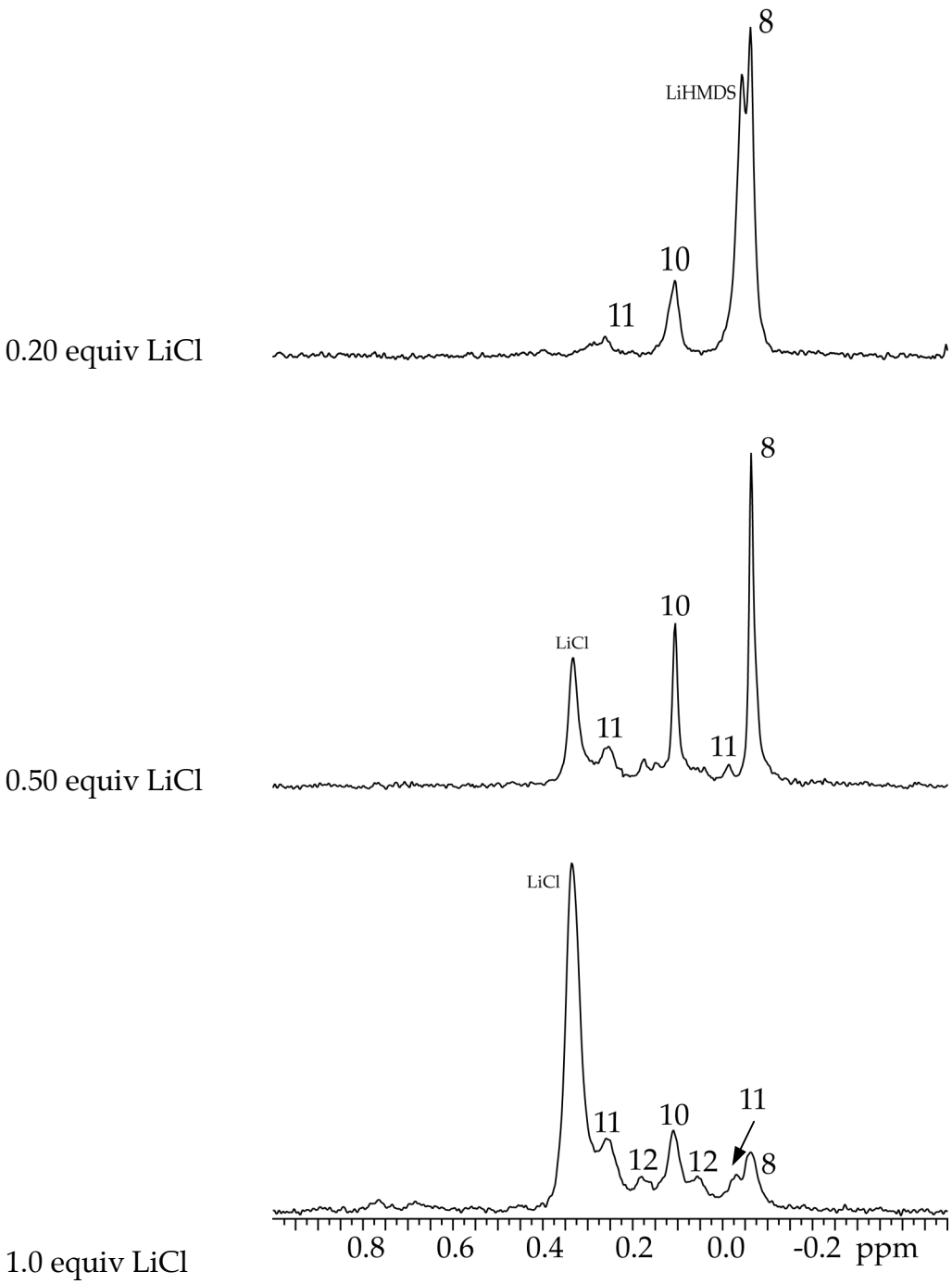

Figure II.5. ^{6}Li NMR spectra of enolate **8** (0.10 M) with various equivalents of LiCl in neat THF at -110 °C. **12** may correspond to the 2:2 enolate-LiCl mixed tetramer.

Adding LiCl to cyclohexanone-derived enolate (generated in situ from recrystallized $Et_3N{\cdot}HCl$[19]) in varying THF concentrations led to another anomaly. The samples were prepared and stored in a -78 °C bath and observed by ^{6}Li NMR spectroscopy at -110 °C (Figure II.6). The resulting spectra show large amounts of noise in the baseline and an equally large number of virtually indistinguishable resonances (Figure II.6A-C). Warming the samples to 0 °C for 30 minutes and re-recording the spectra at -110 °C results in sharp, baseline-separated resonances (Figure II.6D-F). This pronounced aging effect also suggests that there may be an equilibration problem.

Similar mixed aggregate studies were performed with LiBr, again formed in situ by adding $Et_3N{\cdot}HBr$/LiHMDS stock solution to the enolate solution. The ^{6}Li NMR spectra display significantly less mixed aggregates than were observed using LiCl (Figure II.7).

^{1}H NMR spectroscopy proved to be a useful tool in monitoring the behavior of the enolate-LiCl mixed aggregates. In THF-d_8, the vinyl proton of each species has a distinct resonance (Figure II.8), allowing us to monitor all components of the reaction simultaneously. Injecting TMSCl directly into the enolate solution while collecting ^{1}H spectra enables us to observe the reaction in its entirety. The enolate decay and silyl enol ether formation show sigmoidal curvature as expected and the maximum concentration of enolate-LiCl mixed aggregates correlates with the maximum rate of enolate decay (Figure II.9).

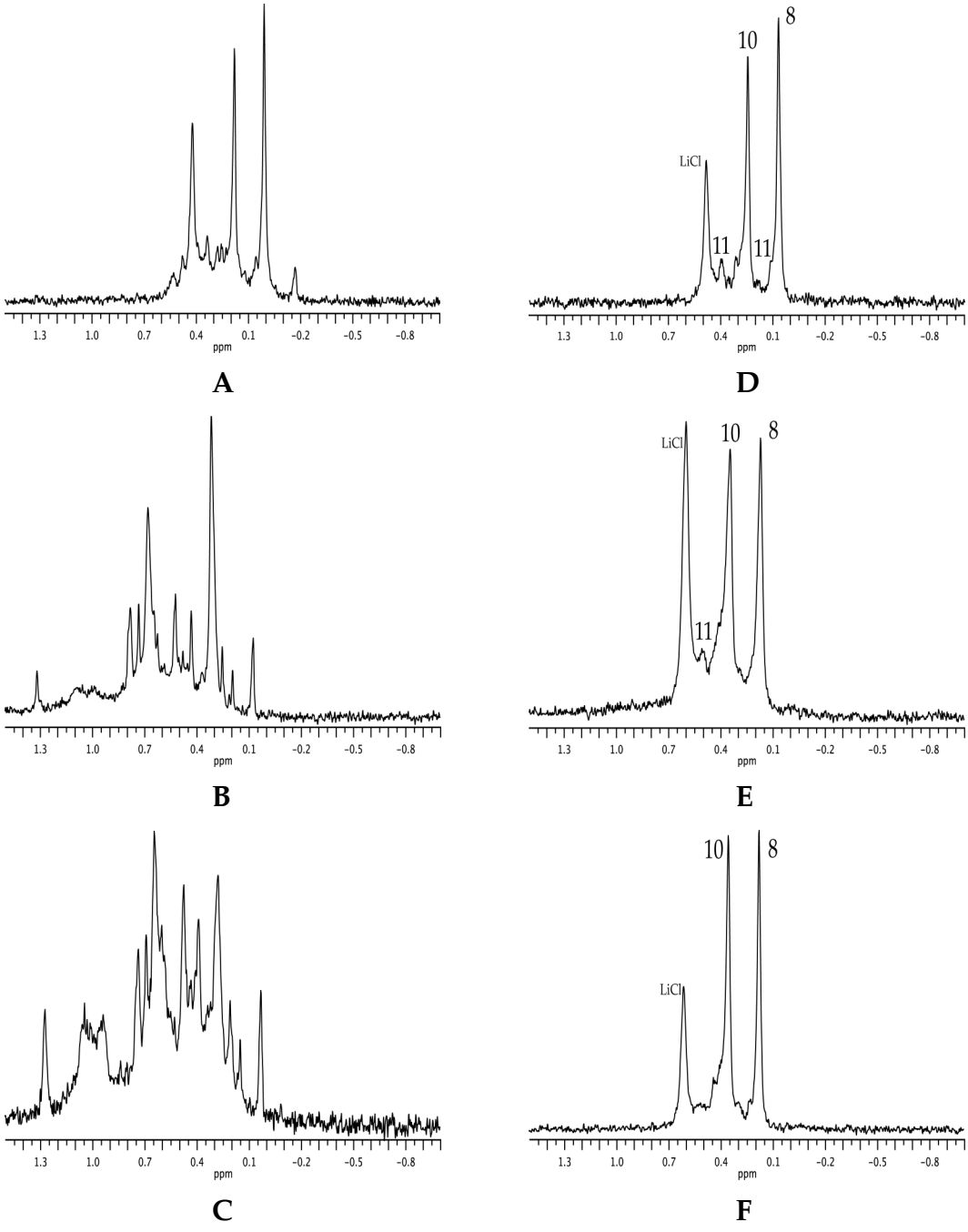

Figure II.6. ^{6}Li NMR spectra of enolate **8** (0.10 M) with LiCl (0.50 equiv) in (**A**,**D**) 9.0 M THF/pentane, (**B**,**E**) 6.0 M THF/pentane, and (**C**,**F**) 4.0 M THF/pentane at -110 °C.

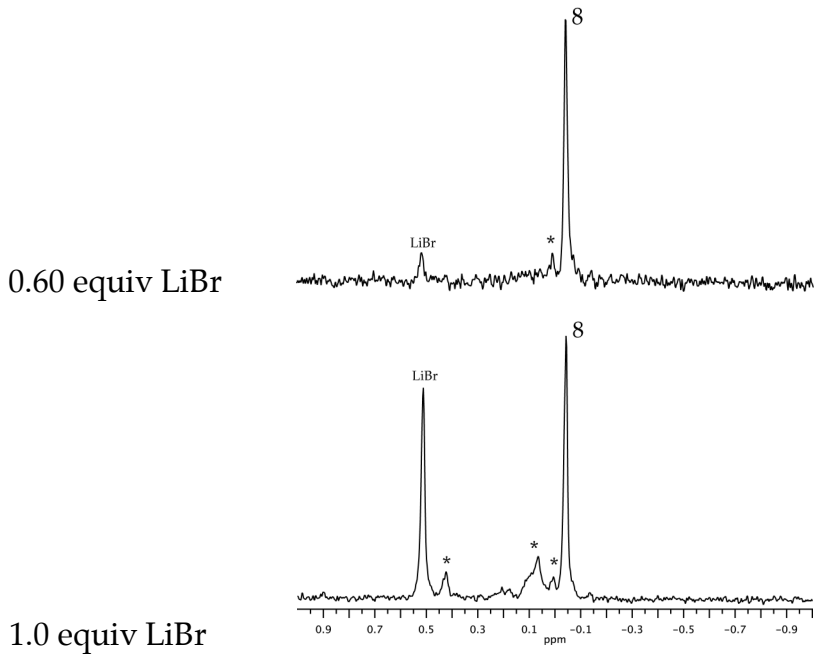

Figure II.7. ^{6}Li NMR spectra of enolate **8** (0.10 M) with various equivalents of LiBr in neat THF at -110 °C. * Denotes probable enolate-LiBr mixed aggregates.

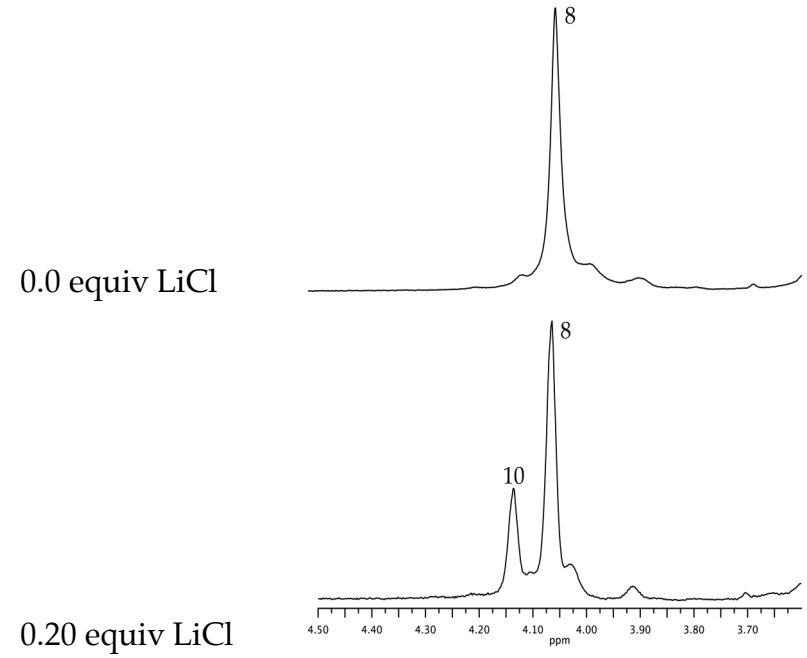

Figure II.8. ^{1}H NMR spectra of enolate **8** (0.10 M) with various equivalents of LiCl in neat THF-d_8 at -110 °C. The resonances shown correspond to the vinyl proton of the indicated species.

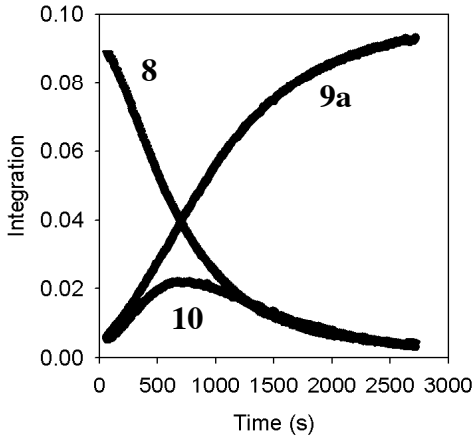

Figure II.9. Plot of the decay of enolate **8** (0.10 M), formation of silyl enol ether **9a**, and enolate-LiCl mixed dimer **10** in neat THF at -90 °C by monitoring the vinyl proton resonances by ^{1}H NMR spectroscopy. TMSCl (5.0 equiv) was added to the enolate solution.

In the reactions described previously, TMSCl was added to a solution of enolate **8**. However, a commonly used technique involves mixing the lithium amide base and the silylating agent prior to ketone addition, a so-called in situ trap. Following this procedure gave vastly different results.

Mixing LDA and TMSCl in THF at -78 °C prior to adding cyclohexanone results in an initial burst of formation of silyl enol ether **9a**. At approximately 85% conversion, the reaction slows significantly (Figure II.10). We turned to ^{6}Li NMR spectroscopy to determine if LDA was still present in the solution. LDA/TMSCl mixtures were prepared and stored in a -78 °C bath and ^{6}Li NMR reveals that LDA has not reacted with TMSCl and is the sole species observed. If the sample is warmed even slightly, however, TMSCl and LDA react and only LiCl is observed by NMR spectroscopy.

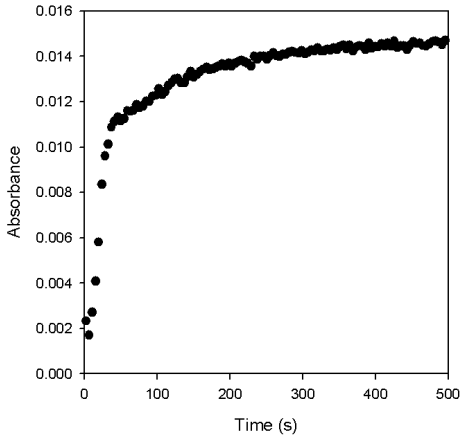

Figure II.10. Plot of the formation of **9a** in neat THF at -78 °C. LDA (0.03 M) and TMSCl (0.25 M) were mixed in the reaction vessel prior to the addition of cyclohexanone (0.025 M).

In addition to the initial burst of reactivity, a second oddity is observed. Monitoring this reaction by in situ IR spectroscopy reveals that there is an absence of both ketone and enolate absorbances, yet product formation is not instantaneous (Figure II.11). The absence of these absorbances indicates that LDA may be reacting with ketone in a 1,2-addition reaction prior to forming silyl enol ether **9a** (eq 3). This type of reaction was previously observed in the Collum group when 2-methylcyclohexanone with LiHMDS/pyrrolidine mixtures resulted exclusively in the 1,2-addition of pyrrolidine.[20]

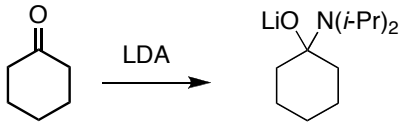

(3)

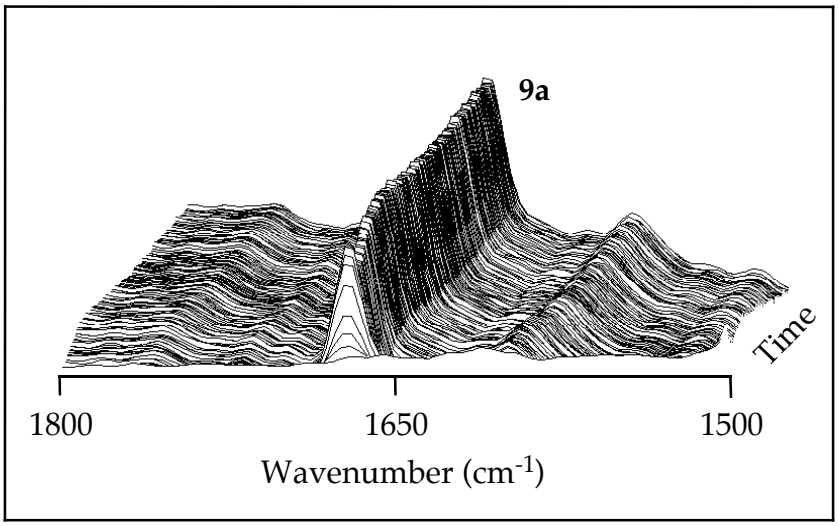

Figure II.11. In situ IR spectra for the silylation of enolate **8** (0.025 M) in neat THF at -78 °C. LDA (0.03 M) and TMSCl (0.25 M) were mixed at -78 °C prior to addition of cyclohexanone (**7**).

Reproducibility of the O-silylation of enolate **8** has been extremely problematic, as the reaction appears to be very sensitive to the reaction conditions. The induction periods vary drastically under theoretically identical conditions (Figure II.12). The cause of the change in induction period could potentially be due to varying amounts of LiCl present in the LDA. Typical curve fitting techniques are difficult due to the extreme irreproducibility of the collected data.

Despite numerous difficulties during these studies, we hoped to obtain data that would provide insight into the reaction mechanism of O-silylations. We attempted to obtain the TMSCl order at low THF concentrations to avoid convolution due to the sigmoidal behavior observed at high THF concentrations; preliminary experiments suggest that the reaction is first order in TMSCl.

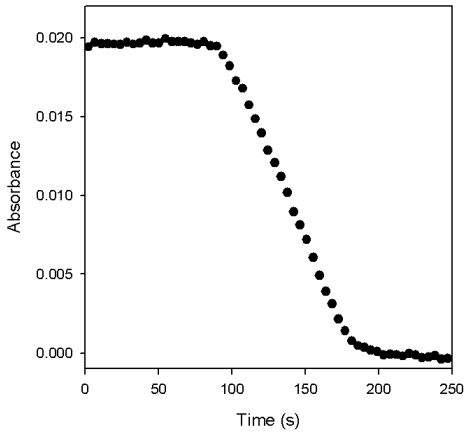

A

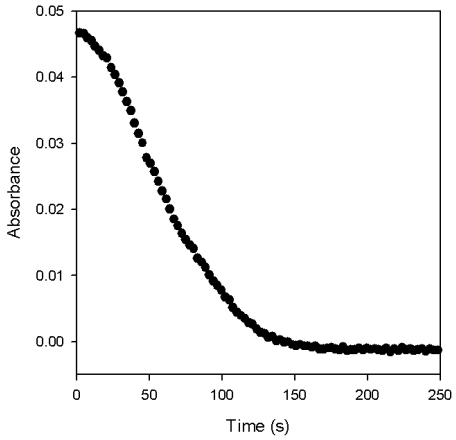

B

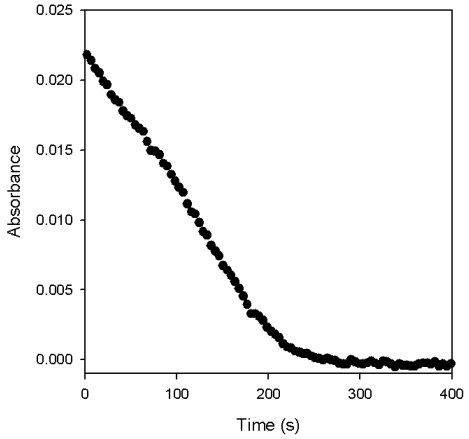

C

Figure II.12. Plots of the decay of enolate **8** (0.025 M) under theoretically identical conditions in neat THF at -78 °C. TMSCl (10 equiv) was added to the enolate solution.

TMSCl Silylations of the Cyclopentanone-derived Enolate. Due to the structural similarity, we had initially assumed that the O-silylation of the cyclopentanone-derived enolate **13** (eq 4) using TMSCl would show a decay comparable to enolate **8**. Once again, our assumption was proven incorrect. While the decay of enolate **13** still shows sigmoidal curvature indicative of autocatalysis, it reacts approximately 10 times faster than enolate **8**. The induction period was difficult to capture, even using a rapid scan interval (a spectrum every 3 seconds) at low temperatures using in situ IR spectroscopy (Figure II.13A). When compared to cyclohexanes, cyclopentanes often show odd reactivities that are normally attributed to changes in hybridization,[21] but there is no change in hybridization during O-silylation.

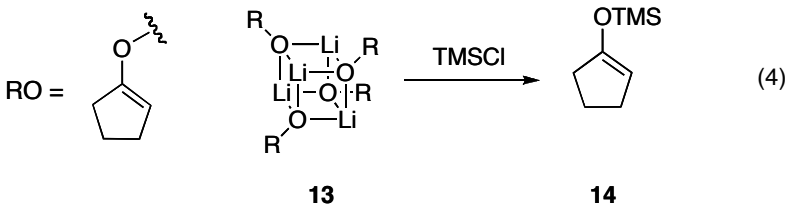

13 **14** (4)

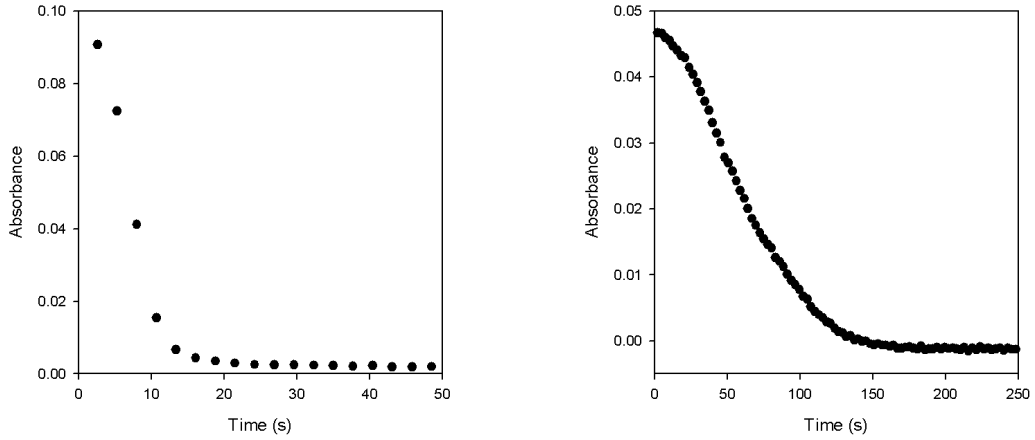

A **B**

(1 spectrum/3 sec) **(1 spectrum/30 sec)**

Figure II.13. Plots of the decay of 0.025 M solutions of enolate (**A**) **13** and (**B**) **8** in neat THF at -78 °C. TMSCl (10 equiv) was added to the enolate solution.

We again turned to ^{6}Li NMR spectroscopic studies to determine the cyclopentanone enolate-LiCl interactions. The spectra show that cyclopentanone enolate forms significant amounts of enolate-LiCl mixed trimer (**16**), but enolate-LiCl mixed dimer (**15**) is not present until at least one equivalent of LiCl has been added to the enolate (Figure II.14). This observation suggests that the enolate-LiCl mixed trimer reacts more rapidly than the corresponding enolate-LiCl mixed dimer.

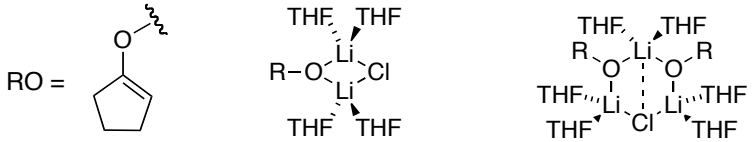

15 **16**

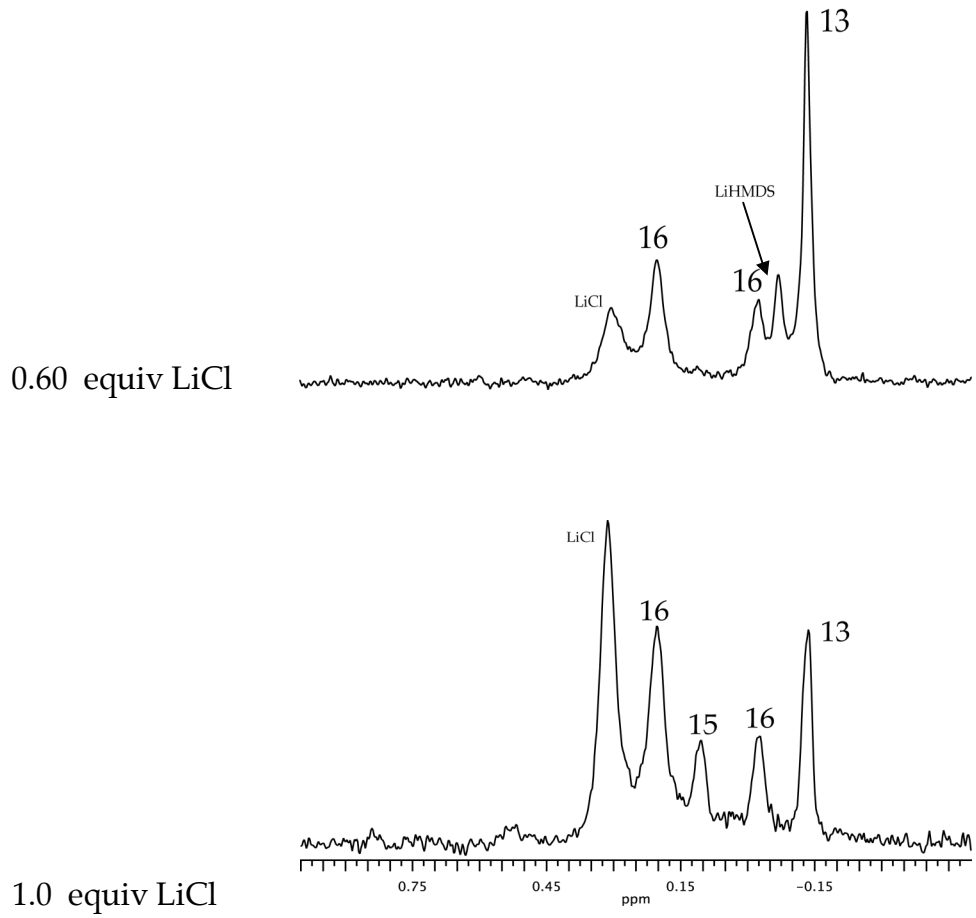

Figure II.14. ^{6}Li NMR spectra of enolate **13** (0.10 M) with various equivalents of LiCl in neat THF at -110 °C.

TMSCl Silylations of the Cycloheptanone-derived Enolate. O-silylation of the cycloheptanone-derived enolate **16** (eq 5) using TMSCl displayed similar behavior to that of cyclohexanone. Monitoring the reaction by in situ IR spectroscopy shows that the reaction rates are nearly identical (Figure II.15), and ^{6}Li NMR spectroscopic studies show a prevalence of enolate-LiCl mixed dimer and very little enolate-LiCl mixed trimer (Figure II.16). One oddity that cannot be ignored is a slight upward curvature during the induction period, perhaps due to an intermediate that coincidentally has the same IR absorbance as the enolate. Further studies to determine the cause

of this behavior have not yet been completed.

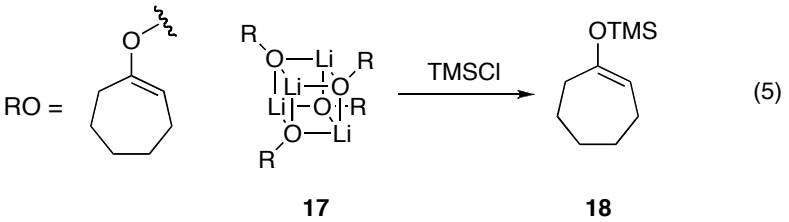

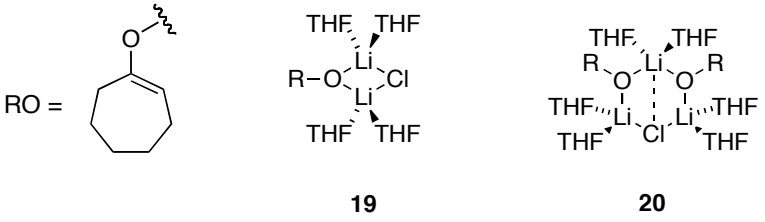

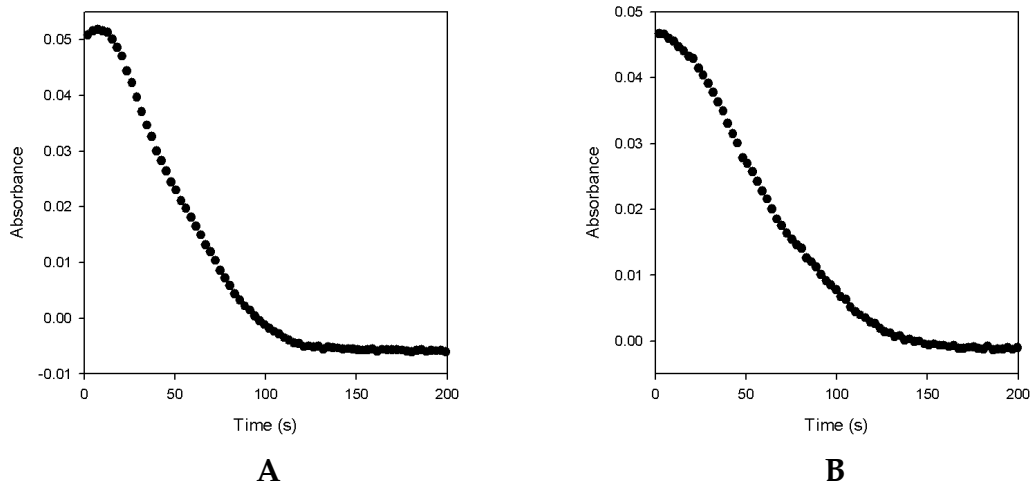

Figure II.15. Plots of the decay of 0.025 M solutions of enolate (**A**) **17** and (**B**) **8** in neat THF at -78 °C. TMSCl (10 equiv) was added to the enolate solution.

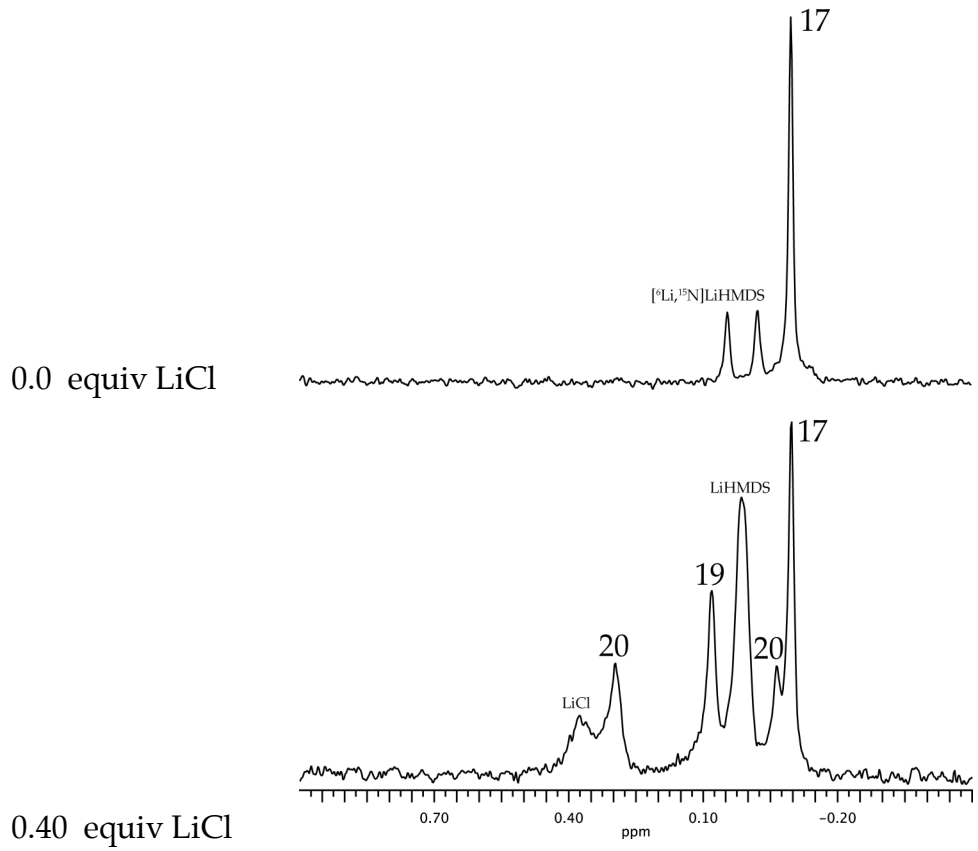

Figure II.16. ^{6}Li NMR spectra of enolate **17** (0.10 M) in neat THF at -110 °C formed from [^{6}Li,^{15}N]LiHMDS. {^{15}N}^{6}Li spectrum of enolate **17** (0.10 M) with 0.40 equiv LiCl in neat THF at -110 °C.

TMSCl Silylations of the Tetralone-derived Enolate. Studies on the O-silylation of the tetralone-derived enolate **21** in THF (eq 6) stem from a potential collaboration with Amgen. Decay of the enolate was monitored by in situ IR spectroscopy. Early experiments showed first-order exponential decay of the enolate (Figure II.17). However, these results were not always reproducible and the resulting plots showed discontinuities in the curves (Figure II.18). These discontinuities were observed at different stages of the reaction, varying solvent concentrations, and emerge as anything from a dip to a break in the curve.

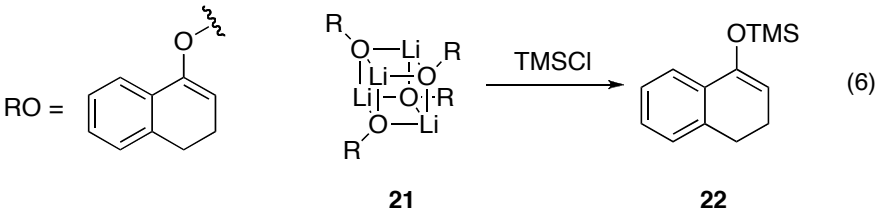

(6)

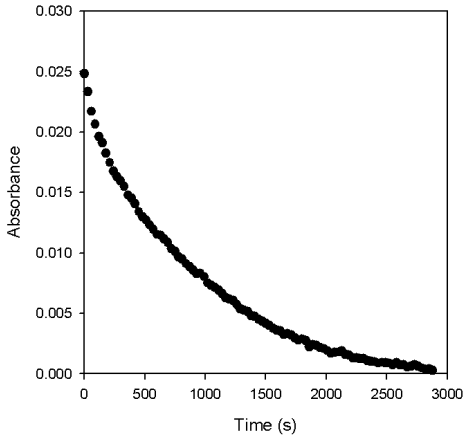

Figure II.17. Plot of the decay of enolate **21** (0.025 M) in 9.0 M THF/pentane at -78 °C. TMSCl (6.0 equiv) was added to the enolate solution.

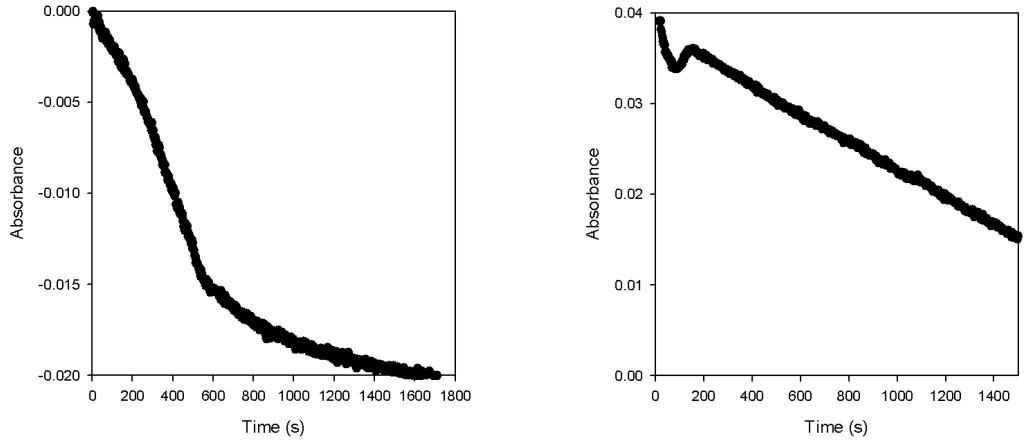

Figure II.18. Plots of the decay of enolate **21** (0.05 M) at -78 °C showing the different types of discontinuities of the decay. TMSCl (6.0 equiv) was added to the enolate solution.

We thought that these problems were mechanical in nature. Several control experiments were performed on the method of data collection, first comparing the normal collection rate versus rapid collect and then comparing the enolate decaying to zero versus monitoring its decay as a negative peak (by zeroing the baseline post enolate formation). Neither of these methods showed any major differences, so we turned to the processing of the data, trying different ways of integrating the IR absorbance of the enolate; however, this was also unsuccessful. The inconsistency of the discontinuities – appearing at varying points in the reaction and looking quite different in each instance – provided little opportunity to determine their origin.

Since the discontinuities in the enolate decays appeared to be experimentally derived, they might stem from solubility issues. Replacing pentane with toluene as the hydrocarbon cosolvent does result in smooth curvature, but also introduces another unexpected observation – a large medium effect. As the concentration of toluene increases, the reaction proceeds at a markedly reduced rate (Figure II.19). This could be due to π interactions between enolate **21** and toluene.

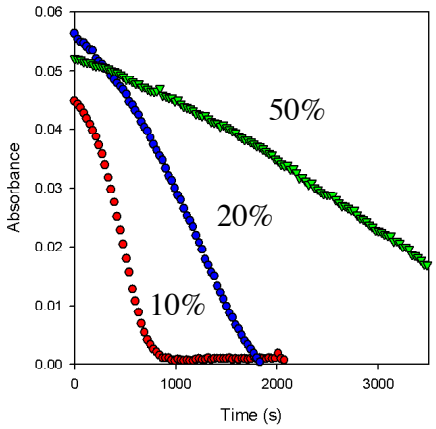

Figure II.19. Plot of the decay of **21** (0.05 M) at -78 °C in 2.0 M THF/pentane/toluene. The percentage of toluene was varied. TMSCl (6.0 equiv) was added to the enolate solution.

TMSCl Silylations of Miscellaneous Enolates. The inconsistent results for the O-silylation of the tetralone-derived enolate **21** directed us to the indanone-derived enolate **23** (eq 7) due to its reliable behavior[3] and structural similarity. O-Silylation with TMSCl in THF results in sigmoidal behavior consistent with LiCl autocatalysis (Figure II.20A). Enolate **23** reacts more rapidly than enolate **21**. This observation is consistent with 5-membered rings being more reactive than their 6-membered ring counterparts, as observed with cyclopentanone versus cyclohexanone.

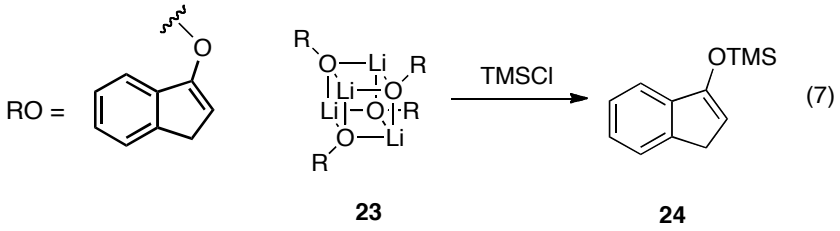

(7)

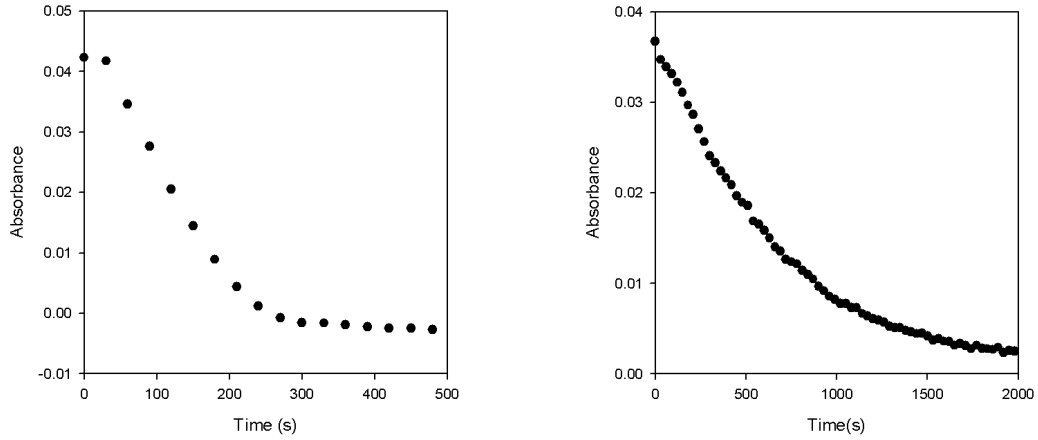

Figure II.20. Plots of the decays of enolate (**A**) **23** (0.025 M) and (**B**) **21** (0.025 M) at -78 °C in 2.0 M THF/pentane. TMSCl (6.0 equiv) was added to the enolate solution.

Introducing a fluorine atom into the ketone increases the reactivity even further. Monitoring a variety of fluorinated enolates by in situ IR spectroscopy shows that many enolates react at intractably high rates even at -78 °C (Figure II.21).

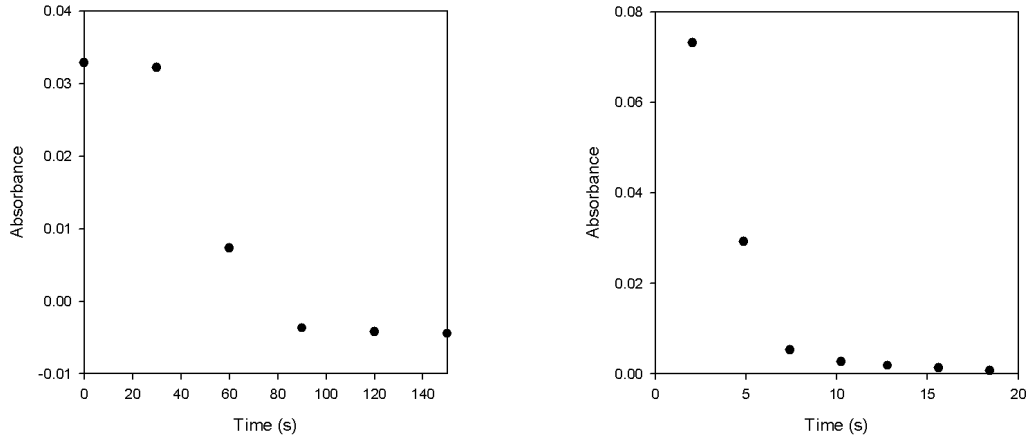

A **B**

(1 spectrum/30 sec) **(1 spectrum/3 sec)**

Figure II.21. (**A**) Plot of the decay of the 5-fluoroindanone-derived enolate (0.025 M) in neat THF. TMSCl (6.0 equiv) was added to the enolate solution. (**B**) Plot of the decay of 2′,3′,4′,5′,6′-pentafluoroacetophenone-derived enolate (0.05 M) in neat THF at -78 °C. TMSCl (10 equiv) was added to the enolate solution.

TMS Imidazole Studies. We thought that we could influence—possibly preclude—mixed aggregates and autocatalysis by using silyl imidazole as the silylating agent.[6] Silylation of enolate **8** using TMS imidazole in neat THF, however, does not give a clean enolate decay (Figure II.22). Using TMS imidazole as the silylating agent for other enolates produced similar results.

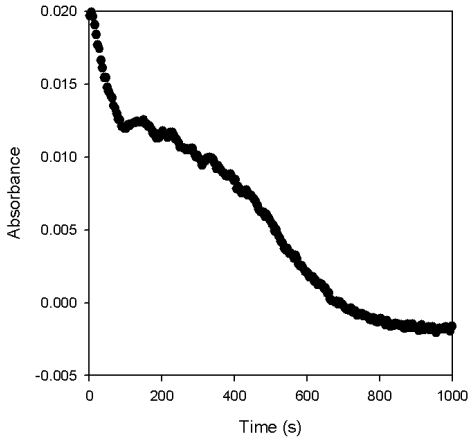

Figure II.22. Plot of the decay of the enolate **8** (0.025 M) in neat THF at -78 °C using TMS imidazole (10 equiv) as the silylating agent.

Silyl Triflate Studies. We turned our attention to silyl triflates (eq 8) as a potentially cleaner silylating agent.[5] We focused our attention on cyclohexanone-derived enolate **8** and used a variety of silyl triflates. Initially, we turned to the commonly used trimethylsilyl trifluoromethanesulfonate (TMSOTf). Enolate **8** reacts cleanly and at a tractable rate, but it does not follow a first order exponential decay, indicating underlying mechanistic complexity (Figure II.23).

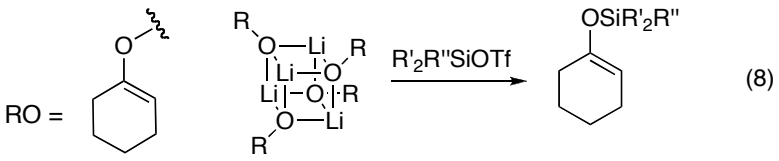

(8)

8

9b: R' = R'' = *i*-Pr

9c: R' = R'' = Et

9d: R' = Me, R'' = *t*-Bu

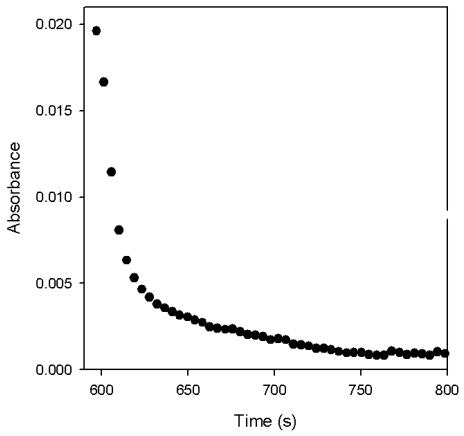

Figure II.23. Plot of the decay of the enolate **8** (0.025 M) in neat THF at -78 °C using TMSOTf (10 equiv) as the silylating agent. Complete enolate formation was allowed prior to addition of TMSOTf.

Triisopropylsilyl trifluoromethanesulfonate (TIPSOTf), another commonly used silyl triflate, was also tested as the silylating agent in neat THF. Under these conditions, enolate **8** displays an initial burst of reactivity, followed by a significant stalling of the reaction (Figure II.24). The substantial decrease in reactivity relative to the TMSOTf experiments could be due to a more sterically hindered silyl triflate. In addition to the stalling of the reaction, it appears that cyclohexanone may reform during the reaction. In situ IR spectroscopy shows a peak appearing at exactly the same absorbance as the carbonyl group of cyclohexanone (Figure II.25). We typically do not see reversible enolization, so this could also be attributed to C-silylation of cyclohexanone.

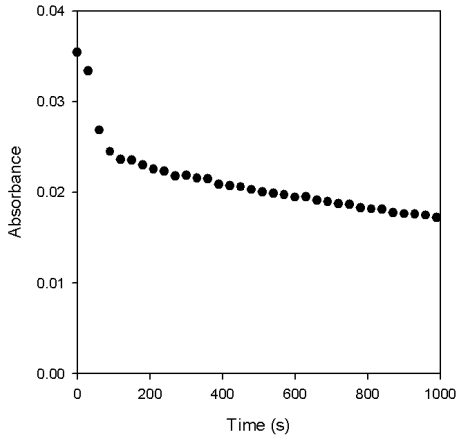

Figure II.24. Plot of the decay of the enolate **8** (0.025 M) in neat THF at -78 °C using TIPSOTf (10 equiv) as the silylating agent.

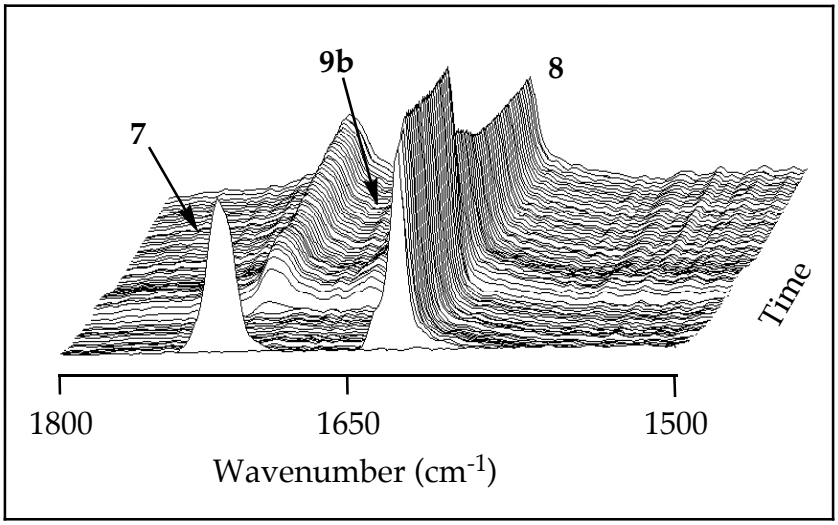

Figure II.25. In situ IR spectra for the silylation of enolate **8** (0.025 M) in neat THF at -78 °C using TIPSOTf (10 equiv) as the silylating agent.

Upon reacting with triethylsilyl trifluoromethanesulfonate (TESOTf), enolate **8** follows a sigmoidal decay with a small induction period (Figure II.26). A peak coinciding with the absorbance of cyclohexanone appears in this reaction, similar to what was observed with TIPSOTf (Figure II.27).

Again, this could be due to a reversible enolization or C-silylation of cyclohexanone.

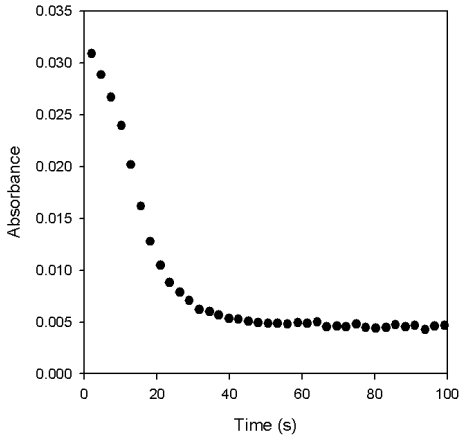

Figure II.26. Plot of the decay of the enolate **8** (0.025 M) in neat THF at -78 °C using TESOTf (10 equiv) as the silylating agent.

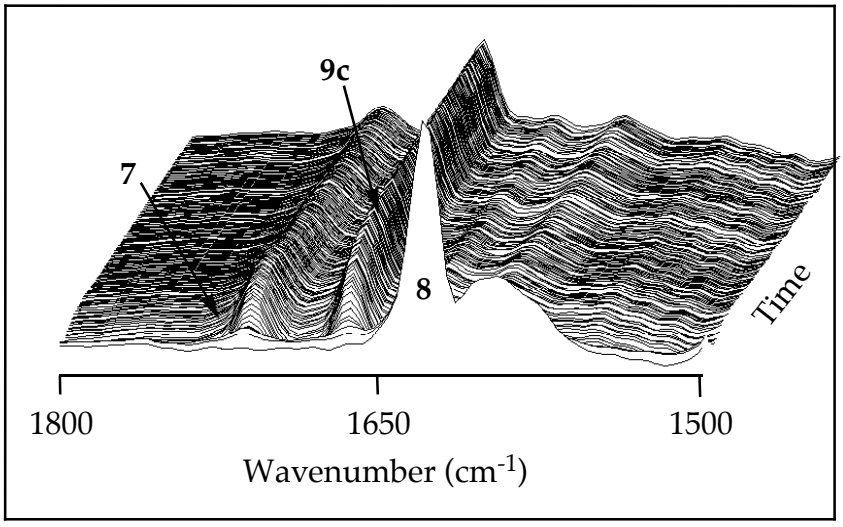

Figure II.27. In situ IR spectra for the silylation of enolate **8** (0.025 M) in neat THF at -78 °C using TESOTf (10 equiv) as the silylating agent.

Lastly, we turned to *tert*-butyldimethylsilyl trifluoromethanesulfonate (TBSOTf) studies in neat THF. Monitoring enolate decay by in situ IR, a sigmoidal curve is observed with a significant induction period (Figure II.28). Following the same pattern as the other silyl triflate studies, a peak appears at exactly the same absorbance as cyclohexanone; however, this species is depleted as the reaction continues, unlike the other silyl triflate experiments. Furthermore, the maximum concentration of the new species correlates with the maximum reactivity of the enolate, similar to what would be observed with autocatalysis. While it seems highly unlikely that either C-silylated cyclohexanone would cause autocatalysis, it is an odd coincidence that we cannot ignore.

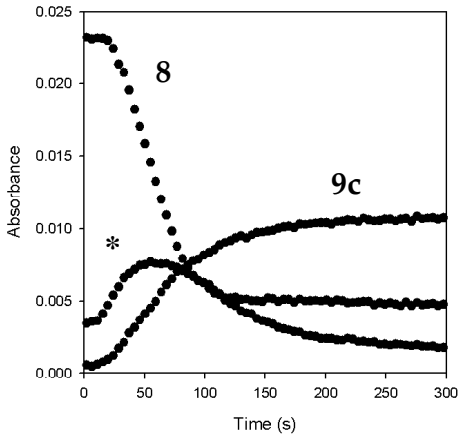

Figure II.28. Plot of the decay of the enolate **8** (0.025 M) in neat THF at -78 °C using TBSOTf (10 equiv) as the silylating agent. * Corresponds to the new species.

Silyl Triflate Studies (in situ traps). The initial silyl triflate studies involved complete formation of the enolate prior to adding the silyl triflate. However, it is common practice to mix lithium amide base and silyl triflate

prior to ketone addition, a so-called in situ trap of the enolate.

Mixing LDA or LiHMDS with TMSOTf in neat THF at -78 °C followed by addition of cyclohexanone does not result in the formation of silyl enol ether **9a**. In situ IR spectroscopy shows only an absorbance for cyclohexanone. Applying the same method using LDA and TIPSOTf in neat THF at -78 °C results in the formation of a small amount of silyl enol ether **9b**, while a significant amount of cyclohexanone remains (Figure II.29). Similar results were observed using LDA and TESOTf (Figure II.30).

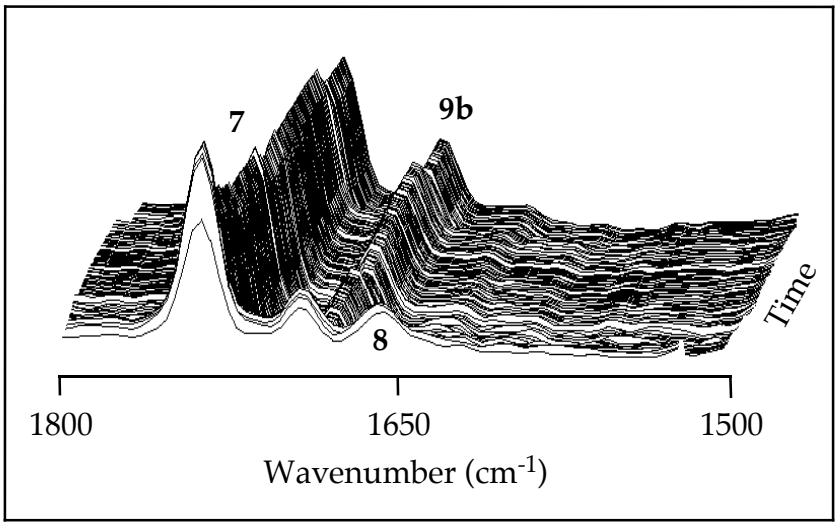

Figure II.29. In situ IR spectra for the silylation of enolate **8** (0.025 M) in neat THF at -78 °C using TIPSOTf (10 equiv) as the silylating agent.

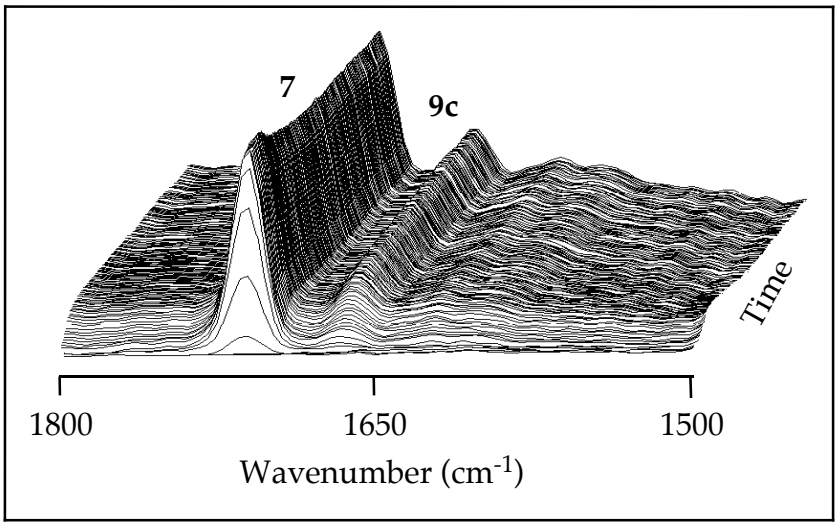

Figure II.30. In situ IR spectra for the silylation of enolate **8** (0.025 M) in neat THF at -78 °C using TESOTf (10 equiv) as the silylating agent.

Mixing LDA and TBSOTf in neat THF at -78 °C followed by addition of cyclohexanone results in unexpected behavior. Cyclohexanone is depleted at a tractable rate and formation of silyl enol ether **9d** appears to follow a first order growth, although the fit is admittedly not perfect (Figure II.31). Whereas **9d** did form, the IR spectra show no significant enolate formation, indicating that the product forms directly from the starting ketone (Figure II.32).

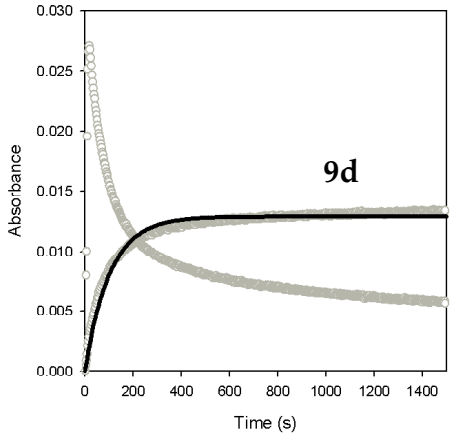

Figure II.31. Plot of the decay of the ketone **7** (0.025 M) and growth of the silyl enol ether **9d** in neat THF at -78 °C using TBSOTf (10 equiv) as the silylating agent. LDA and TBSOTf were mixed prior to ketone addition.

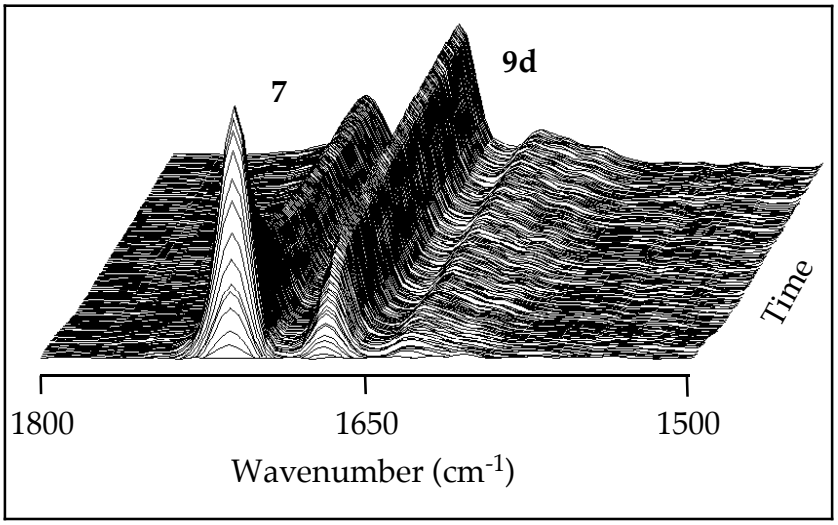

Figure II.32. In situ IR spectra for the silylation ketone **7** (0.025 M) in neat THF at -78 °C using TBSOTf (10 equiv) as the silylating agent.

We turned to NMR spectroscopy to gain insight into the behavior of LDA and silyl triflates. A sample of 10:1 silyl triflate:[^{6}Li]LDA shows only a single resonance by ^{6}Li NMR spectroscopy (Figure II.33). The resonance appears at the same chemical shift for mixtures of LDA and TESOTf, TIPSOTf,

and TBSOTf, indicating that the new species is independent of the silyl group and is, therefore, lithium triflate (LiOTf) (eq 9). ^{29}Si NMR spectra display a resonance for silyl triflate as well as a new resonance, presumed to be silylamine. These observations are both odd and intriguing – what we thought to be enolate chemistry clearly is not, yet the silyl enol ether product still forms.

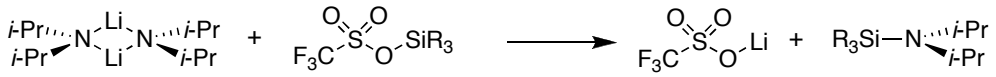

(9)

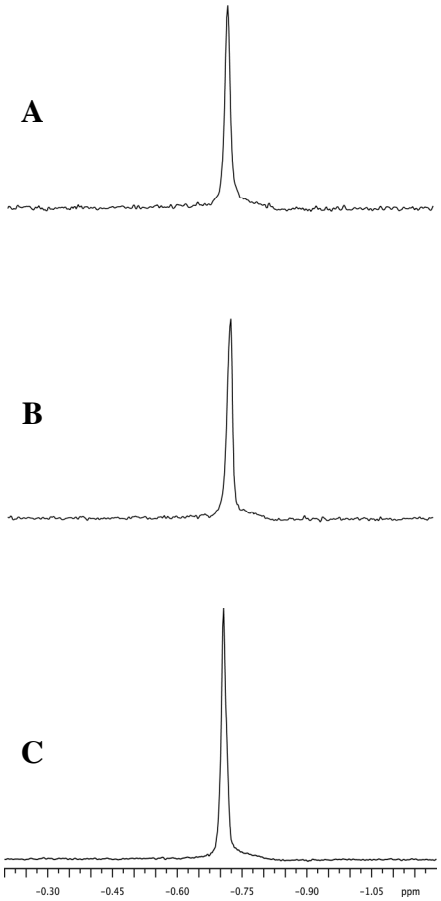

Figure II.33. ^{6}Li NMR spectra of mixtures of 10:1 silyl triflate:[^{6}Li]LDA at -78 °C. The samples contain the following silyl triflates: (**A**) TESOTf, (**B**) TIPSOTf, and (**C**) TBSOTf. The observed species is [^{6}Li]LiOTf.

Lithium Triflate Experiments. Due to the formation of silyl enol ether in the presence of lithium triflate and silylamine, enolate formation appears to be unnecessary. Several control experiments were performed to determine the reactive species. Lithium triflate is eliminated from the reaction simply by adding commercial silylamine to cyclohexanone in neat THF. There is no reaction at -78 °C; however, warming to 0 °C shows a small amount of silyl enol ether formation, which converts back into the starting ketone (Figure II.34). This shows that lithium triflate is required for the reaction to take place.

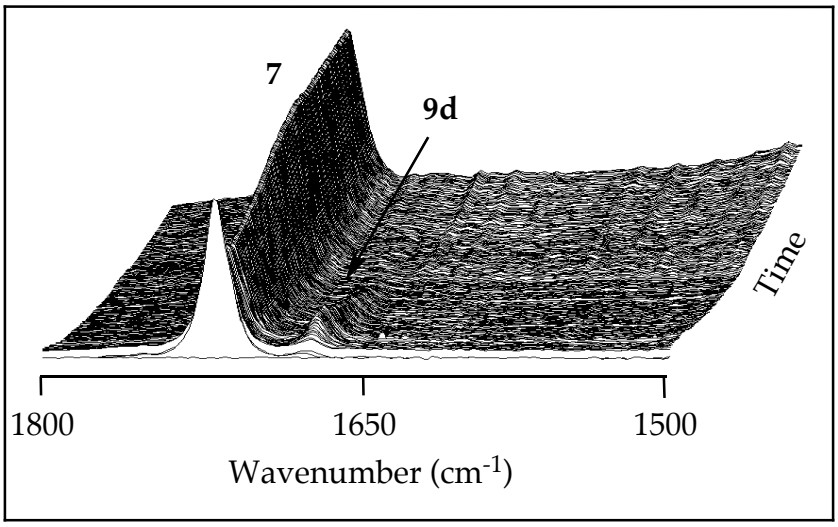

Figure II.34. In situ IR spectra for the silylation of ketone **7** (0.025 M) in neat THF at 0 °C using TBSOTf (10 equiv) as the silylating agent.

We began to wonder if excess silyl triflate was necessary in the reaction. Cyclohexanone was added to a reaction containing LDA and a slight deficiency of TBSOTf. At -78 °C, no reaction is observed. Upon adding additional TBSOTf, silyl enol ether **9d** does form, indicating that excess silyl triflate is indeed a requirement for the reaction.

The last set of control experiments involved eliminating the silylamine

from the reaction. Adding cyclohexanone to a mixture of 1.2 equiv commercial LiOTf, 1.2 equiv Et_3N, and 10 equiv TBSOTf in neat THF at -78 °C results in silyl enol ether forming immediately, followed by stalling of the reaction. The reaction goes to completion upon adding an additional 2.8 equiv Et_3N (Figure II.35).

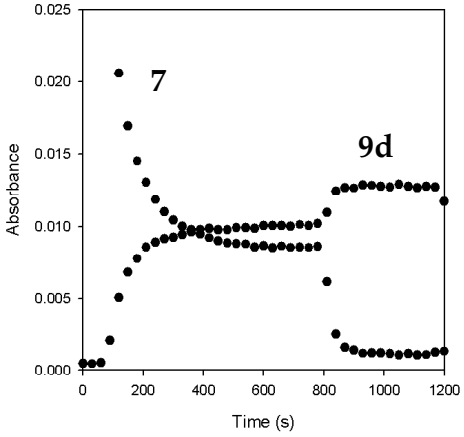

Figure II.35. Plot of the decay of ketone **7** (0.025 M) and growth of the silyl enol ether **9d** in neat THF at -78 °C using TBSOTf (10 equiv) as the silylating agent in the presence of LiOTf and Et_3N. Additional Et_3N was added approximately 800 seconds into the reaction.

The new protocol for silyl enol ether formation was tested using 4-*t*-butylcyclohexanone as a substrate. Ketone was added to a vessel containing 1.2 equiv LiOTf, 4.0 equiv Et_3N, and 8.0 equiv TBSOTf in neat THF at -78 °C. After 1 hr, the reaction was quenched with distilled water and subjected to a typical aqueous workup. The silyl enol ether product was isolated in 89% yield. Not only is this new method for synthesizing silyl enol ethers simple and fast, but also the conditions are mild and the use of lithium amides can be avoided.

We then turned to 3-pentanone (**25**) as a substrate, hoping that the new silyl enol ether synthesis would result in good E/Z selectivities (eq 10). After many attempts at controlling selectivities, the results show that the Z enolate is always favored and the selectivities are modest at best (~5:1).

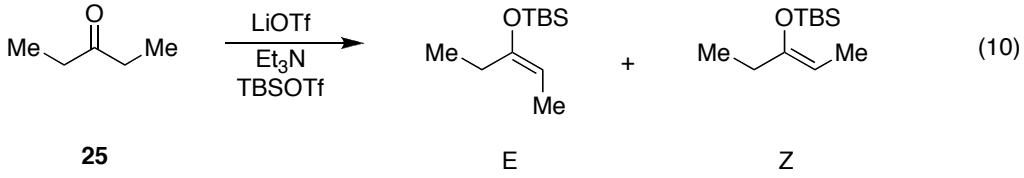

Lastly, we decided to test the new reaction using an alcohol rather than ketone. Upon adding 1,1-diphenylethanol (**26**) to a mixture of lithium triflate, Et_3N, and TBS triflate, no reaction is observed. Adding cyclohexanone to this reaction results in the rapid formation of silyl enol ether **9d** (eq 11, Figure II.36). This may be significant in multi-step syntheses involving multiple functional groups since the silyl triflate will react with only ketone and not tertiary alcohols. It is important to note, though, that further experiments would have to be completed before this method can be generalized.

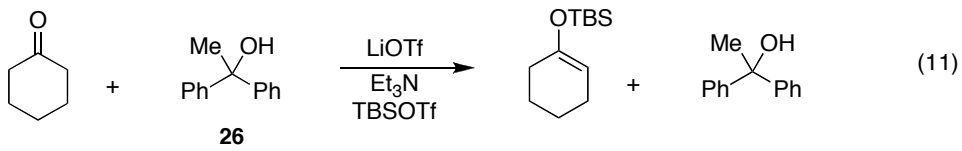

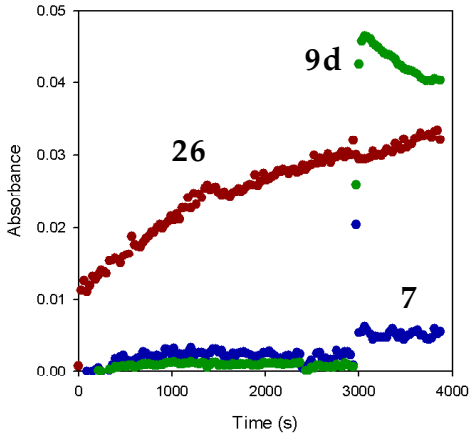

Figure II.36. Plot of the decay of ketone **7** (0.025 M) and growth of the silyl enol ether **9d** in neat THF at -78 °C. TBSOTf (10 equiv) was used as the silylating agent in the presence of **26**, LiOTf, and Et_3N. Cyclohexanone was injected after 3000 seconds.

1,2-addition of LDA to Ketone. Throughout the O-silylation studies, a variety of other odd observations were noted. Using in situ IR spectroscopy, enolate formation was monitored to ensure completion before a silylating agent was added to the reaction vessel. In several instances, the enolate peak grew in at a tractable rate, but the ketone peak disappeared instantly (Figure II.37). We began to wonder if the LDA was reacting with the ketone and forming a 1,2-addition product (eq 3). As a control experiment, enolization of cyclohexanone-2,2,6,6-d_4 using LDA was monitored by in situ IR. The slow enolization and absence of starting ketone suggests that a 1,2-addition of LDA to ketone is possible (Figure II.38).

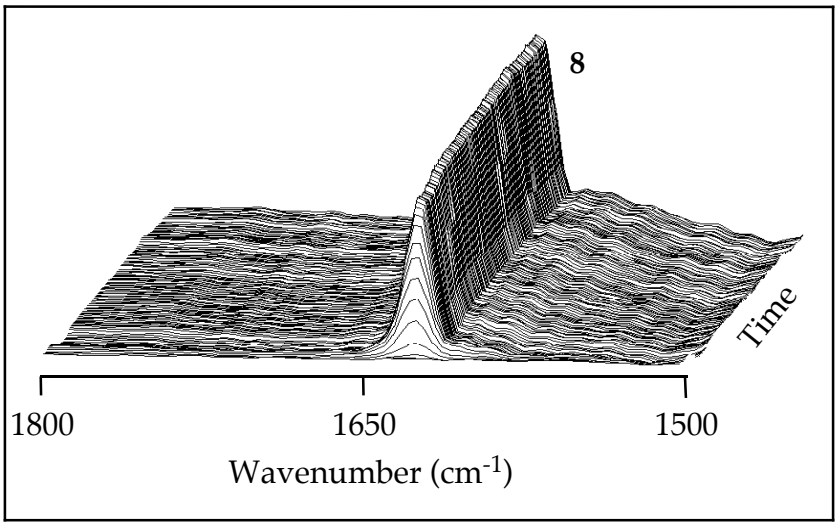

Figure II.37. In situ IR spectra for the enolization ketone **7** (0.025 M) using LDA (0.03 M) in neat THF at -78 °C.

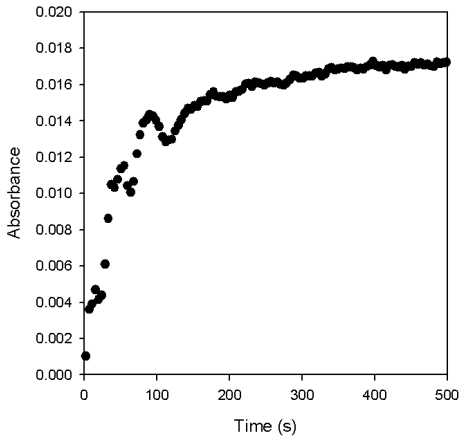

Figure II.38. Plot for the enolization of cyclohexanone-2,2,6,6-d_4 (0.025 M) using LDA (0.03 M) in neat THF at -78 °C.

Side Product Formation. During the initial silylation studies of the cyclohexanone-derived enolate, a side product was often observed during enolization at low THF concentrations. The side product appears immediately and at a slightly lower wavenumber than the cyclohexanone absorbance and

then decays slowly (Figure II.39). Although the product has not yet been isolated or characterized, we believe that this is aldolate product (**27**) formed from cyclohexanone reacting with its own enolate. Control experiments show that upon adding an additional equivalent of cyclohexanone to the enolate, the side product appears, even in neat THF. As this side product increases in concentration, enolate concentration decreases concurrently, which supports the observation of the aldolate product (Figure II.40).

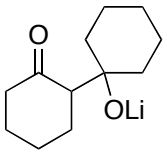

27

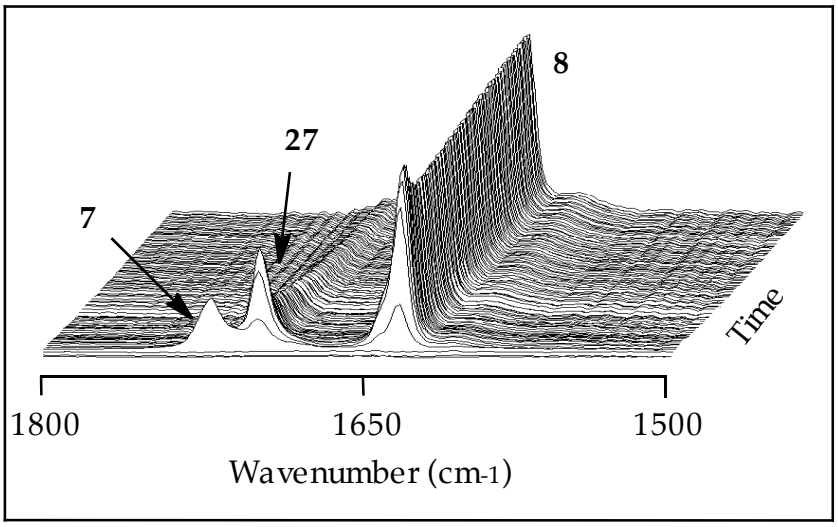

Figure II.39. In situ IR spectra for the enolization of ketone **7** (0.05 M) using LiHMDS (0.06 M) in 2.0 M THF/pentane at -78 °C.

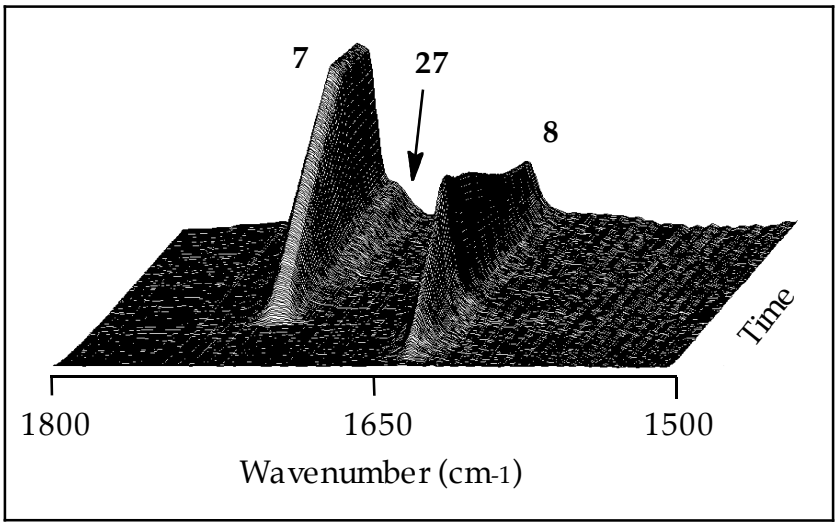

Figure II.40. In situ IR spectra for the enolization of ketone **7** (1.2 M) using LiHMDS (0.06 M) in neat THF at -78 °C.

Perhaps the most perplexing piece of this puzzle is a very broad, strong peak that sporadically appears in the IR spectra. When this absorbance does appear, it forms during the enolization and often varies in size (Figure II.41). Upon addition of a silylating agent, the broad peak is depleted, as if it was being silylated. This reactivity led us to believe that whatever this species is, it does contain lithium. This species, however, does not react at the same rate as the enolate, indicating that the two species are likely not directly related (Figure II.42). The most troubling part is that the species would only appear sporadically. We thought that it might be related to the rate of ketone injection or even due to the rate of stirring (or lack thereof). Despite numerous attempts to determine its origin, we were left empty-handed. We also tried to isolate the species on several occasions but to no avail.

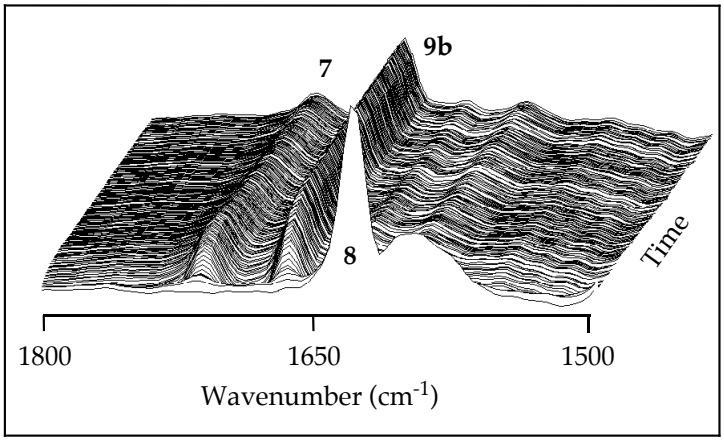

A

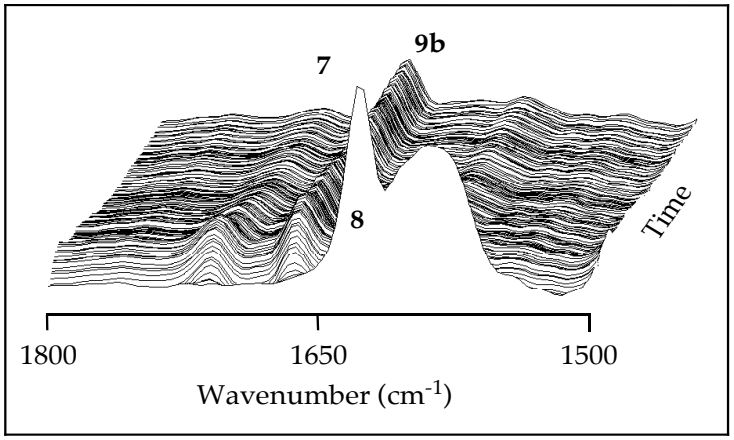

B

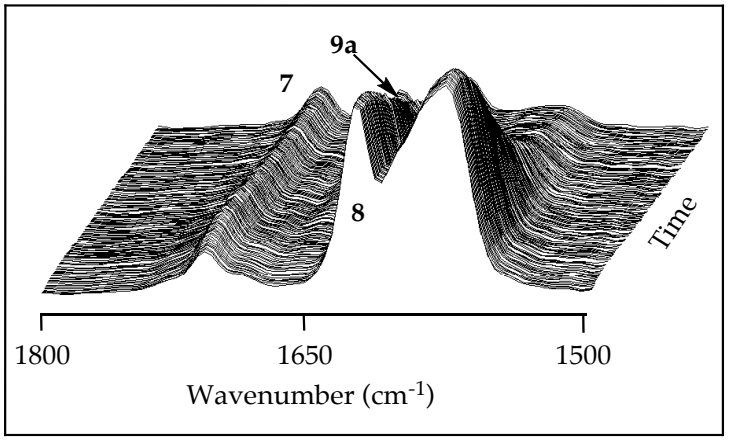

C

Figure II.41. In situ IR spectra showing the side product formation, which appears at 1579 cm^{-1}. The absorbance can range from a smaller shoulder (**A**) to a very large peak (**C**).

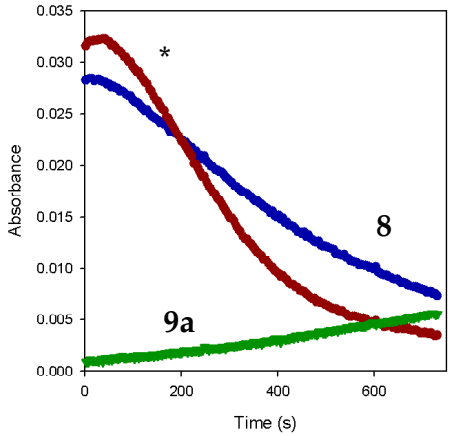

Figure II.42. Plot for silylation of enolate **8** (0.025 M) using TMSCl (1.0 equiv) in neat THF at -78 °C. * Corresponds to the large, broad peak.

Conclusion

We chose to study O-silylations of lithium enolates due to the prevalence of the reaction, as well as the outward appearance of simplicity. We were hoping that silylations would serve as a benchmark for future enolate reactivity studies. Although we observed formation of unexpected side products and had a very difficult time reproducing data, we did gain insight into the effects of LiCl on enolate structure and reactivity.

Although we were not able to elucidate a mechanism for O-silylation reactions, we uncovered many pieces to this complex puzzle and think that each part could be very beneficial to the synthetic community. During our studies, we also developed a way to synthesize silyl enol ethers in high yield and under mild conditions.

A mechanism for this reaction is certainly within reach. We must first understand each of the unexpected observations, why they may have occurred, their effects (if any) on the rate laws, and whether they can be

prevented. Once these relationships are understood, we believe that rate studies will move forward and the mechanism of O-silylations of lithium enolates with a variety of silylating agents will be determined.

Experimental Section

Reagents and Solvents. Substrates are commercially available. THF was distilled from solutions containing sodium benzophenone ketyl. Hydrocarbon solvents were distilled from blue solutions containing sodium benzophenone ketyl with approximately 1% tetraglyme to dissolve the ketyl. [^{6}Li]LiHMDS and [^{6}Li,^{15}N]LiHMDS were prepared and recrystallized as described previously.[22] Air- and moisture-sensitive materials were manipulated under argon using standard glove box, vacuum line, and syringe techniques. Samples for spectroscopic studies were prepared as described in Appendix II.

APPENDIX II

Sample Preparation. Ketone and LiHMDS stock solutions were prepared at room temperature. LDA was cooled to 0 °C prior to adding solvent followed by warming to room temperature. Lithium enolates were prepared from [^{6}Li]LiHMDS or [^{6}Li]LDA in THF/hydrocarbon cosolvent at -78 °C. TMSCl over CaH_2 was freshly distilled. TMSCl was then added to Et_3N (3:1 mole ratio) and centrifuged to separate the $Et_3N{\cdot}HCl$ salt. Silyl triflates were stored under argon and in the freezer if necessary.

Upon complete enolate formation, the silylating agent was added directly to the reaction vessel. The lithium amide base and the silylating agent were mixed in the reaction vessel at -78 °C prior to ketone addition for the in situ trap studies.

The O-silylations were performed under pseudo-first-order conditions ([TMSCl] ≥ 10 x [enolate]). Rates were monitored using in situ IR spectroscopy and ^{1}H NMR spectroscopy.

NMR Spectroscopic Sample Preparation. Ketone stock solutions were prepared at room temperature. LDA mixed with $Et_3N{\cdot}HCl$ was cooled to 0 °C prior to adding solvent followed by warming to room temperature. After flame drying the NMR tube on a Schlenk line and placing it under argon, the tube was placed in a -78 °C dry ice/acetone bath. The appropriate amounts of the base followed by the ketone were added via syringe. All samples had a total volume of 0.60 mL. The tube was sealed under partial vacuum and immediately vortexed for 10 - 15 seconds before being replaced into a -78 °C bath.

REFERENCES

1. (a) Gil, V. M. S.; Oliveira, N. C. *J. Chem. Educ.* **1990**, *67*, 473. (b) Huang, C. Y. *Method Enzymol.* **1982**, *87*, 509. (c) Hirose, K. *J. Incl. Phenom.* **2001**, *39*, 193. (d) Likussar, W.; Boltz, D. F. *Anal. Chem.* **1971**, *43*, 1265.

2. Job, P. *Ann. Chim.* **1928**, *9*, 113.

3. Liou, L. R.; McNeil, A. J.; Ramirez, A.; Toombes, G. E. S.; Gruver, J. M.; Collum, D. B. *J. Am. Chem. Soc.* **2008**, *130*, 4859.

4. (a) *The Claisen Rearrangement: Methods and Applications*; Hiersemann, M.; Nubbemeyer, U.; Wiley: Weinheim, 2007. Kobayashi, S.; Manabe, K.; Ishitani, H.; Matsuo, J.-I. In *Science of Synthesis*; Georg Thieme Verlag: New York, 2005; Vol. 8a, p 173.

5. "New Trialkylsilyl Enol Ether Chemistry: N-Tosylamination of Triisopropylsilyl Enol Ethers". Magnus, P.; Lacour, J.; Coldham, I.; Mugrage, B.; Bauta, W. B. *Tetrahedron* **1995**, *51*, 11087.

6. "The Aldol-Annulation-Fragmentation Strategy Toward the Taxoid Diterpene Framework Revisited. Instructive Failures in the Chemistry of Medium Ring Containing Systems". Hamon, S.; Del Rosario Rico Ferreira, M.; Quilez del Moral, J.; Martin Hernando, J. I.; Candela Lena, J. I.; Birlirakis, N.; Toupet, L.; Arseniyadis, S. *Tetrahedron: Asymmetry* **2005**, *16*, 3241. "Study on the Organosilylazole Series. II. Reaction of Nucleophilic Addition to the Carbonyl Derivatives". Gasparini, J. P.; Gassend, R.; Maire, J. C.; Elguero, J. *J. Organomet. Chem.* **1981**, 208, 309.

7. For leading references and discussions of mixed aggregation effects, see: (a) Tchoubar, B.; Loupy, A. *Salt Effects in Organic and Organometallic Chemistry*; VCH: New York, 1992; Chapters 4, 5, and 7. (b) Briggs, T. F.; Winemiller, M. D.; Xiang, B.; Collum, D. B. *J. Org. Chem.* **2001**, *66*, 6291. (c) Caubère, P. *Chem. Rev.* **1993**, *93*, 2317.

8. (a) Seebach, D. In *Proceedings of the Robert A. Welch Foundation Conferences on Chemistry and Biochemistry*; Wiley: New York, 1984. (b) Caubere, P. *Chem. Rev.* **1993**, *93*, 2317. (c) Juaristi, E.; Beck, A. K.; Hansen, J.; Matt, T.; Mukhopadhyay, M.; Simson, M.; Seebach, D. *Synthesis* **1993**, 1271.

9. (a) Kummer, D. A.; Chain, W. J.; Morales, M. R.; Quiroga, O.; Myers, A. G. *J. Am. Chem. Soc.* **2008**, *130*, 13231. (b) Galiano-Roth, A. S.; Kim, Y.-J.; Gilchrist, J. H.; Harrison, A. T.; Fuller, D. J.; Collum, D. B. *J. Am. Chem. Soc.* **1991**, *113*, 5053. (c) Lipshutz, B. H.; Wood, M. R.; Lindsley, C. W. *Tetrahedron Lett.* **1995**, *36*, 4385. (d) Dyke, A. M.; Gill, D. M.; Harvey, J. N.; Hester, A. J.; Lloyd-Jones, G. C.; Munoz, M. P.; Shepperson, I. R. *Angew. Chem. Int. Ed.* **2008**, *47*, 5067. (e) Cottet, F.; Schlosser, M. *Eur. J. Org. Chem.* **2004**, 3793.

10. Seebach, D. *Angew. Chem., Int. Ed. Engl.* **1988**, *27*, 1624.

11. Gupta, L.; Hoepker, A. C.; Singh, K. J.; Collum, D. B. *J. Org. Chem.* **2009**, *74*, 2231.

12. Jackman, L. M.; Haddon, R. C. *J. Am. Chem. Soc.* **1973**, *95*, 3687-3692.

13. Jackman, L. M.; Szeverenyi, N. M. *J. Am. Chem. Soc.* **1977**, *99*, 4954.

14. Henderson, K. W.; Dorigo, A. E.; Liu, Q-Y.; Williard, P. G.; Schleyer, P. v. R.; Bernstein, P. R. *J. Am. Chem. Soc.* **1996**, *118*, 1339.

15. Henderson, K. W.; Dorigo, A. E.; Williard, P. G.; Bernstein, P. R. *Angew. Chem., Int. Ed. Engl.* **1996**, *35*, 1322.

16. Jackman, L. M.; Lange, B. C. *J. Am. Chem. Soc.* **1981**, *103*, 4494.

17. McNeil, A. J.; Toombes, G. E. S.; Gruner, S. M.; Lobkovsky, E.; Collum, D. B.; Chandramouli, S. V.; Vanasse, B. J.; Ayers, T. A. *J. Am. Chem. Soc.* **2004**, *126*, 16559.

18. Zhao, P.; Collum, D. B. *J. Am. Chem. Soc.* **2003**, *125*, 14411.

19. (a) Snaith and co-workers clearly articulated the merits of NH_4X salts as precursors to anhydrous LiX salts: Barr, D.; Snaith, R.; Wright, D. S.; Mulvey, R. E.; Wade, K. *J. Am. Chem. Soc.* **1987**, *109*, 7891. Also, see: (b) Hall, P. L.; Gilchrist, J. H.; Collum, D. B.; Willard, P. G. *J. Org. Chem.* **1991**, *113*, 9571.

20. Zhao, P.; Condo, A.; Keresztes, I.; Collum, D. B. *J. Am. Chem. Soc.* **2004**, *126*, 3113.

21. Eliel, E. L.; Wilen, S. H.; Mander, L. N. *Stereochemistry of Organic Compounds*; Wiley: New York, 1994; pp 758-762.

22. Romesberg, F. E.; Bernstein, M. P.; Gilchrist, J. H.; Harrison, A. T.; Fuller, D. J.; Collum, D. B. *J. Am. Chem. Soc.* **1993**, *115*, 3475.

CHAPTER III

Experimental Characterization and Computational Study of Unique C,N-Chelated Lithium Dianions

Experimental Characterization and Computational Study
of Unique C,N-Chelated Lithium Dianions*

Structural studies of lithiated anions in solution are important given the ubiquity of these intermediates in organic synthesis.[1] Despite the remarkable advances that have been made in the investigation of C-, O-, and N-lithiated species, dianionic compounds (e.g., C-Li/N-Li) have received relatively little attention.[2] During a recent total synthesis study of the *Lycopodium* alkaloid lyconadin A (**4**), Sarpong et al. discovered that amine **1** was converted to pentacycle **3** by the sequential addition of *n*-BuLi (2 equiv) and iodine (1 equiv).[3] This C-N bond forming reaction was hypothesized to proceed via the intermediacy of a C,N-chelated lithium dianion intermediate (**2**) of ill-defined structure.

Scheme 1

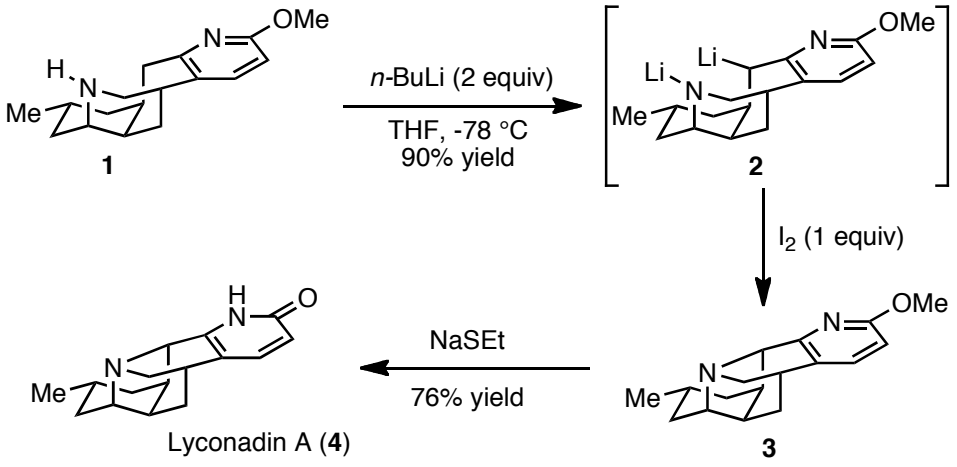

* This work was a collaboration with Dr. Richmond Sarpong and Scott P. West from the University of California, Berkeley. It is currently being prepared for publication.

To gain insight into the solution structure of the dianion intermediates, which may enable the generalization of the C-N bond-forming sequence, we have undertaken an in-depth structural study of these unique species. In this communication, we report the synthesis of a ^{15}N-incorporated isotopomer related to **1** as well as NMR and computational studies that have resulted in the structural characterization of the affiliated lithium dianion.

Because of its ease of synthesis, desmethyl analog [^{15}N]**8** (Scheme 1), lacking a methyl group on the A-ring, was targeted for synthesis and subsequent NMR spectroscopic studies. Coupling **5**[4] with [^{15}N]NH_4Cl using standard amidation conditions[5] gave [^{15}N]**6** in 91% yield. Hofmann rearrangement of [^{15}N]**6**, mediated by $Pb(OAc)_4$, in the presence of benzyl alcohol yielded carbobenzoxy-protected amine [^{15}N]**7**, which was converted to [^{15}N]**8** in three steps using a previously established protocol.[6]

Scheme 2

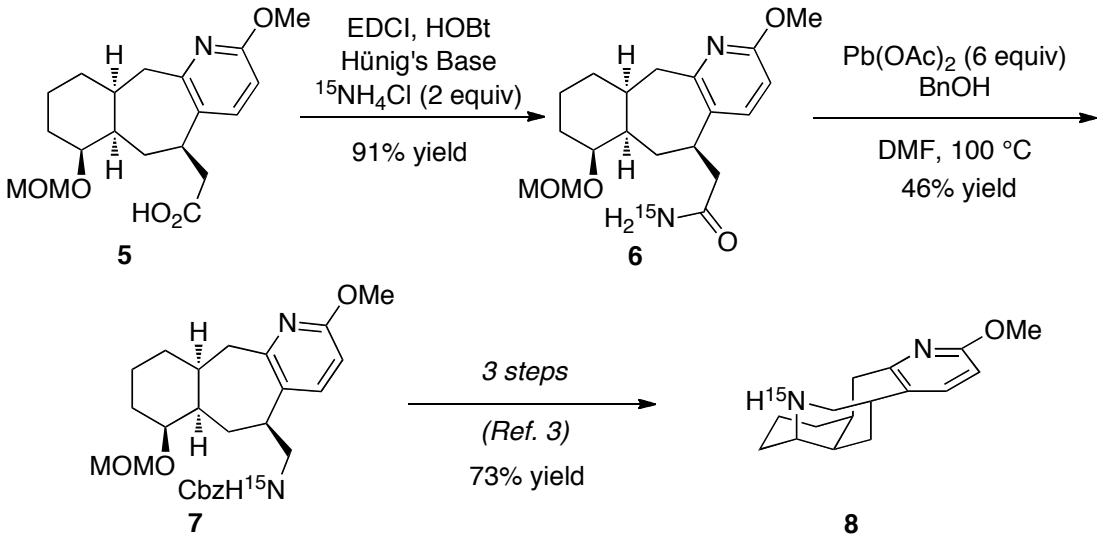

With [^{15}N]**8** in hand, we performed a series of ^{6}Li and ^{15}N NMR studies. Treatment of [^{15}N]**8** in THF-d_8 at -78 °C with [^{6}Li]*n*-BuLi (2 equiv) recrystallized from pentane[7] afforded the putative dianion. The ^{6}Li NMR spectrum of the dianion generated from [^{15}N]**8**—recorded at -90 °C (Figure III.1A)—contains two distinct doublets, indicating that each lithium is bound and couples to the isotopically labeled nitrogen. The ^{15}N decoupled ^{6}Li NMR observations (Figure III.1B) shows two singlets. The ^{15}N NMR spectrum, also recorded at -90 °C (Figure III.1C), contains a quintet, which confirms the N-Li-N connectivity. The structures of open dimer **9** (Figure III.2) and cyclic dimer **10** are consistent with the ^{6}Li and ^{15}N NMR spectral data and are well-precedented structural motifs.[2,8] Dilithio compound **11** also seems plausible but is inconsistent with the data.

^{13}C NMR spectra were recorded at -100 °C (Figure III.1D) to distinguish open isomer **9** from the chelated dilithio compound **10** by ^{6}Li-^{13}C coupling. A combination of 2-D NMR techniques including ^{1}H-^{1}H gCOSY, ^{1}H-^{13}C gHMBC, and ^{1}H-^{13}C HSQC were used to identify the chemical shift of the benzylic carbon. Unfortunately, the ^{13}C spectrum shows no signs of ^{6}Li-^{13}C scalar coupling. This absence is consistent with previous observations. For example, Fraenkel et al.[9] described difficulties observing an analogous coupling in benzyllithium that could be traced, in part, to small ^{1}J(^{6}Li-^{13}C) coupling.

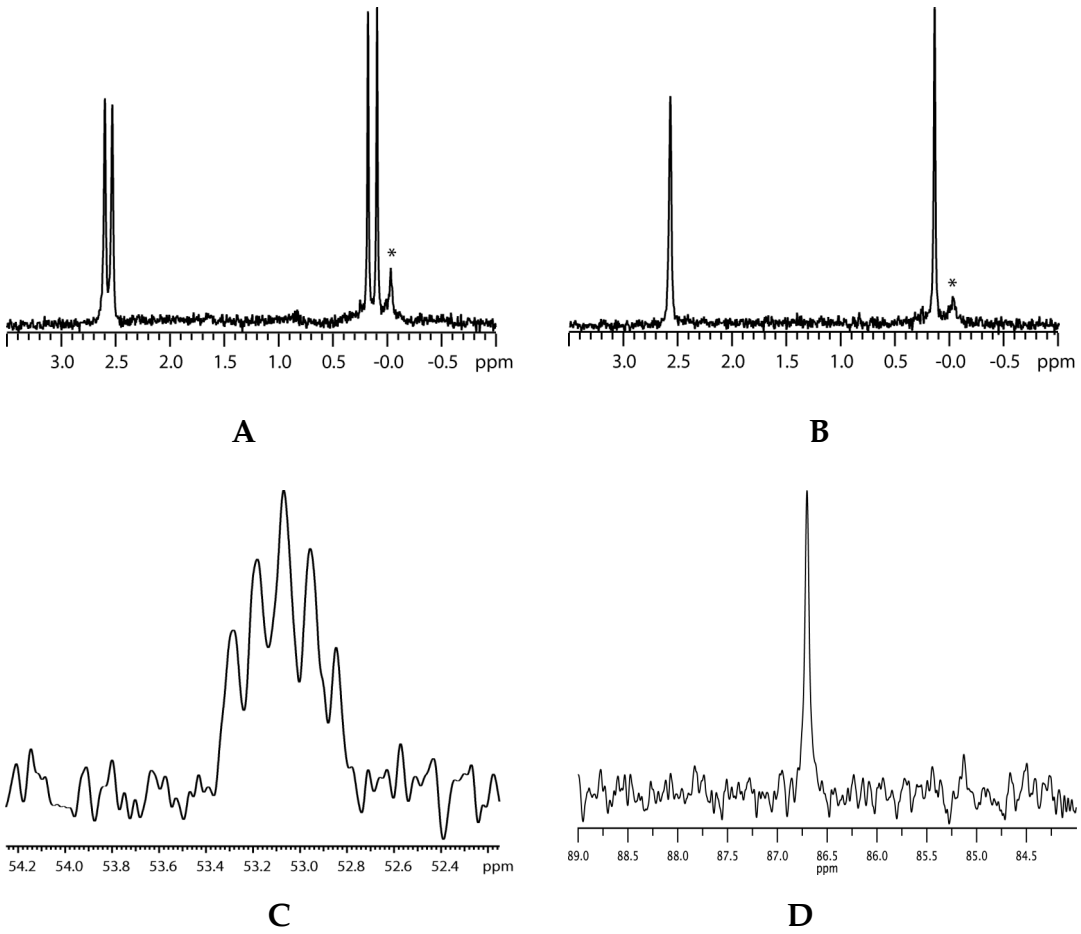

Figure III.1. NMR spectra of key resonances of the dianion of [^{15}N]**8**. (A) ^{6}Li NMR spectrum of 0.05 M [^{15}N]**8** and 2.0 equiv [^{6}Li]*n*-BuLi in THF-d_8 at -90 °C. (B) {^{15}N}^{6}Li NMR spectrum of 0.05 M [^{15}N]**8** and 2.0 equiv [^{6}Li]*n*-BuLi in THF-d_8 at -90 °C. (C) ^{15}N NMR spectrum of 0.05 M [^{15}N]**8** and 2.0 equiv [^{6}Li]*n*-BuLi in THF-d_8 at -90 °C. (D) ^{13}C NMR spectrum of 0.025 M **8** and 2.0 equiv [^{6}Li]*n*-BuLi in THF-d_8 at -100 °C, expanded around the benzylic carbon resonance. *Denotes an impurity from [^{6}Li]*n*-BuLi.

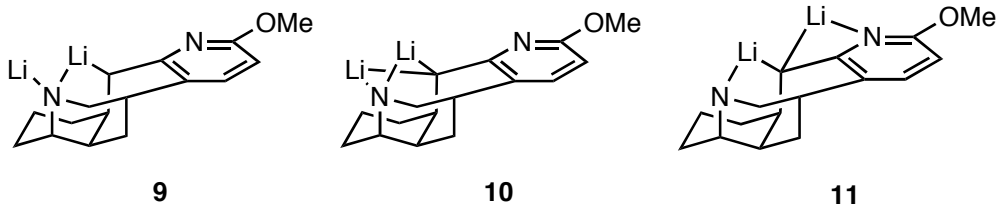

Figure III.2. Possible structures for dilithio anion generated from **8**.

We turned to density functional theory computational studies to provide insight into the dianion intermediate. The relative free energies (ΔG, kcal/mol) of various forms of the dianion intermediate at -78 °C were calculated at the B3LYP/6-31G(d) level of theory with single-point MP2 correction.[10] The relative energies for the computationally most viable dilithio isomers are illustrated in Scheme 3 in monotonically increasing stability at -78 °C. Tetrasolvated open dimer **9c** was calculated to be most stable in energy. Additional structures and their associated relative energies are reported in the part C of Appendix III. On the basis of these results, we conclude that open isomers of type **9** benefit from high solvation numbers.

Scheme 3

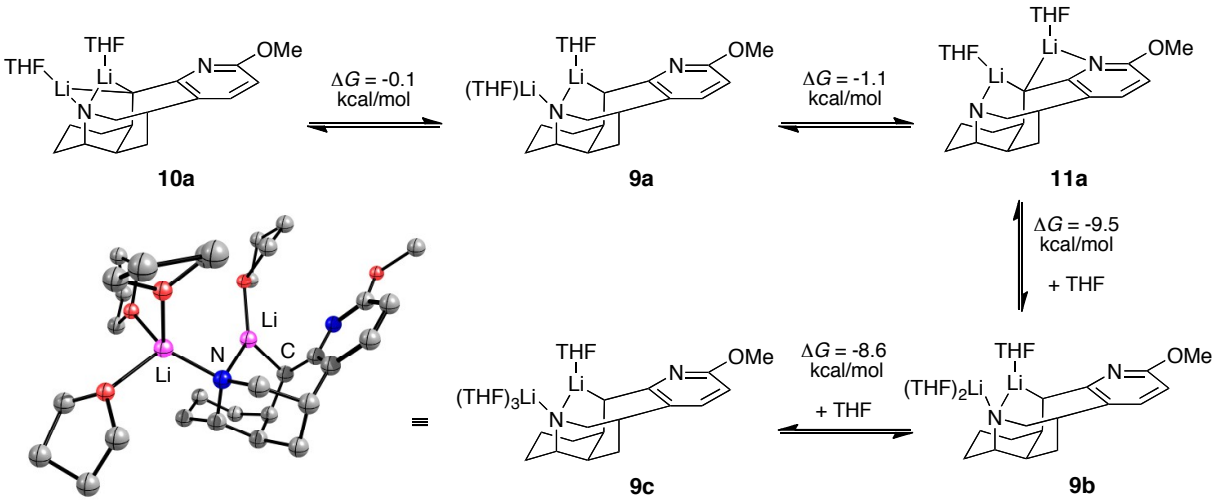

Our studies support the existence of the C,N-chelated dilithio dianion as a monomeric species that is solvated by four molecules of solvent (see **9c**) at concentrations that are relevant to oxidative conversion to **3** (see Scheme 1). Furthermore, we have amassed support for the persistence of **9c** as a highly organized dianion at low temperature. This structural organization may be

critical to the oxidative C-N bond forming process. We expect that ^{15}N and ^{6}Li NMR spectroscopy in conjunction with the computational methods used to characterize dianion **9c** could be predictive. Using this combined approach, the solution structures of a range of such C,N-chelated dianions may be readily determined. These insights will serve as a starting point in our efforts to extend the scope of the oxidative C-N bond-forming reaction.

Acknowledgment. RS is grateful to the National Institute of General Medical Sciences (RO1 GM086374-01) for support of part of this work. DBC thanks the National Science Foundation (CHE 0650880) and the National Institutes of Health (GM39764) for direct support of this work, and Dr. Ivan Keresztes for assistance with 2-D NMR spectroscopy.

APPENDIX III

A. Experimental Methods.

1. Reagents and Solvents.

[^{6}Li]*n*-BuLi was prepared and recrystallized in *n*-pentane as described previously.[7] An aliquot was removed and the pentane was evaporated and replaced with freshly distilled cyclopentane. *n*-BuLi was then titrated using diphenylacetic acid to determine the precise molarity. THF-d_8 was distilled from a solution containing sodium benzophenone ketyl. Cyclopentane was distilled from a blue solution containing sodium benzophenone ketyl with approximately 1% tetraglyme to dissolve the ketyl. Air- and moisture-sensitive materials were manipulated under argon using standard glove box, vacuum line, and syringe techniques.

2. Sample Preparation.

A stock solution of **8** was prepared at room temperature. After flame drying the NMR tube under vacuum and flushing with argon, the tube was placed in a -78 °C dry ice/acetone bath. The appropriate amount of the amine and THF-d_8 was added via syringe, followed by dropwise addition *n*-BuLi. All samples had a total volume of 0.60 mL. The tube was sealed under partial vacuum and immediately vortexed for approximately 5 seconds before being replaced into a -78 °C bath. The samples were stored in a -94 °C freezer.

3. Spectroscopic Analysis.

NMR spectra were recorded at -90 °C or -100 °C on a 500 or 600 MHz spectrometer with a delay between scans set to >5 x T1 to ensure accurate

integrations. ^{6}Li chemical shifts are reported relative to a 0.30 M ^{6}LiCl/MeOH standard (0.0 ppm) and ^{15}N chemical shifts are reported relative to a neat *N,N*-dimethylethylamine (DMEA) standard (25.6 ppm).

B. NMR Spectroscopic Studies.

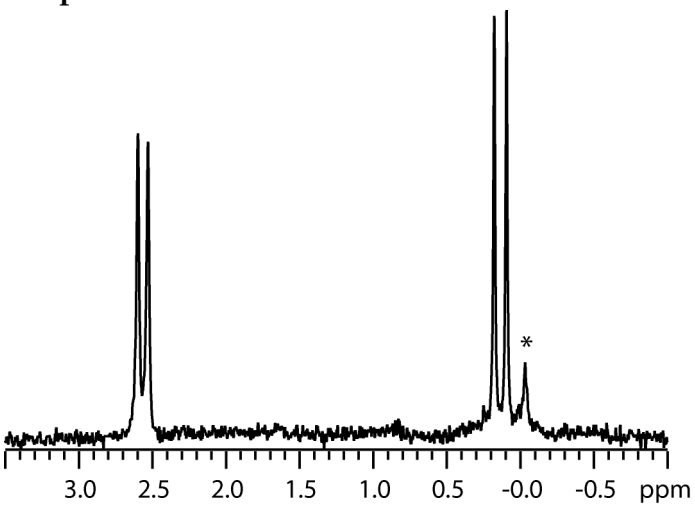

Figure AIII.1a. ^{6}Li NMR spectrum of 0.05 M [^{15}N]**8** and 2.0 equiv [^{6}Li]*n*-BuLi in THF d_8 at -90 °C. * Denotes an impurity from [^{6}Li]*n*-BuLi.

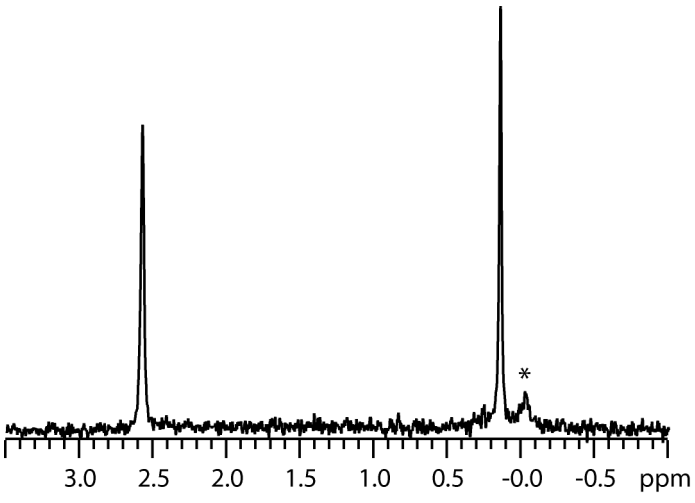

Figure AIII.1b. {^{15}N}^{6}Li NMR spectrum of 0.05 M [^{15}N]**8** and 2.0 equiv [^{6}Li]*n*-BuLi in THF-d_8 at -90 °C. * Denotes an impurity from [^{6}Li]*n*-BuLi.

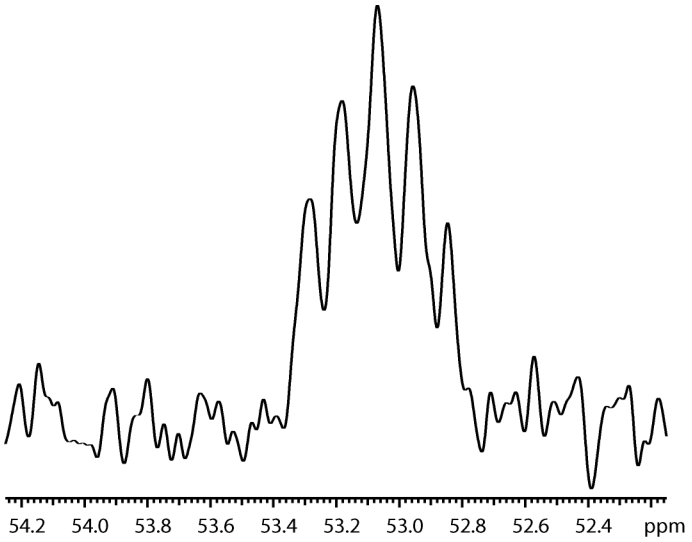

Figure AIII.2. ^{15}N NMR spectrum of 0.05 M [^{15}N]**8** and 2.0 equiv [^{6}Li]*n*-BuLi in THF-d_8 at -90 °C.

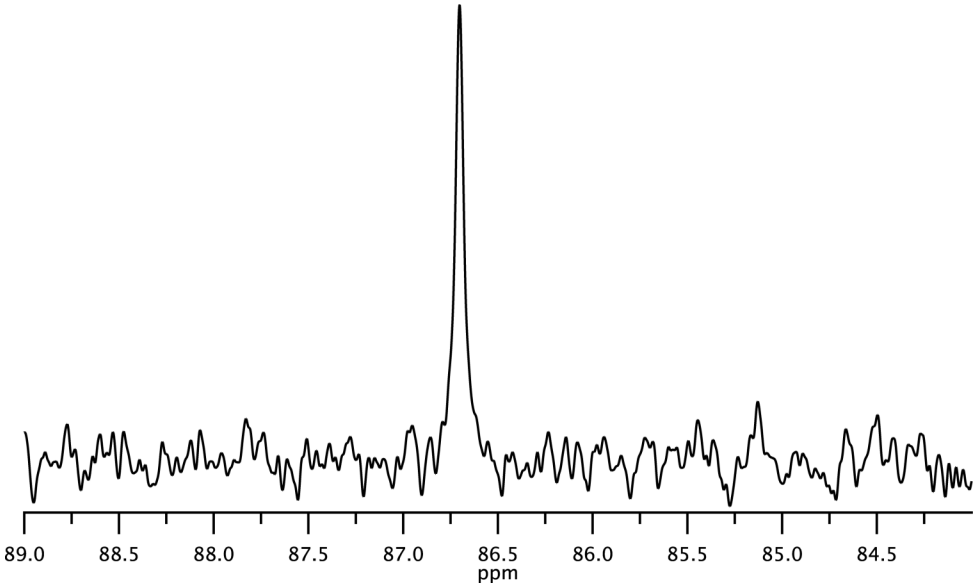

Figure AIII.3. ^{13}C NMR spectrum of 0.025 M [^{14}N]**8** and 2.0 equiv [^{6}Li]*n*-BuLi in THF-d_8 at -100 °C expanded around the benzylic carbon resonance. 2-D NMR techniques (COSY, HMBC, and HSQC) were used to identify the chemical shift of the benzylic carbon.

C. DFT Computational Studies.

Table AIII.1. Relative free energies (ΔG, kcal/mol) of **9**, **10**, and **11** at -78 °C calculated using B3LYP level of theory with 6-31G(d) basis set.

Structure	Free Energy (ΔG, kcal/mol)
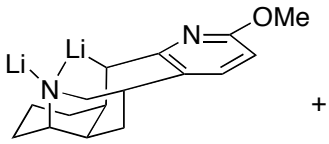	0.0
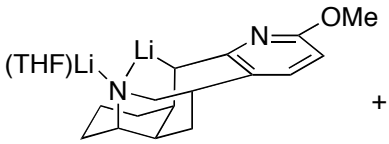	-19.9
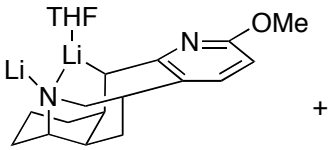	-19.5
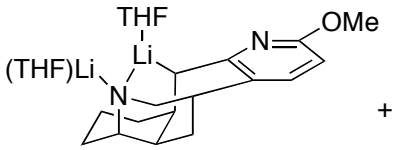	-32.0
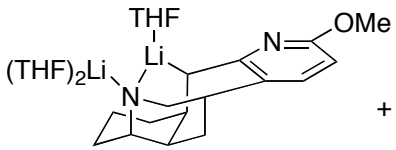	-38.9

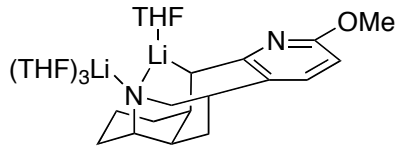	-38.3
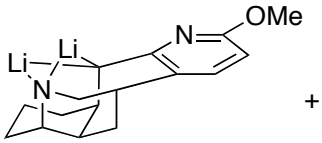 + 4 THF	+4.2
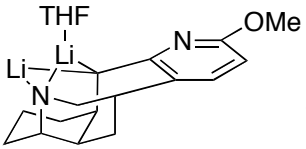 + 3 THF	-13.7
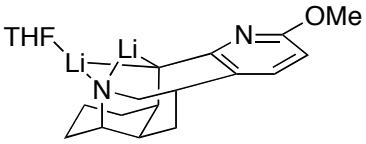 + 3 THF	-13.8
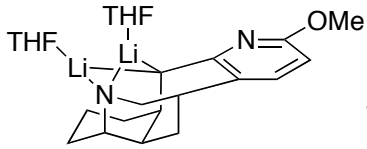 + 2 THF	-33.7
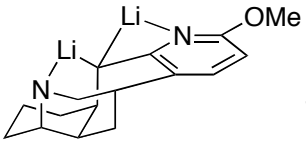 + 4 THF	-3.2
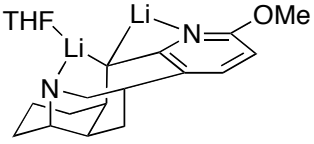 + 3 THF	-20.1

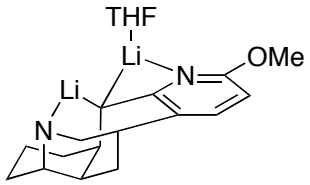 + 3 THF	-21.7
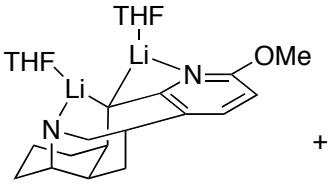 + 2 THF	-34.2

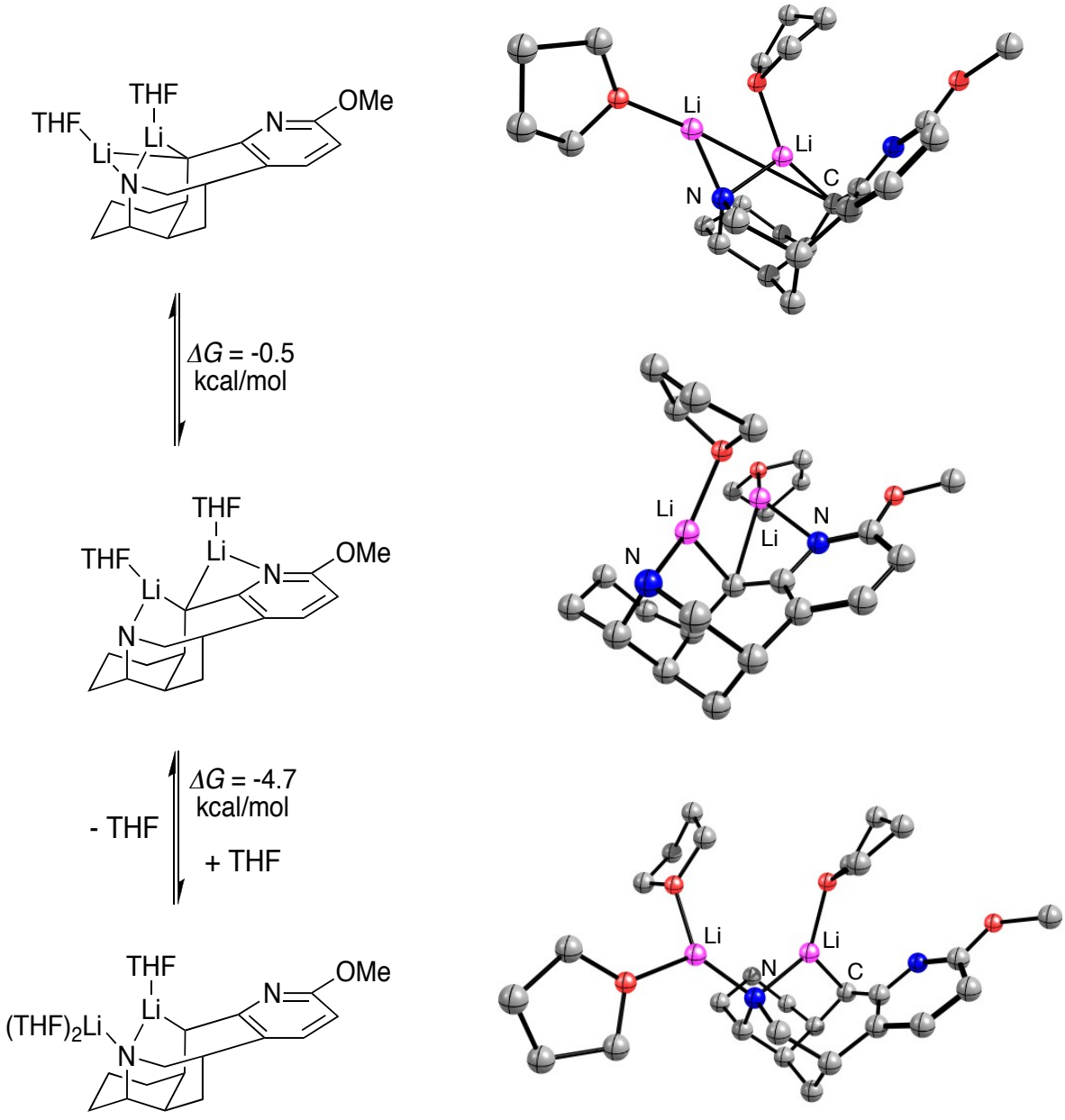

Figure AIII.4. The relative energies of the three most stable solvates of **9**, **10**, and **11** at -78 °C calculated using B3LYP level of theory with 6-31G(d) basis set.

Table AIII.2. Optimized geometries at B3LYP level of theory with 6-31G(d) basis set for the serial solvation of open dimer **9** at -78 °C with free energies (Hartrees), and Cartesian coordinates (X,Y,Z).

G = -232.349373

Atom	X	Y	Z
C	-0.73320	0.75864	-0.22699
C	-1.16581	-0.66851	0.13194
O	-0.00087	-1.49011	-0.00008
C	1.16504	-0.66980	-0.13184
C	0.73406	0.75792	0.22693
H	-1.94955	-1.06099	-0.52668
H	-1.53562	-0.72079	1.16790
H	1.94831	-1.06314	0.52684
H	1.53490	-0.72246	-1.16775
H	0.79733	0.91645	1.31025
H	1.34480	1.52213	-0.26387
H	-1.34309	1.52360	0.26368
H	-0.79630	0.91704	-1.31034

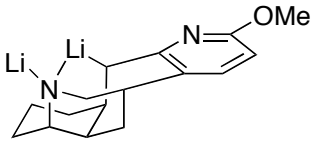

G = -821.216489

Atom	X	Y	Z
C	1.97800	0.16056	-1.07595
C	1.08536	1.27946	-1.63224
C	0.06500	1.80926	-0.60906
C	0.82403	2.17404	0.70033
N	1.56463	1.04524	1.28409
Li	0.07796	-0.24644	1.35783
C	-1.16941	-0.53398	-0.33765
C	-1.15770	0.92251	-0.37087
C	-2.37975	1.57434	-0.18801
C	-3.57699	0.90717	0.05562
C	-3.48012	-0.49681	0.11532
N	-2.36783	-1.17142	-0.06179

O	-4.56014	-1.30534	0.36818
C	-5.82550	-0.69476	0.53221
C	-0.03579	-1.39625	-0.35170
C	1.29217	-1.22905	-1.07691
C	2.31111	-2.27048	-0.54857
C	2.83793	-1.92082	0.85109
C	3.48114	-0.52575	0.84944
C	2.57229	0.59600	0.29494
Li	2.54569	0.93106	2.82224
H	-6.13322	-0.13966	-0.36469
H	-6.53202	-1.50979	0.70642
H	-5.84589	-0.01291	1.39417
H	-4.50565	1.44819	0.18038
H	-2.39512	2.66278	-0.24873
H	-0.34480	-2.44062	-0.30360
H	1.15068	-1.46174	-2.15099
H	1.85128	-3.26593	-0.53059
H	3.16450	-2.32860	-1.24167
H	3.57247	-2.66651	1.18307
H	2.00297	-1.96319	1.56476
H	4.39248	-0.55789	0.23730
H	3.86727	-0.28042	1.87035
H	3.23669	1.45699	0.06100
H	0.10385	2.55703	1.43713
H	1.51212	3.01390	0.46069
H	-0.32116	2.75893	-1.00724
H	1.72729	2.12244	-1.92843
H	0.57489	0.93560	-2.54074
H	2.83930	0.06285	-1.75710

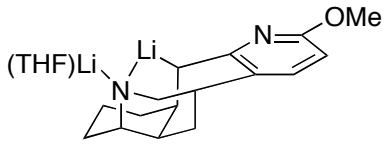

G = -1053.597570

Atom	X	Y	Z
C	-0.81251	2.61978	0.72957
C	-1.59588	2.07544	1.93227
C	-1.60155	0.53835	2.00677
C	-0.12942	0.04090	1.89639
N	0.55216	0.46565	0.66373
Li	-0.73130	-0.14367	-0.68249
C	-2.81619	0.21535	-0.33777

C	-2.54256	-0.17664	1.03936
C	-3.19573	-1.31131	1.52109
C	-4.04773	-2.09741	0.74661
C	-4.19679	-1.67814	-0.58876
N	-3.62716	-0.61231	-1.10113
O	-4.96644	-2.36188	-1.50070
C	-5.66155	-3.50849	-1.05378
C	-2.19301	1.26037	-1.07108
C	-1.62740	2.58818	-0.58922
C	-0.75854	3.21833	-1.70765
C	0.58957	2.50249	-1.87444
C	1.37470	2.49875	-0.55407
C	0.58732	1.94273	0.65065
Li	2.25446	-0.19297	0.28248
O	3.85554	-1.12731	-0.03982
C	4.36164	-2.21186	0.79214
C	5.80102	-2.43174	0.33157
C	5.72099	-2.07731	-1.16171
C	4.75409	-0.89393	-1.16415
H	-6.37458	-3.27104	-0.25201
H	-6.21227	-3.88401	-1.91988
H	-4.97870	-4.29276	-0.69655
H	-4.54705	-2.96291	1.16204
H	-3.03364	-1.59249	2.56208
H	-2.60353	1.32848	-2.07893
H	-2.46116	3.29703	-0.41390
H	-1.30732	3.20487	-2.65763
H	-0.56864	4.27572	-1.46659
H	1.18636	2.98747	-2.65915
H	0.40738	1.47364	-2.21722
H	2.32924	1.94733	-0.67538
H	1.66893	3.53239	-0.32277
H	1.12329	2.28616	1.56479
H	5.30498	-2.91418	-1.73367
H	6.69018	-1.81675	-1.59539
H	5.27014	0.05841	-0.99680
H	4.14986	-0.81884	-2.07253
H	6.47928	-1.74811	0.85447
H	6.13978	-3.45512	0.51399
H	3.73690	-3.09644	0.62158
H	4.27113	-1.90523	1.83773
H	-0.12417	-1.05806	1.95901
H	0.40926	0.41492	2.79740
H	-1.93907	0.26772	3.01839
H	-1.12388	2.44878	2.85359
H	-2.62247	2.46426	1.92211
H	-0.61795	3.68738	0.92532

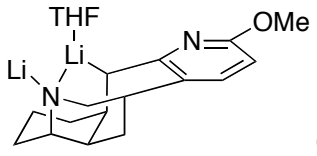

G = -1053.596858

Atom	X	Y	Z
C	2.94948	-1.21605	0.20671
C	2.36883	-2.40472	-0.57313
C	1.07866	-2.05675	-1.33681
C	1.35510	-0.76866	-2.17061
N	1.75790	0.38141	-1.35363
C	3.02957	0.04968	-0.70303
C	3.61424	1.23527	0.08715
C	2.95822	1.46475	1.45695
C	2.95148	0.17788	2.29455
C	2.24028	-0.99282	1.56789
C	0.73869	-0.75715	1.58250
Li	0.33474	0.55909	0.02708
C	-0.30023	-1.30161	0.80356
N	-1.58342	-1.01801	1.27723
C	-2.65291	-1.48730	0.67462
C	-2.63634	-2.25433	-0.50113
C	-1.36882	-2.42042	-1.07565
C	-0.19550	-1.93426	-0.50977
O	-3.82356	-1.09504	1.29416
C	-5.04179	-1.60764	0.78852
Li	0.93187	1.93302	-1.89819
O	-0.73145	2.15005	-0.83572
C	-2.01317	1.58912	-1.31806
C	-3.04811	2.04363	-0.29726
C	-2.51208	3.41890	0.13168
C	-1.00207	3.19470	0.16721
H	-2.19907	2.00563	-2.31541
H	-1.89639	0.50444	-1.38136
H	-3.07761	1.34505	0.54486
H	-4.04842	2.09921	-0.73637
H	-2.89356	3.73988	1.10474
H	-2.76944	4.18712	-0.60697
H	-0.66556	2.81382	1.13682
H	-0.41283	4.07679	-0.10012
H	-5.06777	-2.70491	0.82011
H	-5.82799	-1.21329	1.43710
H	-5.23108	-1.28169	-0.24463
H	-3.52323	-2.66671	-0.96356

H	-1.29714	-2.95324	-2.02412
H	0.37397	-0.38713	2.54172
H	2.46876	-1.90369	2.15519
H	2.47381	0.36206	3.26558
H	3.99294	-0.10880	2.50487
H	3.48513	2.26665	1.99226
H	1.92114	1.81818	1.33540
H	4.68417	1.04309	0.25198
H	3.55854	2.14496	-0.53327
H	3.77142	-0.20226	-1.49089
H	0.44083	-0.52403	-2.74158
H	2.13408	-1.01764	-2.92365
H	0.90139	-2.86594	-2.06109
H	3.11111	-2.73067	-1.31695
H	2.20274	-3.25601	0.10057
H	3.99046	-1.47357	0.46193

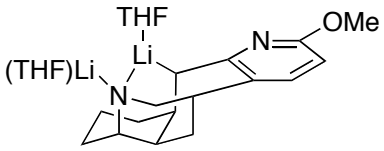

G = -1285.966188

Atom	X	Y	Z
C	-1.94928	0.30529	0.97763
C	-1.04147	1.45296	1.43264
C	-0.04467	1.89226	0.34764
C	-0.84906	2.11093	-0.98902
N	-1.59576	0.93906	-1.43191
Li	0.27675	0.33016	-1.66575
C	1.17796	0.97062	0.21094
C	1.14263	-0.47499	0.08524
C	-0.06834	-1.27731	-0.05542
C	-1.25098	-1.08056	0.93675
C	-2.35868	-2.14540	0.72134
C	-3.20520	-1.92784	-0.55352
Li	-1.53203	-0.93384	-1.61062
C	-3.64017	-0.44481	-0.75709
C	-2.60348	0.66025	-0.38875
N	2.31362	-1.16053	-0.08929
C	3.47768	-0.53848	-0.11368
C	3.62221	0.85310	0.03068
C	2.44305	1.57355	0.18873

O	4.53038	-1.38709	-0.29037
C	5.83918	-0.84148	-0.30303
H	6.08141	-0.34255	0.64461
H	6.51326	-1.68861	-0.44430
H	5.97733	-0.13016	-1.12850
H	4.58307	1.35133	0.03002
H	2.50430	2.65429	0.30813
H	0.23044	-2.32952	-0.05668
H	-0.86798	-1.25464	1.95765
H	-1.92468	-3.15290	0.70537
H	-3.03602	-2.10827	1.58525
H	-4.10704	-2.54880	-0.51259
H	-2.68225	-2.35298	-1.43589
H	-4.50249	-0.28414	-0.10029
H	-3.99713	-0.28259	-1.78416
H	-3.21175	1.57381	-0.23363
H	-0.14667	2.43680	-1.78252
H	-1.50924	2.98895	-0.82703
H	0.35380	2.87519	0.63637
H	-1.67808	2.31724	1.67293
H	-0.51066	1.18331	2.35552
H	-2.75396	0.21841	1.72658

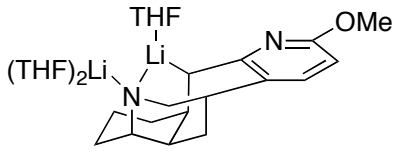

G = -1518.326520

Atom	X	Y	Z
C	-0.14256	-2.84415	1.75587
C	-0.69798	-3.69209	0.60475
C	-1.01575	-2.86277	-0.65290
C	0.23532	-1.99347	-0.98694
N	0.68035	-1.10768	0.09055
C	1.02303	-1.94678	1.24523
C	1.59952	-1.13164	2.42060
C	0.53931	-0.37493	3.23387
C	-0.56930	-1.32553	3.70803
C	-1.24354	-2.07923	2.53362
C	-2.15655	-1.12917	1.77466
Li	-0.91724	0.00494	0.45899
C	-2.78741	-1.28306	0.52132

N	-3.91530	-0.48834	0.33418
C	-4.59414	-0.52358	-0.79064
C	-4.26936	-1.31599	-1.90020
C	-3.09225	-2.06580	-1.76302
C	-2.31232	-2.06619	-0.61476
O	-5.67375	0.34542	-0.78697
C	-6.57585	0.27406	-1.87440
O	-1.45892	1.80457	-0.14748
C	-2.36207	2.47232	0.78171
C	-3.01751	3.56554	-0.05373
C	-3.22775	2.84030	-1.39364
C	-1.99604	1.92534	-1.49719
Li	2.11940	0.07233	-0.41532
O	3.68236	-0.55649	-1.38824
C	3.92552	-1.97622	-1.56693
C	5.41395	-2.07979	-1.88635
C	5.64430	-0.80604	-2.71544
C	4.73538	0.21313	-2.01763
O	2.57677	1.95635	-0.03258
C	1.70593	3.08966	-0.32250
C	2.01961	4.15686	0.74135
C	2.71843	3.35315	1.85111
C	3.47513	2.30540	1.04158
H	-1.20265	2.35751	-2.11957
H	-2.24672	0.92886	-1.87162
H	-4.13898	2.23855	-1.34437
H	-3.30306	3.52374	-2.24529
H	-3.95450	3.91788	0.38742
H	-2.34324	4.42404	-0.16827
H	-3.09394	1.74055	1.14019
H	-1.75182	2.84016	1.61163
H	-6.99672	-0.73383	-1.98882
H	-7.38249	0.97558	-1.64588
H	-6.10536	0.56795	-2.82393
H	-4.86004	-1.35628	-2.80597
H	-2.77067	-2.68197	-2.60316
H	-2.76602	-0.52802	2.45216
H	-1.85990	-2.87531	2.99829
H	-1.32562	-0.76823	4.27602
H	-0.12964	-2.05808	4.40262
H	1.01192	0.11855	4.09543
H	0.09385	0.42625	2.62648
H	2.37106	-0.43500	2.05012
H	2.12086	-1.82521	3.09687
H	1.82362	-2.66861	0.94451
H	1.98453	2.86245	2.49975
H	3.37840	3.96367	2.47431

H	0.67467	2.73058	-0.26860
H	1.91800	3.43759	-1.33964
H	2.69804	4.91785	0.33973
H	1.11576	4.66483	1.08893
H	4.40701	2.71270	0.62299
H	3.70419	1.39113	1.59534
H	0.01376	-1.39860	-1.88765
H	1.03826	-2.71566	-1.27676
H	-1.12086	-3.57307	-1.48720
H	0.06251	-4.43769	0.32591
H	-1.58368	-4.25216	0.93383
H	0.30236	-3.54045	2.48707
H	6.68911	-0.48289	-2.73543
H	5.31955	-0.96420	-3.75017
H	6.00658	-2.05416	-0.96418
H	5.66267	-2.99730	-2.42724
H	3.30496	-2.34136	-2.39421
H	3.61726	-2.48231	-0.64974
H	4.28095	0.93176	-2.70673
H	5.26736	0.76776	-1.23567

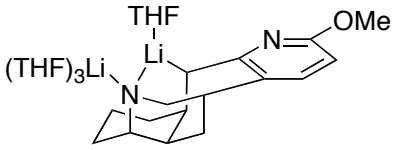

G = -1750.675050

Atom	X	Y	Z
C	0.27008	-3.49201	-0.53640
C	0.84109	-3.79257	0.85397
C	1.20335	-2.51858	1.63560
C	-0.02202	-1.55477	1.58299
N	-0.47221	-1.18152	0.24411
C	-0.85881	-2.42177	-0.43850
C	-1.45124	-2.17987	-1.83977
C	-0.40102	-1.87491	-2.91740
C	0.67621	-2.96876	-2.95786
C	1.36401	-3.16958	-1.58381
C	2.31918	-2.01689	-1.31548
Li	1.13445	-0.37266	-0.60520
C	2.97808	-1.64330	-0.12488
N	4.13449	-0.88961	-0.31041
C	4.84367	-0.46757	0.71236
C	4.52439	-0.69089	2.05847

C	3.32333	-1.38464	2.27065
C	2.51394	-1.85013	1.24409
O	5.95496	0.26423	0.32226
C	6.88198	0.63245	1.32510
O	1.81939	1.46662	-0.94108
C	2.66034	1.52356	-2.12961
C	3.42449	2.83427	-1.98793
C	3.72821	2.84621	-0.48038
C	2.47881	2.19231	0.13397
Li	-1.82108	0.28609	0.24311
O	-1.72346	1.66736	1.79272
C	-0.59612	2.07535	2.58234
C	-1.02909	1.83521	4.03507
C	-2.57383	1.99948	3.98566
C	-2.88120	2.16536	2.48198
O	-3.77815	-0.29864	0.54241
C	-3.97732	-1.42112	1.43859
C	-4.97736	-2.33093	0.72985
C	-5.86318	-1.31200	-0.00425
C	-4.84567	-0.24920	-0.43286
O	-2.02437	1.69576	-1.28718
C	-2.40167	1.50670	-2.67002
C	-1.63725	2.56798	-3.46126
C	-1.56062	3.72032	-2.44933
C	-1.34970	2.97226	-1.13121
H	1.76132	2.93336	0.50771
H	2.72911	1.49225	0.93657
H	4.60962	2.23218	-0.27777
H	3.90057	3.85216	-0.08434

Table AIII.3. Optimized geometries at B3LYP level of theory with 6-31G(d) basis set for the serial solvation of closed dimer **10** at -78 °C with free energies (Hartrees), and Cartesian coordinates (X,Y,Z).

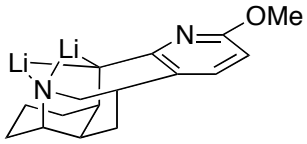

G = -821.209733

Atom	X	Y	Z
C	-1.94928	0.30529	0.97763
C	-1.04147	1.45296	1.43264
C	-0.04467	1.89226	0.34764
C	-0.84906	2.11093	-0.98902
N	-1.59576	0.93906	-1.43191
Li	0.27675	0.33016	-1.66575
C	1.17796	0.97062	0.21094
C	1.14263	-0.47499	0.08524
C	-0.06834	-1.27731	-0.05542
C	-1.25098	-1.08056	0.93675
C	-2.35868	-2.14540	0.72134
C	-3.20520	-1.92784	-0.55352
Li	-1.53203	-0.93384	-1.61062
C	-3.64017	-0.44481	-0.75709
C	-2.60348	0.66025	-0.38875
N	2.31362	-1.16053	-0.08929
C	3.47768	-0.53848	-0.11368
C	3.62221	0.85310	0.03068
C	2.44305	1.57355	0.18873
O	4.53038	-1.38709	-0.29037
C	5.83918	-0.84148	-0.30303
H	6.08141	-0.34255	0.64461
H	6.51326	-1.68861	-0.44430
H	5.97733	-0.13016	-1.12850
H	4.58307	1.35133	0.03002
H	2.50430	2.65429	0.30813
H	0.23044	-2.32952	-0.05668
H	-0.86798	-1.25464	1.95765
H	-1.92468	-3.15290	0.70537
H	-3.03602	-2.10827	1.58525
H	-4.10704	-2.54880	-0.51259
H	-2.68225	-2.35298	-1.43589
H	-4.50249	-0.28414	-0.10029

H	-3.99713	-0.28259	-1.78416
H	-3.21175	1.57381	-0.23363
H	-0.14667	2.43680	-1.78252
H	-1.50924	2.98895	-0.82703
H	0.35380	2.87519	0.63637
H	-1.67808	2.31724	1.67293
H	-0.51066	1.18331	2.35552
H	-2.75396	0.21841	1.72658

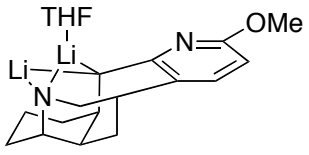

G = -1053.587758

Atom	X	Y	Z
C	0.38485	-0.68113	1.52926
C	-0.68069	-1.21976	0.77151
N	-1.94052	-0.77359	1.16320
C	-3.04079	-1.17524	0.56429
C	-3.07511	-2.05765	-0.53007
C	-1.81989	-2.47296	-0.98979
C	-0.61064	-2.08225	-0.41195
Li	-0.49997	-0.07445	-1.40411
C	1.12040	-1.37369	-2.11410
C	0.66697	-2.50583	-1.13841
C	1.87350	-2.86536	-0.25880
C	2.54809	-1.63949	0.37333
C	2.74430	-0.50892	-0.68627
N	1.50522	-0.15889	-1.40561
Li	0.81908	0.83629	0.12451
O	-0.78709	1.77581	-0.75727
C	-0.39255	2.90261	-1.58887
C	-0.48431	4.13338	-0.66569
C	-1.36675	3.65939	0.52607
C	-1.85798	2.27282	0.10474
C	3.46256	0.69738	-0.03307
C	2.93295	1.14616	1.34774
C	2.69574	-0.04234	2.29783
C	1.82882	-1.15710	1.65796
O	-4.17053	-0.60740	1.10078
C	-5.42744	-1.01958	0.59300

H	2.23407	0.31117	3.22898
H	3.67335	-0.46499	2.57078
H	3.65082	1.84739	1.79258
H	2.01101	1.75770	1.27607
H	4.51082	0.40558	0.11477
H	3.46986	1.53715	-0.74188
H	3.47090	-0.90744	-1.42475
H	-1.09767	2.97275	-2.42697
H	0.60322	2.67310	-1.97358
H	-0.92678	4.98130	-1.19609
H	0.50654	4.44416	-0.32158
H	-2.20106	4.33714	0.72672
H	-0.77227	3.58653	1.44226
H	-1.99013	1.53555	0.89961
H	-2.77379	2.33006	-0.49777
H	0.29290	-1.17368	-2.83463
H	1.93583	-1.75970	-2.76065
H	-1.78037	-3.14270	-1.84912
H	-3.98782	-2.40677	-0.99384
H	-5.58024	-2.10010	0.71279
H	-6.17810	-0.48518	1.17973
H	-5.54887	-0.75950	-0.46792
H	0.41338	-3.39416	-1.73679
H	2.60543	-3.37246	-0.90478
H	1.58843	-3.58609	0.51982
H	3.55351	-1.95528	0.69783
H	1.87060	-2.01505	2.35695
H	0.01821	-0.20473	2.44125

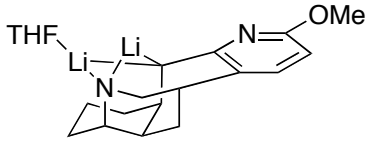

G = -1053.587786

Atom	X	Y	Z
C	0.38604	-0.68139	1.52950
C	-0.67918	-1.22069	0.77177
N	-1.93932	-0.77565	1.16375
C	-3.03930	-1.17778	0.56468
C	-3.07306	-2.05975	-0.53008
C	-1.81758	-2.47399	-0.99003
C	-0.60857	-2.08272	-0.41205
Li	-0.49939	-0.07510	-1.40252

C	1.12147	-1.37149	-2.11423
C	0.66927	-2.50469	-1.13905
C	1.87623	-2.86371	-0.25989
C	2.54990	-1.63762	0.37275
C	2.74512	-0.50645	-0.68635
N	1.50560	-0.15678	-1.40518
Li	0.81862	0.83765	0.12544
O	-0.78864	1.77493	-0.75551
C	-0.39727	2.90152	-1.58870
C	-0.48769	4.13218	-0.66559
C	-1.37342	3.65994	0.52453
C	-1.86039	2.27076	0.10617
C	3.46290	0.69991	-0.03286
C	2.93331	1.14775	1.34820
C	2.69670	-0.04118	2.29786
C	1.83045	-1.15628	1.65770
O	-4.16942	-0.61100	1.10146
C	-5.42604	-1.02334	0.59314
H	2.23485	0.31175	3.22914
H	3.67456	-0.46334	2.57067
H	3.65096	1.84905	1.79332
H	2.01127	1.75899	1.27675
H	4.51138	0.40868	0.11450
H	3.46946	1.54001	-0.74129
H	3.47167	-0.90420	-1.42529
H	-1.10485	2.97086	-2.42484
H	0.59769	2.67279	-1.97598
H	-0.92657	4.98163	-1.19649
H	0.50344	4.43980	-0.31944
H	-2.21016	4.33633	0.71966
H	-0.78225	3.59191	1.44318
H	-1.98999	1.53472	0.90258
H	-2.77671	2.32377	-0.49591
H	0.29350	-1.17172	-2.83430
H	1.93690	-1.75647	-2.76138
H	-1.77761	-3.14327	-1.84970
H	-3.98555	-2.40929	-0.99395
H	-5.57857	-2.10395	0.71240
H	-6.17704	-0.48942	1.17987
H	-5.54724	-0.76284	-0.46771
H	0.41634	-3.39284	-1.73798
H	2.60849	-3.36984	-0.90625
H	1.59187	-3.58509	0.51839
H	3.55560	-1.95280	0.69699
H	1.87302	-2.01449	2.35633
H	0.01920	-0.20580	2.44184

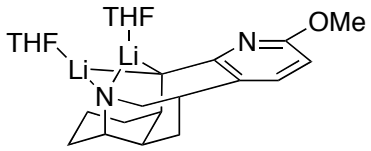

G = -1285.968944

Atom	X	Y	Z
C	2.09242	1.88821	0.65619
C	2.42116	0.93273	-0.32537
Li	0.56999	0.46714	0.66269
N	-1.00095	1.19399	-0.26824
C	-0.74153	0.97299	-1.69081
C	0.62296	1.54880	-2.18029
C	0.62236	3.06060	-1.89069
C	0.22288	3.40060	-0.44765
C	-1.07993	2.63835	-0.04779
C	-1.47861	2.99415	1.39635
C	-0.33205	2.87415	2.41130
C	0.89973	3.67027	1.95641
C	1.39676	3.23679	0.55337
C	1.80426	0.75291	-1.63920
C	2.30688	-0.26213	-2.44432
C	3.30717	-1.15571	-2.03663
C	3.73837	-0.99032	-0.71069
N	3.32347	-0.04344	0.09983
O	4.62627	-1.85693	-0.10149
C	5.22027	-2.86105	-0.90067
Li	-1.77091	-0.36869	0.44408
O	-0.11954	-1.34861	1.27767
C	0.55914	-2.41938	0.53044
C	1.57930	-2.99394	1.50544
C	0.85211	-2.86490	2.85367
C	0.11715	-1.53098	2.71599
O	-3.44532	-1.23476	0.13850
C	-4.42535	-0.35853	-0.49264
C	-4.99055	-1.17793	-1.64783
C	-4.99253	-2.59837	-1.05940
C	-3.70806	-2.61659	-0.22202
H	1.71051	3.56447	2.68908
H	0.63629	4.73867	1.93042
H	-0.66920	3.22202	3.39772
H	-0.04798	1.81842	2.54720
H	-1.83488	4.03465	1.40858
H	-2.33460	2.36988	1.69811

H	-1.87522	3.05726	-0.70612
H	-3.89736	0.55120	-0.78808
H	-5.19636	-0.11072	0.24744
H	-4.32656	-1.11793	-2.51764
H	-5.98468	-0.83836	-1.95189
H	-4.99764	-3.38253	-1.82159
H	-5.86934	-2.74394	-0.41834
H	-3.79737	-3.20501	0.69616
H	-2.85065	-2.98568	-0.79791
H	-0.85178	-1.50265	3.22322
H	0.72814	-0.68888	3.05751
H	0.13714	-3.68493	2.99085
H	1.53471	-2.86287	3.70791
H	2.49470	-2.39426	1.48422
H	1.83664	-4.02884	1.26111
H	1.00076	-1.97253	-0.36342
H	-0.20057	-3.15762	0.24277
H	-0.75384	-0.11007	-1.91439
H	-1.53701	1.43100	-2.32549
H	1.89475	-0.37038	-3.44802
H	3.68683	-1.91923	-2.70270
H	5.77821	-2.43472	-1.74516
H	5.91481	-3.39623	-0.24808
H	4.47854	-3.57160	-1.29423
H	0.64257	1.42773	-3.27416
H	-0.10687	3.52425	-2.57211
H	1.60024	3.50067	-2.12864
H	-0.02906	4.47391	-0.42575
H	2.13809	3.99921	0.24197
H	2.75073	1.81627	1.52325

Table AIII.4. Optimized geometries at B3LYP level of theory with 6-31G(d) basis set for the serial solvation of open dimer **11** at -78 °C with free energies (Hartrees), and Cartesian coordinates (X,Y,Z).

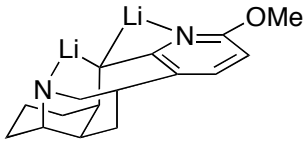

G = -821.221522

Atom	X	Y	Z
C	-0.04831	-1.28687	0.36150
C	1.09130	-0.36630	0.27578
N	2.28548	-1.04204	0.09818
Li	1.35915	-2.50059	-0.67832
Li	-0.78124	-0.75706	-1.61410
N	-1.60479	0.85167	-1.45276
C	-0.85716	2.03225	-1.11054
C	-0.13673	1.94701	0.28859
C	-1.17739	1.56158	1.35737
C	-2.07920	0.39323	0.93866
C	-2.66454	0.66804	-0.47741
C	-3.63816	-0.45932	-0.87067
C	-3.04858	-1.87009	-0.70926
C	-2.43825	-2.08179	0.68497
C	-1.39914	-0.99560	1.06405
C	1.09393	1.06404	0.24945
C	2.34056	1.67725	0.13483
C	3.54593	0.97877	-0.00044
C	3.44661	-0.40832	-0.04546
O	4.48921	-1.26449	-0.24802
C	5.78773	-0.70337	-0.39339
H	-1.98654	-3.08180	0.75633
H	-3.25183	-2.05424	1.42393
H	-3.82382	-2.62528	-0.89463
H	-2.29157	-2.07905	-1.49068
H	-4.52951	-0.39252	-0.23000
H	-3.96848	-0.29856	-1.90456
H	-3.27674	1.59426	-0.38313
H	-0.09812	2.23994	-1.87938
H	-1.50186	2.93953	-1.05683
H	2.37711	2.76470	0.14900
H	4.48922	1.50221	-0.08333
H	6.08711	-0.15103	0.50591

H	6.46283	-1.54809	-0.54016
H	5.84276	-0.03684	-1.26339
H	0.22363	2.95777	0.53171
H	-1.81974	2.43902	1.51981
H	-0.68644	1.35088	2.31898
H	-2.91675	0.35975	1.65671
H	-1.20655	-1.11453	2.14472
H	0.30890	-2.20409	0.86598

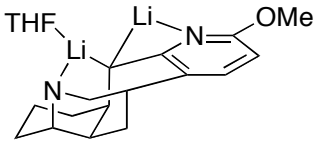

G = -1053.600380

Atom	X	Y	Z
C	-0.22661	-0.95184	-1.50516
C	0.89495	-1.22052	-0.64299
Li	1.17093	0.71857	-1.86312
Li	-0.75521	0.73993	-0.23691
O	0.72577	2.16329	-0.57080
C	1.44353	2.23696	0.70585
C	0.48851	3.02812	1.58867
C	-0.07436	4.09489	0.61902
C	0.10766	3.47166	-0.78339
N	-1.67385	0.10007	1.21746
C	-0.97020	-0.73540	2.15860
C	-0.33555	-2.03254	1.53360
C	-1.44356	-2.81097	0.80064
C	-2.30279	-1.92727	-0.11362
C	-2.78344	-0.66702	0.67139
C	-3.70229	0.18335	-0.22676
C	-3.10383	0.49846	-1.60750
C	-2.61466	-0.77014	-2.32446
C	-1.62337	-1.60235	-1.47210
C	0.90003	-1.73165	0.70736
C	2.14393	-1.91590	1.29547
C	3.36292	-1.57160	0.68370
C	3.26373	-0.96643	-0.56222
N	2.10149	-0.79265	-1.19095
O	4.31852	-0.45527	-1.26859
C	5.61878	-0.63042	-0.72602
H	-2.15901	-0.51071	-3.29082
H	-3.49094	-1.39472	-2.55120

H	-3.84546	1.01771	-2.22981
H	-2.27241	1.22472	-1.52260
H	-4.64147	-0.36550	-0.38894
H	-3.95712	1.11056	0.30289
H	-3.42668	-1.05616	1.49506
H	-0.16540	-0.16451	2.65087
H	-1.63409	-1.09745	2.97911
H	2.17732	-2.35177	2.29240
H	4.30748	-1.74846	1.18083
H	5.86352	-1.69363	-0.60876
H	6.30664	-0.17834	-1.44301
H	5.72407	-0.12908	0.24526
H	0.00586	-2.66001	2.37093
H	-2.10191	-3.24167	1.56908
H	-1.02158	-3.65737	0.23915
H	-3.19724	-2.51546	-0.38204
H	-1.52713	-2.57906	-1.97956
H	0.11773	-0.96583	-2.55072
H	1.63031	1.21056	1.02540
H	2.39719	2.75341	0.53597
H	0.77136	4.06555	-1.42157
H	-0.83068	3.29253	-1.31503
H	0.48424	5.03326	0.68911
H	-1.12435	4.31173	0.83041
H	0.99183	3.46996	2.45341
H	-0.31306	2.36644	1.93703

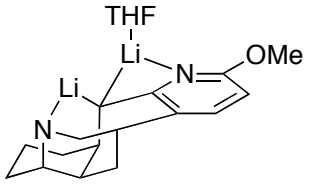

G = -1053.597904

Atom	X	Y	Z
C	0.76082	-0.14560	-1.04856
C	0.34107	1.16581	-0.57334
N	-1.01291	1.38336	-0.76569
Li	-1.38633	-0.51425	-0.72952
Li	0.99034	-0.86132	0.96709
N	2.57849	-0.26833	1.61954
C	2.74754	1.14570	1.83561
C	2.56288	2.01802	0.53765
C	3.49601	1.47222	-0.55944

C	3.43406	-0.05389	-0.70844
C	3.59798	-0.72174	0.68974
C	3.61392	-2.25467	0.53767
C	2.43045	-2.80510	-0.27413
C	2.28158	-2.09123	-1.62701
C	2.18833	-0.54978	-1.49196
C	1.10821	2.15567	0.13080
C	0.43569	3.31732	0.49540
C	-0.92781	3.54006	0.25604
C	-1.61035	2.50024	-0.36417
O	-2.95934	2.49739	-0.61947
C	-3.69080	3.66974	-0.28898
O	-2.91715	-1.51967	-0.31574
C	-4.21787	-0.86905	-0.28119
C	-4.93705	-1.53312	0.88680
C	-4.46035	-2.99075	0.76275
C	-3.00821	-2.84174	0.28414
H	1.40645	-2.47822	-2.16924
H	3.16102	-2.33370	-2.24116
H	2.55174	-3.88522	-0.43326
H	1.48739	-2.72709	0.30075
H	4.54058	-2.54853	0.02299
H	3.63783	-2.70975	1.53591
H	4.61289	-0.43073	1.04809
H	2.03646	1.50300	2.59599
H	3.76394	1.39681	2.21960
H	1.00242	4.09909	0.99751
H	-1.40458	4.46393	0.55578
H	-3.31223	4.54340	-0.83364
H	-4.72207	3.47618	-0.59064
H	-3.65911	3.87625	0.78876
H	2.90478	3.03587	0.77949
H	4.52436	1.74027	-0.27662
H	3.29635	1.96648	-1.52177
H	4.29412	-0.35270	-1.33275
H	2.31929	-0.14204	-2.51029
H	0.12001	-0.42245	-1.90358
H	-2.72173	-3.58674	-0.46430
H	-2.29127	-2.87971	1.11167
H	-4.04064	0.20332	-0.17534
H	-4.73188	-1.05760	-1.23289
H	-4.60665	-1.09421	1.83526
H	-6.02415	-1.43196	0.82169
H	-4.52674	-3.54642	1.70205
H	-5.05774	-3.52285	0.01434

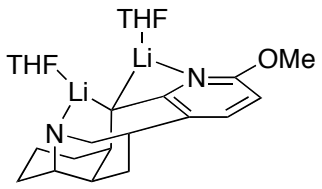

G = -1285.969673

Atom	X	Y	Z
C	0.41673	-0.40731	-1.29588
C	0.10538	0.98000	-1.14063
N	-1.24650	1.20878	-0.88814
Li	-1.36952	-0.39714	0.20848
Li	1.19591	-0.32929	0.73346
O	-0.38129	-0.09716	1.98793
C	-0.21949	1.23672	2.56287
C	0.83265	1.02023	3.64267
C	0.42681	-0.34665	4.23946
C	-0.33544	-1.04944	3.09333
N	2.93850	0.26398	0.64784
C	3.12855	1.64315	0.27281
C	2.52357	2.02349	-1.12876
C	3.10876	1.06723	-2.18465
C	3.05202	-0.40803	-1.76528
C	3.62956	-0.56738	-0.32406
C	3.63001	-2.05676	0.07146
C	2.27667	-2.75370	-0.13791
C	1.74177	-2.54293	-1.56283
C	1.64970	-1.04594	-1.95598
C	1.00878	2.11176	-1.09805
C	0.42987	3.36566	-0.97702
C	-0.95371	3.58402	-0.82813
C	-1.73410	2.43873	-0.75279
O	-3.08795	2.43760	-0.50516
C	-3.73322	3.69638	-0.38968
O	-2.85922	-1.62444	0.26168
C	-4.15418	-1.00682	-0.01432
C	-4.81925	-1.86499	-1.10688
C	-3.65366	-2.69881	-1.66914
C	-2.77996	-2.88919	-0.43435
H	0.75983	-3.02613	-1.67859
H	2.42069	-3.04984	-2.26426
H	2.36907	-3.82825	0.07335
H	1.53214	-2.39342	0.59627
H	4.37644	-2.58450	-0.54067
H	3.94906	-2.14440	1.11816

H	4.70101	-0.26526	-0.40011
H	0.07642	1.90156	1.75018
H	-1.18651	1.55959	2.97161
H	0.83857	1.82099	4.38790
H	1.82094	0.95775	3.17333
H	-0.22852	-0.22093	5.10733
H	1.29903	-0.92286	4.55851
H	-1.36414	-1.30780	3.36692
H	0.16550	-1.94534	2.71672
H	2.68372	2.31127	1.02917
H	4.20826	1.92213	0.21687
H	-1.72516	-3.07952	-0.64985
H	-3.16291	-3.68659	0.21768
H	-3.97754	-3.64718	-2.10777
H	-3.10394	-2.13424	-2.43017
H	-5.58116	-2.52117	-0.67191
H	-5.30305	-1.24918	-1.86988
H	-4.73191	-0.98995	0.91610
H	-3.95535	0.01896	-0.33549
H	1.08544	4.23466	-0.99775
H	-1.35772	4.58498	-0.75468
H	-3.63270	4.28405	-1.31096
H	-4.78893	3.48010	-0.21289
H	-3.33643	4.27994	0.45140
H	2.88135	3.03599	-1.37141
H	4.16623	1.33933	-2.31788
H	2.62213	1.21503	-3.16012
H	3.71142	-0.96481	-2.45352
H	1.47577	-1.02567	-3.04796
H	-0.47477	-0.95102	-1.63799

REFERENCES

1. For a review of lithiated anions, see: Langer, P.; Freiberg, W. *Chem. Rev.* **2004,** *104,* 4125-4149.

2. For crystallographically characterized N,C-chelated dianions, see: (a) Selinka, C.; Stalke, D. *Z. Naturforsch., B: Chem. Sci.* **2003**, *58*, 291. (b) Konrad, T. M.; Grunwald, K. R.; Belaj, F.; Mosch-Zanetti, N. C. *Inorg. Chem.* **2009**, *48*, 369. (c) Williard, P. G.; Jacobson, M. A. *Org. Lett.* **2000**, *2*, 2753.

3. (a) Bisai, A.; West, S. P.; Sarpong, R. *J. Am. Chem. Soc.* **2008**, *130*, 7222-7223. (b) West, S. P.; Bisai, A.; Lim, A. D.; Narayan, R. R.; Sarpong, R. *J. Am. Chem. Soc.* **2009**, *131*, 11187-11194.

4. Tricycle **5** was prepared as previously reported by Sarpong et al. See Ref. 3.

5. Kalgutkar Amit, S.; Crews Brenda, C.; Saleh, S.; Prudhomme, D.; Marnett Lawrence, J. *Bioorg. Med. Chem.* **2005**, *13*, 6810.

6. For a recent example of Hofmann rearrangement using $Pb(OAc)_4$, see: Evans, D. A.; Scheidt, K. A.; Downey, C. W. *Org. Lett.* **2001**, *3*, 3009.

7. (a) Rennels, R. A.; Maliakal, A. J.; Collum, D. B. *J. Am. Chem. Soc.* **1998**, *120*, 421. (b) Kottke, T.; Stalke, D. *Angew. Chem., Int. Ed. Engl.* **1993**, *32*, 580.

8. (a) Collum, D. B. *Acc. Chem. Res.* **1993**, *26*, 227. (b) For leading references to open dimers, see: Ramirez, A.; Sun, X.; Collum, D. B. *J. Am. Chem. Soc.* **2006**, *128*, 10326.

9. Fraenkel, G.; Martin, K. V. *J. Am. Chem. Soc.* **1995**, *117*, 10336.

10. Frisch, M. J.; Trucks, G. W.; Schlegel, H. B.; Scuseria, G. E.; Robb, M. A.; Cheeseman, J. R.; Montgomery, Jr., J. A.; Vreven, T.; Kudin, K. N.; Burant, J. C.; Millam, J. M.; Iyengar, S. S.; Tomasi, J.; Barone, V.; Mennucci, B.; Cossi, M.; Scalmani, G.; Rega, N.; Petersson, G. A.; Nakatsuji, H.; Hada, M.; Ehara, M.; Toyota, K.; Fukuda, R.; Hasegawa, J.; Ishida, M.; Nakajima, T.; Honda, Y.; Kitao, O.; Nakai, H.; Klene, M.; Li, X.; Knox, J. E.; Hratchian, H. P.; Cross, J. B.; Bakken, V.; Adamo, C.; Jaramillo, J.; Gomperts, R.; Stratmann, R. E.; Yazyev, O.; Austin, A. J.; Cammi, R.; Pomelli, C.; Ochterski, J. W.; Ayala, P. Y.; Morokuma, K.; Voth, G. A.; Salvador, P.; Dannenberg, J. J.; Zakrzewski, V. G.; Dapprich, S.; Daniels, A. D.; Strain, M. C.; Farkas, O.; Malick, D. K.; Rabuck, A. D.; Raghavachari, K.; Foresman, J. B.; Ortiz, J. V.; Cui, Q.; Baboul, A. G.; Clifford, S.; Cioslowski, J.; Stefanov, B. B.; Liu, G.; Liashenko, A.; Piskorz, P.; Komaromi, I.; Martin, R. L.; Fox, D. J.; Keith, T.; Al-Laham, M. A.; Peng, C. Y.; Nanayakkara, A.; Challacombe, M.; Gill, P. M. W.; Johnson, B.; Chen, W.; Wong, M. W.; Gonzalez, C.; and Pople, J. A. *Gaussian 03*, revision B.04; Gaussian, Inc.: Wallingford, CT, 2004.